Physics – Uspekhi **57** (10) 990 – 1021 (2014)

INSTRUMENTS AND METHODS OF INVESTIGATION PACS numbers: 28.41.Kw, **52.30.–q**, 52.35.Tc, 52.40.Fd, **52.50.–b**

On the theory of plasma processing of spent nuclear fuel

A V Timofeev

DOI: 10.3367/UFNe.0184.201410g.1101

Contents

Abstract. This paper reviews the current theory of the processing of spent nuclear fuel by a plasma method using ion-cyclotron heating. The method consists of selectively heating ash ions, followed by their extraction from the cold plasma flow of nuclear fuel. It is shown that these processes are realizable for moderate values of system parameters. Through the analysis of spent fuel processing data, results useful for other applications are also obtained. A theory of helical wire antennas that are often used in plasma research is developed. A new interpretation is offered for the amplification effect of an HF electric field excited by such antennas. The concept of spatial instability is introduced for the stationary flow of a continuous medium, a phenomenon that leads to the downstream enhancement of perturbations due to nonmoving objects and can occur, for example, in a subsonic plasma flow along a magnetic field.

1. Purpose and principles of spent nuclear fuel processing

1.1 Conditions for spent nuclear fuel processing

At present, problems to be resolved by nuclear power engineering include nuclear fuel (NF) breeding and the transition to closed-cycle operation of nuclear reactors. Closed-cycle operation assumes that all the natural uranium, which consists mainly of ^{238}U, is transformed into products of NF fission, i.e., into nuclear ash (NA). In the closed cycle, ^{238}U undergoes a sophisticated evolution, beginning with the attachment of a single neutron to its nucleus and the subsequent β-decay and the transformation into fissioning nuclei of the ^{239}Pu. Further irradiation by neutrons may cause fissioning of the plutonium nuclei with a release of energy, or their transformation into nuclei of the so-called minor actinides (americium, curium, etc.). These elements have half-life periods of $\geqslant 10^3$ years, and their appearance in the ambient environment is extremely undesirable. The closed fuel cycle implies the 'burning out' of minor actinides under the influence of neutrons in nuclear reactors. The closed fuel cycle providing for nuclear fuel breeding can be realized in fast reactors (FRs).

The nuclear ash resulting from the decay of NF nuclei hinders the course of the chain fission reaction; therefore, all reactors must be reloaded when the NA concentration reaches a critical value, which in the FR case amounts approximately to 10%. If the NA is extracted from the spent nuclear fuel (SNF), then the remaining part of the latter can be used as full-value NF for fast reactors.

When the SNF of fast reactors is processed, it is desirable to reduce the NA content by an order of magnitude to 1% [1]. However, the higher the quality of processing, the more effort it requires. For this reason, it may turn out to be more expedient to leave a greater part of NA in the NF and to reload the reactor more often. Thus, for example, if the concentration of the remaining NA is reduced to 2.5%, the

A V Timofeev National Research Centre 'Kurchatov Institute', pl. Akademika Kurchatova 1, 123182 Moscow, Russian Federation
E-mail: avtim@nfi.kiae.ru, timofeev_av@nrcki.ru

Received 2 October 2013, revised 7 November 2013
Uspekhi Fizicheskikh Nauk **184** (10) 1101 – 1133 (2014)
DOI: 10.3367/UFNr.0184.201410g.1101
Translated by G Pontecorvo; edited by A Radzig

time between the reloadings will only decrease to 5/6 of the initial time.

Sanitary and ecological regulations impose extremely rigorous restrictions on the content of NF (actinides) in the NA: 0.1% of the initial amount [1].

The conditions indicated for processing SNF of fast reactors can be satisfied by presently applied chemical methods. However, their disadvantage consists in the appearance of a large volume of detrimental waste. From this point of view, physical methods, including plasma methods, employing the difference between NT and NA mass numbers may turn out to be more attractive.

It should be noted that separation of the ^{238}U and ^{239}Pu isotopes by physical methods is difficult owing to their masses being close to each other, so the 'nuclear explosive' is naturally involved in the FR closed cycle.

1.2 State of the problem of spent nuclear fuel processing by plasma methods

The goal of SNF processing consists in the separation of particles of different chemical elements in accordance with their masses. The same problem was resolved when the separation of isotopes of the same element was performed. In SNF processing, therefore, it is natural to try applying the methods used for isotope separation, such as various versions of the centrifugation method.

Converting a substance into a plasma state provides us with the possibility of acting upon its particles with electric and magnetic fields. In particular, this permits rotating the plasma in devices possessing no moving parts. In an axially symmetric system placed in crossed fields (axial magnetic and radial electric fields), charged particles, depending on their masses, can both drift in the direction across these fields, i.e., along the azimuth, or move along the electric field with acceleration. This effect was utilized in the so-called 'Archimedean' filter, meant for processing waste from the production of plutonium [2, 3]. However, as pointed out in Ref. [4], the experiments happened to be not quite successful. Hopes were also not justified concerning the method for creating plasma based on injection of the substance to be processed in the form of gas and vapor into a magnetic field and its further ionization with the aid of microwave (UHF) radiation. In our opinion, the employment of end plates, both for introducing a constant electric field into the plasma and for collecting one of the fractions of the substance being processed, was also unsatisfactory. Another method for generating plasma in such systems — with the aid of a plasma-beam discharge — was dealt with in Refs [5, 6].

Fetterman and Fisch [7] proposed to use the so-called Volosov centrifugal trap for SNF processing [8]. By varying the parameters of such a trap, one can direct the NA and NF ions toward different end plates. However, even in this case, it would be necessary to use butt electrodes as the receivers of ions. The same authors note in Ref. [9] that plasma can also be made to rotate in a magnetic field induced in an electrodeless system by transferring the momentum of electromagnetic waves. In Ref. [10], a scheme is proposed for SNF processing that represents a development of so-called plasma-optical schemes (see, for example, paper [11]) and of the electromagnetic isotope separation scheme modified by the introduction of an electromagnetic field orthogonal to the magnetic field.

Another way for electromagnetic waves to act upon charged plasma particles (via energy transfer) was proposed

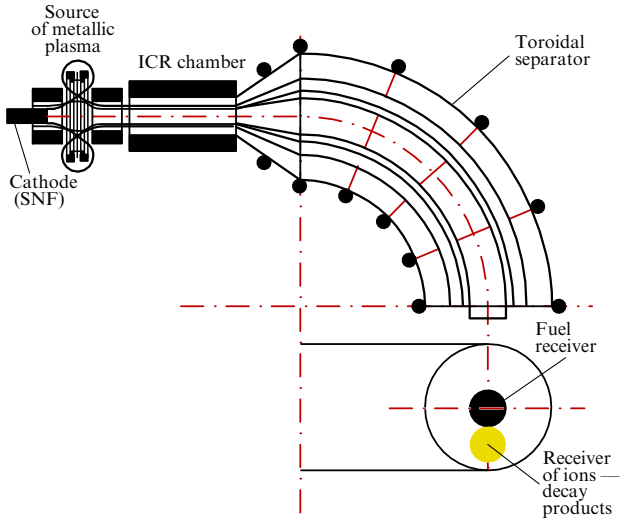

Figure 1. Schematic diagram of the layout for SNF processing.

for SNF processing in Refs [12–14]. This method involves the same stages as the ion-cyclotron resonance (ICR) method of isotope separation: ionization of the substance being processed, selective ICR heating of the target ions and their extraction from the SNF plasma, and separate collection of the target and dump ions. Isotope separation was realized by this method in our country and in the USA and France (see reviews [15, 16]). The schematic diagram of a layout for SNF processing by the ICR method is presented in Fig. 1.

It should be noted that, while in the case of ICR isotope separation the target ions — the ones that are heated — are ions of a sole isotope, in SNF processing it is necessary to heat ions of many chemical elements differing significantly in mass. Therefore, unlike heating in ICR isotope separation systems, the cyclotron heating of various ions has to be performed in an inhomogeneous magnetic field. The features peculiar to the mass distribution of NA ions make it necessary to utilize two high-frequency (HF) fields of different frequencies for the heating.

For the experimental investigation of physical processes occurring during plasma ICR SNF processing, a facility designated as PS-1, in which imitators, namely, stable metals and gases, will be substituted for the SNF substance, has been installed at the Institute of Hydrogenic Power Engineering and Plasma Technologies of the National Research Centre 'Kurchatov Institute' (NRC KI). At present, experiments are under way with the axially symmetric part of the facility. The segment involving a curvilinear magnetic field is planned to be attached later.

A theoretical analysis has hitherto been performed for two stages of SNF processing: the selective heating of NA ions, and their extraction from cold SNF plasma. As to the first stage, i.e., the generation of SNF plasma, its analysis is rendered difficult both by the complex interdisciplinary character of the process of converting the solid SNF substance into plasma and by the lack of data published in the available literature on elementary processes occurring with the atoms and ions of uranium, the main SNF component. The issue of ion collection has not been studied theoretically either.

The analysis of any device involving plasma as the working substance gives rise to numerous and diverse

physical problems. The systems for SNF plasma processing we are interested in are no exception. The present article provides an idea of a certain stage in the theoretical study of such systems. Practice shows that for the creation of a consistent picture of the phenomena taking place in plasma systems a combination of theory and experiment is required. However, no experiments concerning SNF plasma processing have been performed yet. For this reason, experimental results obtained with devices involving the same design elements as used in SNF processing systems are extremely valuable. Such are the devices, mentioned above, applied in ICR isotope separation, as are systems investigated in the 1960s, in which a flow of hydrogen plasma was directed along curved magnetic force lines. Such systems were meant for developing methods of plasma injection into magnetic traps [17]. It turned out that a hydrogen plasma bunch moving along a curvilinear magnetic field segment undergoes decontamination from admixtures of heavy ions [18–21]. The separation of ions by their masses is actually based on the very same process (the drift of charged particles in an inhomogeneous magnetic field) that was proposed in Refs [12–14] to be used for facilitating the separation of NA ions heated by the ICR method and of cold NF ions.

Although the theory of plasma is quite well developed, the analysis of concrete plasma systems and their optimization requires further theoretical studies. In the course of such studies, unexpected aspects of known physical regularities are often revealed. As we shall see below, this assertion also holds valid for the problem, we are interested in, of SNF processing by the ICR plasma method. Thus, for example, the investigation of plasma flows in SNF processing systems led to the introduction of the new concept of spatial instability. The spatial instability that is inherent in subsonic plasma flows in a strong magnetic field causes transverse stratification of these flows. In order to clarify the mechanism of instability development in subsonic flows, it turned out to be useful to introduce the concepts of negative mass and negative heat capacity. Notice that with the aid of the first concept it is possible, in particular, to provide a simple interpretation of the action of a Laval nozzle.

1.3 Heating of nuclear ash ions by the ion-cyclotron resonance method

If a plasma is placed in a magnetic field, the distinction between the masses of NF and NA ions is manifested in the difference between the cyclotron rotation frequencies ω_i. This circumstance can be used to advantage for the selective heating of one of the groups of ions by the ICR method. Selective heating of NA ions permits separating them quite easily in phase space from NF ions with the required high degree of purity. Indeed, charged particles produced in a source of plasma usually have a low energy, of the order of several electron-volts, and their velocity distribution is close to the Maxwellian distribution. This distribution is characterized by a sharp drop in the region of energies exceeding the temperature. Therefore, if the NA ions are heated to an energy $\varepsilon \geqslant 10\,T$, the required degree of separation will be achieved in phase space. However, the purpose of processing consists in finding the spatial separation of the NF and NA ions, at which they can be received by different collectors. To this end, it is possible to make use of the energy dependence of the Larmor radius in a plasma in a magnetic field and, in the case of an inhomogeneous field, of the drift velocity (the systematic shift of a particle across the force lines of the magnetic field). Calculations show (see Section 4) that for the transformation of energy differences into spatial ones the energy of NA ions must be increased by at least one order of magnitude.

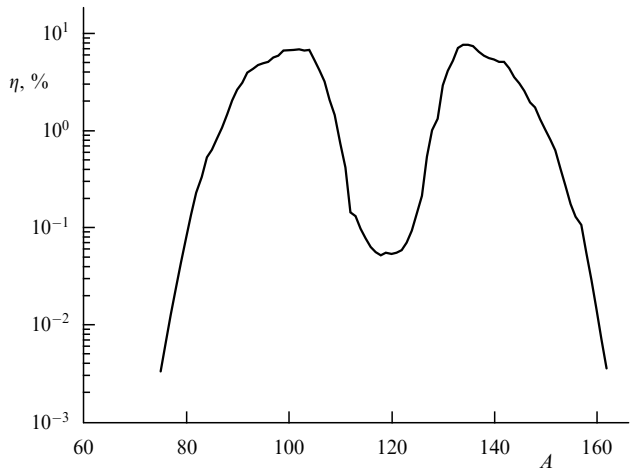

Figure 2. Distribution of chemical elements composing NA over the mass number A; η is the fraction of elements.

The equations of motion describing the behavior of ions in electric and magnetic fields contain the ion masses and charges in the form of ratios Ze/m_i, where Z is the particle charge multiplicity. Therefore, the spread in Z values may conceal in certain cases the influence of the difference among the masses of the particles being separated. This peculiarity makes it difficult to apply plasma methods of SNF processing, including the method based on the selective ICR heating of NA ions.

Fuel and ash nuclei differ in mass by approximately a factor of two. The distribution of chemical elements composing NA over the mass number A is shown in Fig. 2. If one assumes the NA substance to be singly ionized, then in the cyclotron heating of NA ions with $A \approx 120$, doubly charged NF ions ($A \approx 240$) will also undergo heating. The presence of doubly charged NF ions could be neglected if their fraction in the SNF plasma were inferior to 0.1%. However, this can hardly be hoped for, since the first and second ionization potentials of uranium atom differ by a factor of less than two ($U_1 = 6.3$ eV, and $U_2 = 11.2$ eV). Therefore, the requirements that the SNF substance exhibit a high degree of ionization and of the presence of an extremely small fraction of doubly charged uranium ions are difficult to reconcile. Experiments on ICR separation of the isotopes of a number of metals with ionization potentials close to that of uranium atom revealed the presence of a noticeable (of the order of 1%) amount of doubly charged ions in the metal plasma with a temperature near several electron-volts [22, 23].

To exclude the heating of doubly charged actinide ions, the author of Ref. [24] proposed taking advantage of the peculiarities of the mass number distribution of NA elements. Referring to Fig. 2, plotted from the nuclear data of Ref. [25], this distribution is seen to be concentrated in the vicinity of mass number values $A \approx 100$ and $A \approx 140$, and that the fraction of elements with $A \approx 120$ is relatively small. Therefore, if the extraction of fission fragments with $A \approx 120$ is abandoned, the admissible 1% level of NF contamination with fragments will not be exceeded. It must, however, be noted that multiple reloading of a reactor will result in the appearance of NA elements with $A \approx 120$ accumulating in the

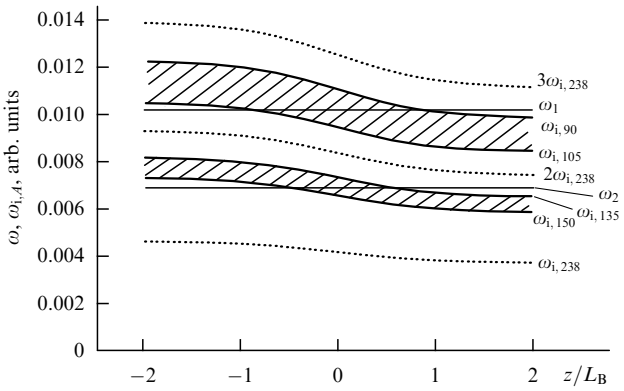

Figure 3. Dependence of the NA ion-cyclotron frequency on the coordinate along the magnetic field: 90% of the ions fall into the shaded regions.

NF. Such accumulation may be prevented by element transmutation processes caused by the neutron field of nuclear reactors.

Selective heating of one group of ions differing in mass was previously used for separating the isotopes of a sole chemical element. In the case of isotope separation, a certain single isotope was usually isolated from a mixture of isotopes. The heating of ions of this isotope can be performed in a homogeneous magnetic field by choosing the HF field frequency from the condition that $\omega \approx \omega_i$, where ω_i is the cyclotron frequency of the (target) isotope being isolated. NA, which has to be extracted from SNF, contains a set of chemical elements with different masses (see Fig. 2) and, consequently, different cyclotron frequencies.

At present, the technique for generating HF fields with frequency spectra close to monochromatic is well developed. To heat NA ions in such a field it is necessary to direct the plasma jet as it leaves the source into a magnetic field weakening along the jet direction. The drop in the magnetic field within the confines of the ICR heating system should be such that each one of the NA ions receives energy from the HF field as it crosses its cyclotron resonance zone. In accordance with the above, ions of $A \approx 120$ with cyclotron frequencies close to the cyclotron frequencies of doubly charged actinide ions are to be excluded. Such heating can be realized with the aid of two monochromatic HF fields, so one of them heats the light fraction of NA elements with $A \approx 100$, while the other one heats the heavy fraction with $A \approx 140$. This heating scheme is illustrated in Fig. 3, which shows the respective magnetic field profile along the axis of the device:

$$B_0(z) = \left(1 - \beta \tanh \frac{z}{L_{B0}}\right) B_0(0)\,, \tag{1.1}$$

in the cyclotron resonance region of the NA and NF ions. Here, β is a parameter determining the degree of inhomogeneity of the magnetic field, and L_{B0} represents the spatial scale of the magnetic field.

Figure 3 demonstrates the possibility, in principle, of selective cyclotron heating of NA ions. The choice of frequencies was based on the calculations described in Section 4. The frequency values were influenced by the Doppler effect, allowing for which the cyclotron resonance condition assumes the form

$$\omega = \omega_i + k_\parallel v_\parallel\,, \tag{1.2}$$

where $k_\parallel$ is the wave vector component along the magnetic field, and $v_\parallel$ is the ion velocity along the same field.

Helical antennas applied for ICR heating excite a spectrum of electromagnetic oscillations of width $\Delta k_\parallel$ of the order of $1/L_A$, where L_A is the antenna length along the magnetic field. Calculations have shown that in the separation process of NA ions that we are interested in, the optimal frequencies are $\omega_1 = \omega_{i,A=97}$, and $\omega_2 = \omega_{i,A=143}$ at $\beta = 0.11$. Here, the cyclotron frequencies are taken at $z = 0$.

The processes of isotope separation and of SNF processing also differ in one more way. While the separation of ions in the first process is based on their mass numbers differing by $\Delta A \sim 1$, the difference between the NA and NF mass numbers in the second process is significantly larger, $\Delta A \sim 100$. In the case of cyclotron heating, the doubly charged NF ions with a cyclotron frequency close to the cyclotron frequency of singly charged NA ions with $A \approx 120$ (see above) should remain cold. However, even taking into account this circumstance the effective difference between the mass numbers, $\Delta A_{\text{eff}} \approx \Delta A/Z$, determining the difference in the cyclotron frequencies of the ions being separated, exceeds the value of the analogous quantity for the mixture of isotopes of a sole chemical element by approximately an order of magnitude. The strength of the magnetic field in which ICR heating is performed depends on the value of ΔA_{eff}. The strength of the magnetic field must be such that the difference between the cyclotron frequencies of the heated 'target' ions and of the 'dump' ions, which must remain cold, exceeds the cyclotron resonance line width due to the Doppler effect and to other factors (see Section 3). Owing to the value of ΔA_{eff} in SNF plasma exceeding this value for a mixture of isotopes, ICR NA heating can be performed in an essentially weaker magnetic field.

1.4 Separation of nuclear ash and nuclear fuel ions

Cyclotron heating causes a predominant increase in the energy $\varepsilon_\perp$ of the Larmor rotation of charged particles, which leads to an increase in their Larmor radius $\rho_i = (2\varepsilon_\perp/m_i)^{1/2}/\omega_i$. If the heating is sufficiently intense and the magnetic field is not too strong, the Larmor circles of the ions will go beyond the confines of the flow of cold SNF plasma, precisely where the ions can be received by their collectors. Unlike the above, the characteristic parameters of systems for ICR isotope separation are such that the Larmor radius of the target ions, even after their heating, remains small compared to the radius of the plasma flow. The target ions are extracted from the flow onto a set of parallel plates oriented along the magnetic field (see Refs [15, 16]). The distance between the plates, Δh, must satisfy the condition $\rho_{ih} > \Delta h > \rho_{ic}$, where ρ_{ih} and ρ_{ic} are the Larmor radii of the target and dump ions, respectively. In this case, most of the heated (target) ions will lodge on the collector plates, while most of the cold (dump) ions will pass between them. To prevent the dump ions from landing on the plates, the front edges of the plates facing the flow must be protected by screens that 'eat up' part of the plasma flow. As a result, the flow between the plates represents a set of streamlets with sharp boundaries. It is quite possible that these streamlets are subject to drift type instabilities (see, for example, Ref. [26]). The development of such instabilities should cause broadening of the streamlets, which could lead to dump ions landing on the plates, thus worsening the quality of separation.

The separation quality of charged particles based on the difference between their energies can be improved by

attaching a magnetic field segment with curved force lines [27] to the axisymmetric ICR heating system. In such a magnetic field, ions shift (drift) along the binormal to the force lines with the velocity $V_{\rm dr} = (v_\parallel^2 + v_\perp^2/2)/(R\omega_{\rm i})$, where R is the radius of curvature of the force lines. The drift velocity depends on the ion energy and on its distribution over the degrees of freedom, but not on the particle mass, while the velocity of motion along the force lines of the magnetic field is proportional to $(\varepsilon/m_{\rm i})^{1/2}$. Therefore, when an ion covers the whole length of a segment of the curvilinear magnetic field, its displacement along the binormal will be $\Delta y_{\rm dr} \propto (m_{\rm i}\varepsilon)^{1/2}$. If the force lines along this segment are bent through an angle $\Delta\varphi$, the displacement is expressed as

$$\Delta y_{\rm dr} = \frac{1}{2}\,\rho_{\rm i}'\Delta\varphi\left(\cos\theta + \frac{1}{\cos\theta}\right), \tag{1.3}$$

where $\rho_{\rm i}'$ is the ion Larmor radius calculated from the total energy, and $\theta = \arctan(v_\perp/v_\parallel)$ is the pitch angle.

If, for instance, $\Delta\varphi \approx \pi$, $\cos\theta \approx 1$, the shift $\Delta y_{\rm dr}$ is approximately three times $\rho_{\rm i}$. Therefore, for the ion to go beyond the confines of the cold plasma stream, it must be heated to an energy one order of magnitude lower than the value determined by the condition $\rho_{\rm i} > r_0$, where r_0 is the radius of the stream.

It is especially expedient to apply ion separation in a curvilinear magnetic field in ICR isotope separation systems. In such systems ICR heating takes place in a homogeneous magnetic field, so the ion pitch angle turns out to be close to $\pi/2$, while the ion shift $\Delta y_{\rm dr}$ may be essentially superior to the Larmor radius of the ions.

Mass separation of ions in a curvilinear magnetic field has been implemented in experiments [18–21], in which hydrogen plasma bunches contaminated with heavy admixture ions were directed through a magnetic field segment with curved force lines. All the ions in the plasma bunches, generated by plasma guns, move along the magnetic field with velocities close to each other, so the kinetic energy of heavy ions exceeds the energy of the light ones. Since the drift velocity in a curvilinear magnetic field is proportional to the energy, a plasma bunch will undergo cleansing from heavy ions lodged on the walls of the vacuum chamber in certain relationships between parameters of the system.

The separation methods discussed in this article imply the exit of heated NA ions from the stream of cold SNF plasma. In this case, a cloud of positive charge forms around the stream, and the stream itself acquires a negative charge. The excess negative charge may leak out onto the collector and the flanks of the plasma source. Neutralization of the positive charge can be effected by ionization of the residual gas. To this end, it might be necessary to ignite a gas discharge.

As a matter of fact, the same problem also appears in the ICR isotope separation, although it is not so pronounced there. Indeed, the heating of ions of the target isotope causes a broadening of its distribution over the radius. Here, the central part of the plasma column is negatively charged, while its periphery is charged positively. This circumstance has led to no difficulties, and it was not mentioned in the descriptions of experimental results. Most probably, such a distribution of the potential was established spontaneously in the plasma source and in the separation system, satisfying the requirement of local plasma quasineutrality.

It should be noted that the problem of maintenance of plasma neutrality also arises when a curvilinear magnetic field is used. As is known, electric polarization of plasma in an inhomogeneous magnetic field can lead to its ejection into the region of a lower magnetic field, i.e., onto the wall of the vacuum chamber. This problem is dealt with in Section 5.

The extraction of heated ions from the cold plasma stream is facilitated as the magnetic field reduces, which leads to an increase in both the Larmor radius of ions and their displacement along the binormal in the curvilinear magnetic field. However, the strength of the magnetic field has a lower bound that is due to the requirements of heating selectivity (see above) and magnetization of the cold NF ions. This is necessary for the isolation of NA ion collectors from the cold dump ions. Analysis of the diffusion of the latter across the magnetic field has shown that for the required isolation it is sufficient to satisfy the approximate condition $\omega_{\rm i}/\nu_{\rm ii} \geqslant 3$, where $\nu_{\rm ii}$ is the frequency of ion–ion collisions (see Section 6). This condition can be presented as

$$\frac{nZ_{\rm f}^3}{BT_{\rm i}^{3/2}} \leqslant 1.15\times 10^{11}\,, \tag{1.4}$$

where n is the mean plasma density [cm^{-3}] in the stream, B is the magnetic field induction [kG], $T_{\rm i}$ is the ion temperature [eV], and $Z_{\rm f}$ is the charge number of NF ions. In inequality (1.4), account is taken of the fact that $\omega_{\rm i} \propto Z_{\rm f}$, and $\nu_{\rm ii} \propto Z_{\rm f}^4$.

1.5 Throughput of the system for spent nuclear fuel processing. The problem of multiply charged ions

A conventional nuclear reactor providing electric power of 1 GW consumes about 20 t of NF per year. If such an amount of SNF is processed applying the plasma method, then during continuous operation of the processing systems the power of the plasma jet through them, measured in equivalent amperes (eA), will run to approximately $J \approx 250$ eA. It is desirable that the number of processing systems mated to a reactor be minimal. The following scheme is optimal: one reactor — one SNF processing system.

The parameters of the plasma jet passing through the system are related to its productivity by the expression

$$J \approx 10^{-14} nS(T_{\rm i} + T_{\rm e})^{1/2}\,, \tag{1.5}$$

where n is the average plasma density [cm^{-3}] in the jet, S is the area [cm^2] of the stream's cross section, $T_{\rm i}$ and $T_{\rm e}$ are the respective ion and electron temperatures [eV], and J is the current [eA] carried by the stream. In expression (1.5), the velocity of the plasma stream is assumed to be equal to the speed of ion sound.

If in formula (1.5), for example, one sets $n = 10^{12}$ cm^{-3}, $r = 15$ cm ($S = \pi r^2$), and $T_{\rm i} = T_{\rm e} = 3$ eV, then the throughput of the system will turn out to be an order of magnitude smaller than required. The adopted parameter values are close to those of the systems examined in Refs [24, 28]. However, these systems were not optimized, and their parameters were selected on the basis of estimates to an order of magnitude. It is not ruled out that a more detailed analysis may result in achievement of the optimal productivity of a single system: $J \approx 250$ eA.

We shall now briefly touch upon the physical processes that can determine the density of the plasma jet through the SNF processing system and, consequently, the productivity of the system. The isolation of NA ion collectors from the flow of cold NF plasma is violated by Coulomb collisions leading to displacements of charged particles across the

magnetic field. The plasma diffusion is due to ion–electron collisions and the diffusion coefficient is expressed as $D_\perp \approx \rho_i^2 \nu_{ie}$, where ν_{ie} is the collision frequency of ions and electrons. The higher the ion–ion collision intensity, the greater the plasma viscosity. The viscosity coefficient is given by the expression $\eta_{\perp i} \approx n m_i \rho_i^2 \nu_{ii}$. For typical values of the plasma parameters, the diffusion time calculated via the average plasma density, $t_d \approx r_0^2/(\rho_i^2 \nu_{ie})$, is about two orders of magnitude longer than the time the plasma flows through the system, $t_0 \approx L/V_s$, where $L \approx 3 \times 10^2$ cm is the length of the system, and $V_s = [(T_e + T_i)/m_i]^{1/2}$ is the speed of ion sound.

It should be noted that the intensity of diffusion in the 'tail' of the radial density distribution, which may reach the NA collectors, drops significantly: $t_d \propto n^{-1}$. Concerning the viscosity, as shown in Ref. [29] (see also Section 6), when using the parameters indicated above, it weakly affects the motion of the plasma across the magnetic field. Therefore, one cannot rule out that the condition of magnetization, $\omega_i/\nu_{ii} \geqslant 3$, presented in Section 1.4, somewhat reduces the required plasma density.

The Coulomb collisions of NA ions, heated by the HF field, with cold NF ions and electrons lead to cooling of the NA ions. The characteristic times of cooling by electrons and ions can be estimated to an order of magnitude as

$$t_{ie} \approx \frac{m_i}{m_e}\frac{2}{\nu_{ie}} \approx 10^{10}\,\frac{T_e^{3/2}}{n} \quad \text{and} \quad t_{ii} \approx \frac{1}{\nu_{ii}} \approx 3 \times 10^6\,\frac{\varepsilon_i^{3/2}}{n}\,,$$

respectively. At electron temperatures of several electron-volts and NA ion temperatures $\varepsilon_i \approx 3 \times 10^2 - 10^3$ eV, these times exceed that required for the plasma jet to flow through the processing system, $t_0 \approx L/V_s$.

Notice that an accurate analysis of the cooling process requires taking into account the fact that the inhomogeneity of the basic magnetic field causes the transverse energy received from the HF field to partially turn into longitudinal energy, and that part of the trajectories of heated NA ions goes beyond the stream of cold SNF plasma. These effects make the cooling deteriorate.

The main energy losses of NA ions are due to so-called distant Coulomb collisions. The rarer 'close' collisions occurring at small values of the impact parameter result in a significant energy transfer in a single collision event. No more than one thousandth of the NF may fall into the NA; consequently, the relative fraction of NF in the released NA cannot exceed 10^{-2}. The latter quantity sets an upper bound on the probability of close collisions during the flight time of an NA ion, $w \approx (L/V_s)(\nu_{ii}/\lambda_C)$, where λ_C is the Coulomb logarithm. The condition $w \leqslant 10^{-2}$ is satisfied at the system parameters indicated above. Naturally, factors weakening the influence of Coulomb collisions (enhancement of the NA ion longitudinal velocity in an inhomogeneous magnetic field, and ion trajectories going beyond the cold SNF plasma flow) also reduce the value of w.

Repeated ionization of NF ions also affects SNF processing negatively. Indeed, to satisfy magnetization condition (1.4) as Z_f increases, it is necessary either to strengthen the magnetic field $B \propto Z_f^3$ for a given density or to reduce the plasma density $n \propto Z_f^{-3}$ in a fixed magnetic field. (The ion temperature will apparently be determined by conditions in the plasma source.) Since for successful separation it is necessary that the Larmor radius of NA ions, $\rho_i \propto \varepsilon_\perp^{1/2} B^{-1} Z_a^{-1}$, be at least within an order of magnitude of the radius of the plasma stream, the energy up to which the NA ions are to be heated, $\varepsilon \propto Z_f^6 Z_a^2$ (where Z_a is the NA ion charge), will undergo a sharp rise.

Calculations show that whereas at $Z = 1$ the SNF separation requires ion heating to an energy on the order of $10^2 - 10^3$ eV (see Refs [24, 28]), in a plasma with doubly charged ions the energy will rise to unacceptably high values of $10^4 - 10^5$ eV. Application of the other possibility (decreasing the plasma density) will noticeably reduce the throughput of the processing system.

It must be noted that, even if plasma with singly charged NF ions enters the system, Z_f may increase significantly as the plasma flows through the processing system. An accurate calculation of Z_f apparently requires taking into account that the influence of inelastic collisions may lead to appearing the far 'tail' of the distribution, responsible for repeated ionization, becoming non-Maxwellian. The cross section of inelastic electron collisions with singly charged ions rises sharply as the atomic number of the chemical element increases. According to Ref. [30], the effective oscillator strength determining this quantity reaches values on the order of 10^3 for uranium. To an order of magnitude, the inelastic collision cross section should be greater than the Bohr radius by a similar factor (see, for example, Ref. [31]). The results of experiments [22] on the ICR separation of calcium and ytterbium ions testify in favor of the above reasoning. Plasmas of these elements may simulate uranium plasma, since their first and second ionization potentials ($U_1 = 6.1$ eV and $U_2 = 11.9$ eV in the case of calcium; $U_1 = 6.2$ eV and $U_2 = 12$ eV in the case of ytterbium) are close to the ionization potentials of uranium, $U_1 = 6.3$ eV and $U_2 = 11.2$ eV. In calcium, the fraction of doubly charged ions amounted only to $\xi = 0.02$ at $T_e = 2.1$ eV and $n \approx 1.6 \times 10^{11}$ cm^{-3}, while in the case of ytterbium the respective quantity amounted to $\xi = 0.003$ at $T_e = 0.6$ eV and $n \approx 1.5 \times 10^{12}$ cm^{-3}.

It cannot be excluded that in a plasma of heavy elements inelastic collisions determine not only the 'tail' of the velocity distribution function, but its main 'body' as well. It might be possible that in experiments [22] the electron temperature and, together with it, the fraction of doubly charged ions in ytterbium plasma precisely for this reason turned out to be much lower than in calcium plasma.

2. Excitation of high-frequency fields in a magnetized plasma

2.1 High-frequency electric field amplification effect

Development of the theory of ICR plasma heating proceeded mainly in applications to thermonuclear systems. The parameters of thermonuclear plasma are essentially different from those of plasma in SNF processing systems and in systems built around ICR isotope separation, which are close to them. In the two latter systems, the plasma density, the radius of the plasma column, and the magnetic field induction have smaller values. The difference manifests itself in the character of HF fields used in ICR heating.

At present, ICR heating of thermonuclear plasma is mainly performed following the small-admixture method through the excitation of magnetoacoustic oscillations (MAOs) (see, for example, Ref. [32]). At the first stages of thermonuclear studies, use was also made of the magnetic-beach method, for which it is necessary to excite Alfven oscillations (AOs) (see, for example, Ref. [33]). The ionic

component in a plasma significantly affects both AOs and MAOs. Anyhow, owing to the characteristic features of plasma indicated above, the condition $N_{\parallel}^2 \gg \varepsilon_{\perp}$ must be fulfilled in SNF processing systems, where $N_{\parallel}$ is the longitudinal component of the refractive index, and $\varepsilon_{\perp}$ is the dielectric plasma response to the transverse electric field (see, for example, Refs [32, 33]). This condition permits us to neglect the influence of ions on oscillations with $\omega \approx \omega_{\mathrm{i}}$. When this condition is fulfilled, the AOs and MAOs, characterized by a small longitudinal electric field component, transform into the so-called TE mode of vacuum waveguides, in which the electric field component parallel to the waveguide axis is zero. If the basic magnetic field is directed along the axis, then $E_{\parallel} = \mathbf{Eb} = 0$ in the TE mode, where $\mathbf{b}$ is the unit vector directed along the basic magnetic field.

In the second fundamental mode of vacuum waveguides (the TM mode), all three components of the electric field differ from zero, while the longitudinal component of the magnetic field vanishes.

Electron mobility along the magnetic field is extremely high. Therefore, even when the plasma density is relatively low, characteristic of SNF processing systems, electrons in the surface layer of the plasma jet have time, by redistributing along the magnetic field, to suppress the longitudinal electric field of the TM mode during a sole oscillation period. As a result, the inner plasma layers are screened from this waveguide mode.

It should be noted that electrons screen the TM mode if their temperature is not too low ($\omega \leqslant k_{\parallel} v_{T_{\mathrm{e}}}$). As a rule, this condition is satisfied. In the case of cold electrons ($\omega \gg k_{\parallel} v_{T_{\mathrm{e}}}$), the amplitude of the electric field in the plasma column can increase significantly due to transformation of the TM mode into eigenoscillations of the plasma column in the magnetic field — the Trivelpiece–Gold mode.

In typical plasma systems, the ion cyclotron frequency is much smaller than the plasma frequencies. Low-frequency electrostatic fields created by external sources are well screened by plasma; therefore, ICR heating is usually performed with the aid of induced fields excited by current antennas made of conductors situated near the plasma. Owing to the low frequency of electromagnetic oscillations, the vacuum wavelength is significantly superior to the dimensions of the system. Such oscillations are closely related to the antennas that excite them, so the analysis of HF antennas is a necessary part of the theory of ICR heating.

Figure 4 schematically shows a helical current antenna used in an ICR isotope separation system. In this antenna, helical current conductors complete half a turn around the plasma column. Such an antenna is called a half-turn or half-wave antenna. There are also helical antennas (single-wave, double-wave) in which conductors revolve about a larger angle (see Section 2.3).

Current antennas simultaneously excite both TM and TE modes. Both modes, when examined separately, involve relatively strong potential electric fields created by charges appearing on the conducting walls of the vacuum chamber. If HF fields are excited by a current antenna, the TE and TM modes should exhibit such phases whereat the potential components of electric fields are mutually suppressed. As a result, only a relatively weak induced electric field remains. Screening of the TM mode by the plasma 'liberates' fields of the TE mode. Here, the role of electric charges on the walls of the vacuum chamber is assumed by charges in the plasma

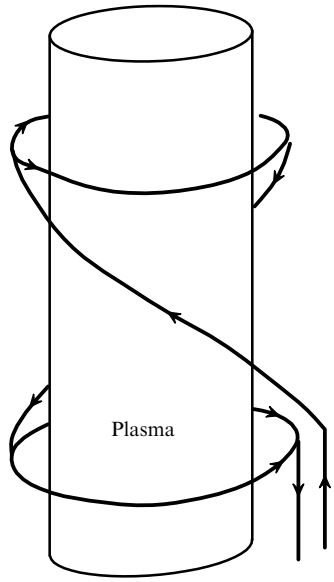

Figure 4. Schematic of a helical half-wave antenna.

surface layer, by which the plasma is screened from the TM mode. These arguments permit calculating in a relatively simple manner the electric field excited by the helical current antennas in the plasma column in a longitudinal magnetic field (see Section 2.2). The idea of utilizing an HF antenna to excite two modes differing in radial wavelengths, one of which (the short-wave mode) is screened by the plasma, was proposed in Ref. [34].

Let us estimate the amplification coefficient of the transverse electric field. Owing to the low frequency, $\omega \ll c/L_{\mathrm{A}}$ (where L_{A} is the antenna length along the basic magnetic field), the magnetic field of current antennas is quasistatic and at the center of the plasma column its induction can be estimated as

$$B_1 \approx \frac{I}{c r_{\mathrm{A}}}\,,$$

where I is the current traversing the antenna, and r_{A} is the antenna radius.

With the aid of the induction equation, we find

$$E \approx \frac{\omega r_{\mathrm{A}}}{c} B_1 \approx \frac{\omega}{c^2} I\,. \tag{2.1}$$

The induced electric field of a separate straight conductor is parallel to it, and since helical conductors are inclined to the magnetic field at an angle of $\approx r_{\mathrm{A}}/L_{\mathrm{A}}$ (usually $r_{\mathrm{A}} \ll L_{\mathrm{A}}$), the transverse component of the electric field has the form

$$E_{\perp} \approx \frac{\omega}{c^2} \frac{r_{\mathrm{A}}}{L_{\mathrm{A}}} I\,. \tag{2.2}$$

A vortex electric field is created by conductors separated azimuthally from each other by an angle $\theta = \pi$, and in which currents are directed oppositely (see Fig. 4). Therefore, the potential field of electrons screening the longitudinal component of the vortex field can be characterized by the wave numbers $k_{\parallel} \approx L_{\mathrm{A}}^{-1}$, $k_{\perp} \approx r_{\mathrm{A}}^{-1}$. Consequently, screening of the longitudinal vortex field (2.1) inevitably gives rise to the transverse electric field

$$E_{\perp} \approx \frac{\omega}{c^2} \frac{L_{\mathrm{A}}}{r_{\mathrm{A}}} I\,.$$

This field exceeds the transverse field (2.2) of a helical antenna in a vacuum by a factor of $K \approx (L_A/r_A)^2$.

The electric field amplification effect by plasma has already been indicated in the first publications concerning ICR isotope separation. The interpretation presented here of this effect, proposed in Refs [35–37], permits the construction of a relatively simple analytical model of the HF field excited by a helical antenna.

2.2 Simplified calculation of high-frequency fields

We shall briefly expound the main points of the model developed in Refs [35–37]. Applying the Maxwell equations, as well as the Poisson equation and the condition of a magnetic field without divergence, we find the excitation of electromagnetic fields in a vacuum to be described by the equations

$$\hat{L}\mathbf{B} = -\frac{4\pi}{\omega}\nabla \times \mathbf{j}_{ex}\,, \qquad \hat{L}\mathbf{E} = \frac{4\pi}{\omega}(c\nabla q_{ex} - \mathrm{i}\,\mathbf{j}_{ex})\,, \tag{2.3}$$

where $\hat{L} = \Delta_\perp - N_\parallel^2 + 1$, $N_\parallel = k_\parallel c/\omega$, we use the dimensionless coordinates $\mathbf{r} \to \mathbf{r}\omega/c$, and $\mathbf{j}_{ex}$ and q_{ex} are the external current and charge, respectively. We consider a system with cylindrical symmetry and a magnetic field directed along the axis of symmetry. The space–time structure of electromagnetic fields is assumed to be of the form $\propto \exp(-\mathrm{i}\omega t + \mathrm{i}m\theta + \mathrm{i}N_\parallel z)\,F(r)$.

The spatial structure of the TE and TM modes can be determined with the aid of the respective longitudinal components of the first and second equations of system (2.3).

With the use of the Maxwell equations, the transverse components of the electric field can be expressed via $B_\parallel$ and $E_\parallel$:

$$\mathbf{E}_\perp = \frac{\mathrm{i}}{1 - N_\parallel^2}(\nabla \times \mathbf{b}B_\parallel + N_\parallel \nabla_\perp E_\parallel)\,, \tag{2.4}$$

where $\mathbf{b}$ is the unit vector directed along the basic magnetic field.

ICR heating is caused by the interaction of ions with the electric field component, which is orthogonal to the basic magnetic field and rotates in the same direction as ions in the Larmor circle (left-polarized field):

$$E_+ = \frac{1}{\sqrt{2}}(E_r + \mathrm{i}E_\theta) = \frac{1}{\sqrt{2}\,(1 - N_\parallel^2)}\left(\frac{\mathrm{d}}{\mathrm{d}r} - \frac{m}{r}\right)(B_\parallel + \mathrm{i}N_\parallel E_\parallel)\,. \tag{2.5}$$

In the case of low-frequency electromagnetic fields excited by an antenna which is stretched out along the magnetic field ($r_A \ll L_A \ll 1$), the radial dependences of $B_\parallel$, $E_\parallel$ have the form $\propto r^{|m|}(1 + O(r^2/L^2))$. From expression (2.5) it follows that wave modes with $m < 0$, running azimuthally in the ion (left) direction, exhibit essentially higher amplitudes of the left-polarized electric field than those of modes running in the opposite direction. This is quite natural, since in the low-frequency, quasistatic, approximation the electric field is potential (see Section 2.1); therefore, its polarization is determined by the spatial dependence of the oscillations considered. The main contribution to ICR heating is due to the mode with the azimuthal wave number $m = -1$. Only this mode has a transverse left-polarized electric field differing from zero on the axis of the system, where the plasma density reaches its maximum.

Let us suppose that a helical current $\mathbf{j}_{ex} = (0, J_\theta, J_\parallel) \times (\omega/c)\,\delta(r - r_A)$ flows across the surface $r = r_A$ and that on the same surface there are electric charges

$$q_{ex} = Q\,\frac{\omega}{c}\,\delta(r - r_A)\,.$$

Assume also that the system examined is confined by a perfectly conducting cylinder of radius $r_B > r_A$. The solutions of equations (2.3) are expressed via modified Bessel functions of the argument $x = r(N_\parallel^2 - 1)^{1/2}$ (see below). Within the region inside the antenna cylinder ($r < r_A$), under the condition of $x \ll 1$ for the mode $m = -1$, making use of Ref. [38] (see also Section 2.3), it is not difficult to obtain

$$B_\parallel + \mathrm{i}N_\parallel E_\parallel \approx x\,\frac{2\pi}{c}\left\{\left[1 - \left(\frac{x_A}{x_B}\right)^2\right]\left(\frac{1}{x_A}\,J_\theta - J_\parallel + cN_\parallel Q\right) + x_A\left[\frac{1}{4}\left(1 - \left(\frac{x_A}{x_B}\right)^2\right) + \ln\frac{x_A}{x_B}\right]J_\theta\right\}, \tag{2.6}$$

where $x_{A,B} = r_{A,B}(N_\parallel^2 - 1)^{1/2}$.

From Eqn (2.3) it follows that a helical current antenna ($J_\theta \neq 0$, $J_\parallel \neq 0$, $Q = 0$) excites both the TE and TM modes. Here, owing to the current continuity condition

$$\frac{m}{r_A}\,J_\theta + N_\parallel J_\parallel = 0\,, \tag{2.7}$$

the following relationship is fulfilled for the largest terms of the field E_+ expansion in the power series of small parameter $x_{A,B} \ll 1$: $B_\parallel + \mathrm{i}N_\parallel E_\parallel = 0$ [see Eqn (2.6)]. In accordance with formula (2.5), this means that the main components of the left-polarized electric field of the TE and TM modes are mutually suppressed and the field of each of the modes turns out to be $(r_A N_\parallel)^{-2} \gg 1$ times larger than the total field E_+ of a helical antenna in a vacuum. With the aid of equation (2.4), it is not difficult to show that the same is also valid for individual components E_r, E_θ of the transverse electric field.

However, the potential components of the TE and TM modes only 'annihilate' in a vacuum. The planned SNF processing systems and the systems for ICR isotope separation must operate in conditions where the plasma significantly weakens the longitudinal electric field, which is due to the interaction with electrons, while the response of the plasma to the transverse field is insignificant. For this purpose, the following conditions must be fulfilled: $|\varepsilon_\parallel| \gg 1$, $|\varepsilon_\perp| \ll N_\parallel^2$, where $\varepsilon_\parallel$ and $\varepsilon_\perp$ are the components of the plasma permittivity, which are determined by the motion of electrons and ions, respectively. In this case, the TM mode, in which $E_\parallel \neq 0$, is screened by the plasma in the narrow boundary layer of the plasma column without reaching its center. As a result, only the TE mode, which is hardly affected by the plasma, is present in the central region.

HF electromagnetic fields in this region are independent of how the TM mode was eliminated — via screening by the plasma or by the choice of such a value of q_{ex} for which the right-hand part of the second equation in system (2.3) turns to zero:

$$j_{\parallel,ex} = cN_\parallel q_{ex}\,. \tag{2.8}$$

For the surface densities of the longitudinal current and charge, from the last formula we obtain

$$J_{\parallel} = cN_{\parallel}Q\,. \tag{2.9}$$

Owing to current continuity condition (2.7) and relation (2.9), the following three quantities turn out to be equal in magnitude to each other: $-(m/x_{\mathrm{A}})J_{\theta}, J_{\parallel}, cN_{\parallel}Q$. Therefore, in the presence of plasma screening the TM mode, the resulting transverse electric field can, with equal success, be considered either as the field of the screening charge [in the right-hand side of expression (2.6), the $cN_{\parallel}Q$ term in round brackets remains intact] or as the TE mode field [it is $(1/x_{\mathrm{A}})J_{\theta}$ that remains].

The first interpretation permits us to propose a rather simple method for calculating the transverse HF field. In the simplest version, a helical current antenna consists of two conductors entwining the plasma column at opposite ends of one diameter. These conductors carry currents flowing in opposite directions:

$$j_{\parallel,\mathrm{ex}} = \left[\delta\left(\theta - \frac{\pi}{2} - A\pi\,\frac{z}{L_{\mathrm{A}}}\right) - \delta\left(\theta + \frac{\pi}{2} - A\pi\,\frac{z}{L_{\mathrm{A}}}\right)\right] \times \cos(\omega t)\,\frac{1}{r_{\mathrm{A}}}\left(\frac{\omega}{c}\right)^2 \delta(r - r_{\mathrm{A}})\,I\,, \qquad |z| < L_{\mathrm{A}}\,, \tag{2.10}$$

where A is the number of turns of the antenna conductors around the plasma column.

In the vicinity of the axis, the left-polarized component of the electric field of interest to us is created only by the azimuthal current harmonic of number $m = -1$:

$$j'_{\parallel,\mathrm{ex}} = \sin\left(\theta + \omega t - A\pi\,\frac{z}{L_{\mathrm{A}}}\right)\frac{1}{\pi r_{\mathrm{A}}}\left(\frac{\omega}{c}\right)^2 \delta(r - r_{\mathrm{A}})\,I\,. \tag{2.11}$$

In the adopted model, the external charge q_{ex} imitates charges arising in the boundary plasma layer upon screening of the TM mode. In such an exchange, it is necessary to conserve the characteristic features of the screening process. If there is no electron emission from the end plates, the total number of electrons per force line of the magnetic field is conserved. Taking this condition into account, the continuity equation for q'_{ex} and the differential relation, equivalent to Eqn (2.8), namely

$$j_{\parallel,\mathrm{ex}} = -\mathrm{i}\,\frac{c^2}{\omega}\,\frac{\partial q_{\mathrm{ex}}}{\partial z}\,, \tag{2.12}$$

we obtain

$$q'_{\mathrm{ex}} = Q'\,\delta(r - r_{\mathrm{A}})\,, \tag{2.13}$$

where

$$Q' = f(\theta, t, z)\,\frac{1}{A\pi^2}\,\frac{L_{\mathrm{A}}}{r_{\mathrm{A}}}\,\frac{\omega}{c^2}\,I\,,$$

$$f(\theta, t, z) = \sin(\theta + \omega t)\,f_{\mathrm{even}}(z) - \cos(\theta + \omega t)\,f_{\mathrm{odd}}(z)\,,$$

$$f_{\mathrm{even}} = \begin{cases} \cos\left(\alpha\,\dfrac{z}{L_{\mathrm{A}}}\right) - \cos\alpha + \dfrac{L_{\mathrm{A}}}{L}\left(\cos\alpha - \dfrac{1}{\alpha}\,\sin\alpha\right), & |z| < L_{\mathrm{A}}\,, \\ \dfrac{L_{\mathrm{A}}}{L}\left(\cos\alpha - \dfrac{1}{\alpha}\,\sin\alpha\right), & |z| > L_{\mathrm{A}}\,, \end{cases}$$

$$f_{\mathrm{odd}} = \begin{cases} \sin\left(\alpha\,\dfrac{z}{L_{\mathrm{A}}}\right), & |z| < L_{\mathrm{A}}\,, \\ \sin\alpha\,\mathrm{sgn}\,z\,, & |z| > L_{\mathrm{A}}\,. \end{cases}$$

Here, L is half the total length of the system along the magnetic field ($L \geqslant L_{\mathrm{A}}$), and $\alpha = A\pi$.

For electromagnetic structures stretched out along the magnetic field ($r \ll L$), we find with the aid of the Poisson equation the following expression for the left-polarized field at the center of the plasma column:

$$E_{+}(t, \theta, z) = -2\sqrt{2}\,\pi Q'(t, \theta, z)\left[1 - \left(\frac{r_{\mathrm{A}}}{r_{\mathrm{B}}}\right)^2\right]. \tag{2.14}$$

The magnetic field in the SNF processing systems under consideration varies in the longitudinal direction. The radius of the bunch of force lines of the magnetic field, along which the plasma jet flows, and the radius of the surface close to the plasma boundary, on which the charges screening the TM mode are located, vary correspondingly. These variations can be taken into account changing the value of $r_{\mathrm{A}} \propto B^{-1/2}$ in the above-presented expression for the effective charge Q'.

The results of calculations by formula (2.14) for different antennas are presented in Fig. 5 by the dotted curves. Referring to the figure, the symmetric and antisymmetric (in the z-coordinate) parts of the electric field can be seen to be segments of sinusoids with equal amplitudes which are shifted by 1/4 of their wavelength. Their time shift also equals 1/4 of the period. Thus, the electric field component inhomogeneous in the z-coordinate represents a wave running along the z-axis. At the same time, the electric field has a homogeneous component that is involved in the symmetric part. This component corresponds to a standing wave.

The field magnitude of a half-wave antenna (Fig. 5a) increases towards its edges and remains at its maximum level right up to the system boundaries. Half-wave antennas were applied most often in experiments on ICR isotope separation. The electric field component symmetric in the z-coordinate and constant beyond the antenna (Fig. 5b, c) 'ensues' mainly from the single-wave (a single turn of the conductors about the plasma column) and two-wave (two turns) antennas. It can be suppressed by using a combination of single-wave and two-wave antennas, with the current in the latter being necessarily doubled (Fig. 6).

The conclusion concerning the absence of an HF field outside the combined antenna in the region $|z| > L_{\mathrm{A}}$ holds valid when the following two conditions are fulfilled: $r_{\mathrm{A}}/L_{\mathrm{A}} \to 0$ and $\delta L_{\mathrm{A}}/L_{\mathrm{A}} = \delta \to 0$, where δL_{A} is the transverse dimension of the helical conductors.

The finiteness of the ratio $r_{\mathrm{A}}/L_{\mathrm{A}}$ is related to the inductive TE-mode electric field $E_{\perp 1} \approx E_{\perp}(r_{\mathrm{A}}/L_{\mathrm{A}})^2$, which, unlike its potential component, is not localized within the confines of the single-wave and two-wave antennas [see formula (2.10) and below].

Owing to the second of the indicated conditions ($\delta \to 0$), the charge component antisymmetric in the z-coordinate and screening the TM mode is absent outside the single-wave and two-wave antennas. Indeed, only in the $\delta \to 0$ limit does any force line of the magnetic field at the radius $r = r_{\mathrm{A}}$ is crossed an even number of times by the conductors of these antennas [see formula (2.10)]. The total current in them is zero and, consequently, in accordance with Eqn (2.13) the density of the screening charge should assume one and the same value in the regions $z > L_{\mathrm{A}}$ and $z < -L_{\mathrm{A}}$. To make it equal to zero in

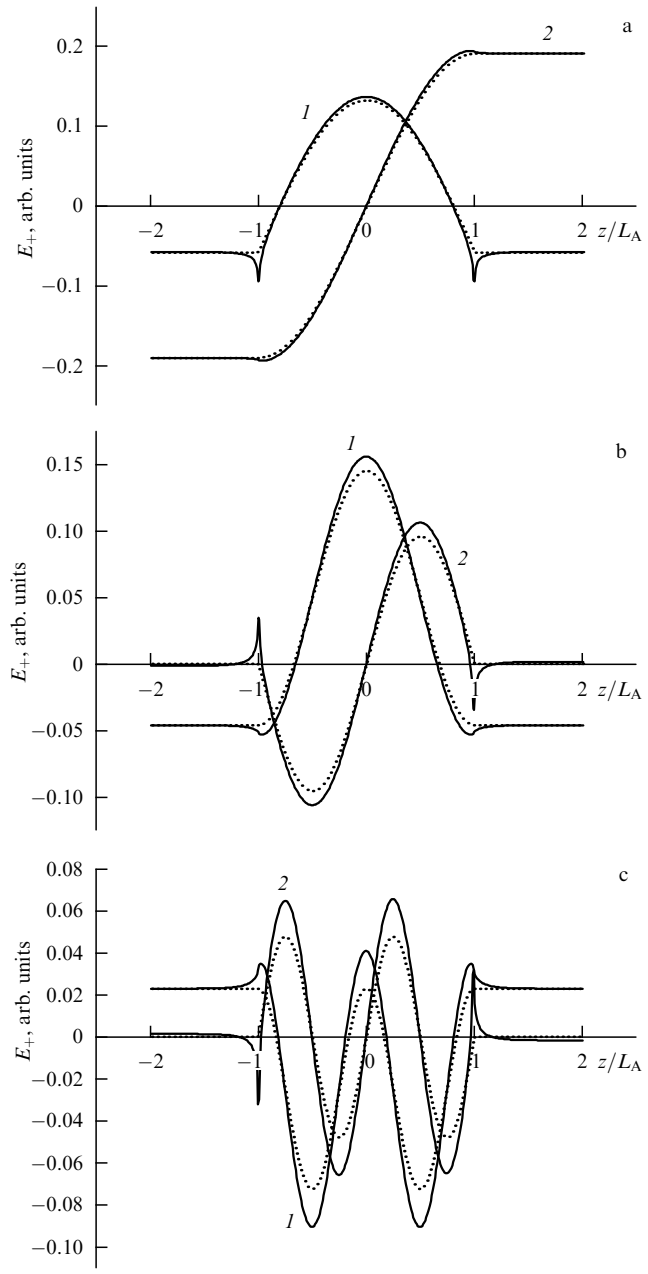

Figure 5. Dependence of the left-polarized electric field of different antennas on the z-coordinate: (a) half-wave antenna, (b) single-wave antenna, and (c) two-wave antenna. Curves *1* are attributed to the symmetric part, and *2* to the antisymmetric part. The solid curves correspond to the exact calculation of the TE-mode field in a vacuum (see Section 2.3), and the dotted curves correspond to calculations by the simplified model (2.14).

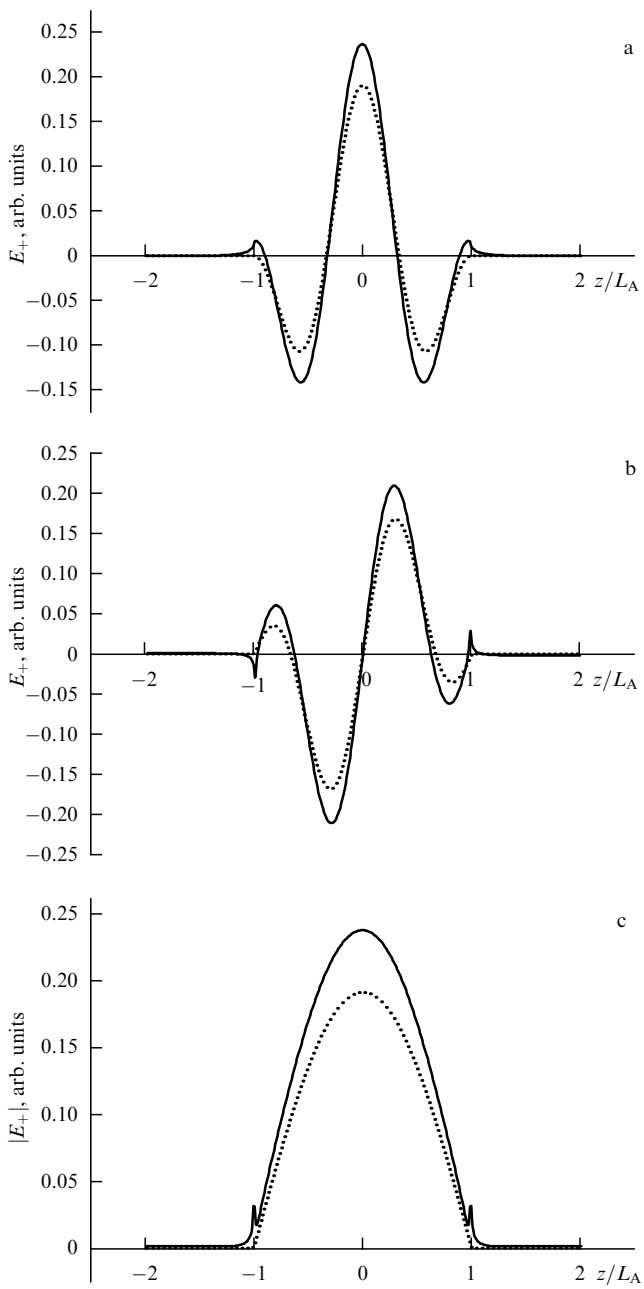

Figure 6. Dependence of the left-polarized electric field of a combined antenna on the z-coordinate: (a) symmetric part, (b) antisymmetric part, and (c) total field modulo. The solid curves correspond to the exact calculation of the TE-mode field in a vacuum (see Section 2.3), and the dotted curves correspond to calculations by the simplified model (2.14).

these regions, a combination of single-wave and two-wave coils (a combined antenna), together with a certain relationship between the currents in them, is necessary.

Figures 5 and 6 demonstrate that a combined antenna composed of single-wave and two-wave antennas actually permits localizing the HF field within its confines. Thus, the possibility is discarded of a parasitic cyclotron resonance, which, generally speaking, can be realized outside the ICR heating system — in the plasma source or on the curvilinear magnetic field segment used for extraction of heated target ions from the cold plasma stream. The magnetic field in these systems is inhomogeneous, which does not exclude the possibility of NF ion heating. If no such danger exists, the radius of curvature of the magnetic force lines along the curvilinear segment, together with the length of the segment itself, can be reduced. This circumstance facilitates fulfilment of the conditions necessary for successful SNF processing (see Section 1.5).

When the finiteness of the transverse dimension of the conductors is taken into account, the abridgement geometry of the helical currents on the flanks of the antenna becomes important. In this article, the model of an HF antenna constructed in Refs [35–37] is utilized. In this model (see, also, Section 2.3), the HF current lines entwine the plasma column through an angle $2\pi - \delta < \Delta\theta < 2\pi$ in a single-wave antenna, and through an angle $4\pi - \delta < \Delta\theta < 4\pi$ in the two-

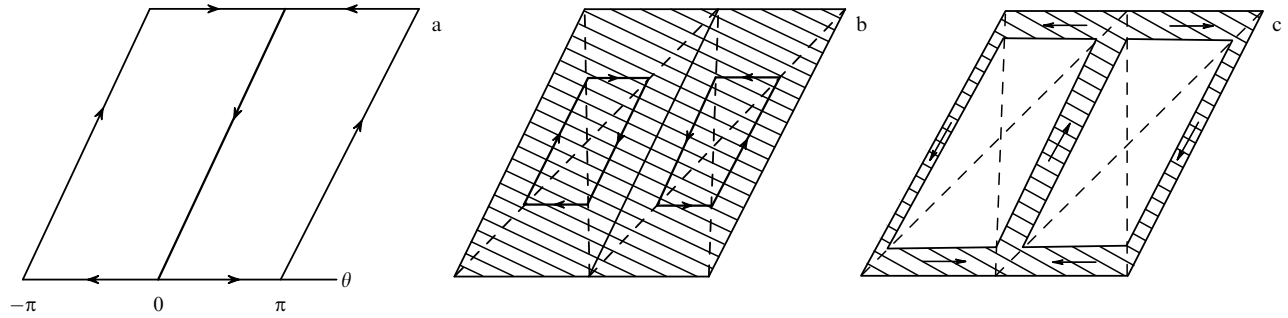

Figure 7. Model of a helical antenna. (a) Unfolding of a half-wave antenna into a plane; arrows indicate the instantaneous direction of the current flow. (b) Currents in the auxiliary element used in simulating the antenna. (c) Currents in the antenna model applied in calculations. The region across which the current flows is shaded.

wave case. Here, on a small part of the force lines, on the order of δ, the electric current turns out not to be compensated. This circumstance is related to the presence of a residual antisymmetric in the z-coordinate electric field $E_{\perp 2} \approx \delta E_{\perp}$ in the regions of $|z| > L_{\mathrm{A}}$.

2.3 Improved calculation of high-frequency fields. A high-frequency antenna model

Applicability of the simplified model of HF antennas for the description of HF electromagnetic fields in SNF processing systems relying on the ICR method is confirmed by the results of more precise calculations of the TE-mode electric field with the use of the longitudinal component of the first equation in system (2.3) [35, 37]. Results of such calculations are depicted by the solid curves in Figs 5 and 6.

In the calculations [35, 37], the restriction $x \ll 1$, on which the analysis performed in Section 2.2 is based, was lifted. For the quantities $B_{\|}$ and $E_{\|}$ entering into Eqn (2.5), use was made of expressions that are solutions of equations (2.3) at arbitrary values of $N_{\|}$:

$$B_{\|} = -\frac{x_{\mathrm{A}}}{I'_m(x_{\mathrm{B}})}\, \Phi''_{x_{\mathrm{A}},x_{\mathrm{B}}}(x_{\mathrm{A}}, x_{\mathrm{B}})\, I_m(x)\, \frac{4\pi}{c}\, J_{\theta}\,, \tag{2.15}$$

$$E_{\|} = \frac{\mathrm{i}}{\sqrt{N_{\|}^2 - 1}}\, \frac{x_{\mathrm{A}}}{I_m(x_{\mathrm{B}})}\, \Phi(x_{\mathrm{A}}, x_{\mathrm{B}})\, I_m(x)\, \frac{4\pi}{c}\, J_{\|}\,, \tag{2.16}$$

where $I_m(x)$, $K_m(x)$ are modified Bessel functions, and $\Phi(x_{\mathrm{A}}, x_{\mathrm{B}}) = I_m(x_{\mathrm{A}})\, K_m(x_{\mathrm{B}}) - I_m(x_{\mathrm{B}})\, K_m(x_{\mathrm{A}})$.

Taking HF fields with arbitrary values of $N_{\|}$ into account accurately also required the construction of the model of an HF antenna, reflecting peculiarities of the current distribution in real antennas. Such a model must satisfy the condition $\operatorname{div} \mathbf{j} = 0$. Violation of this condition is equivalent to the introduction of fictitious electric charges to which potential electric fields are related. Such fields can be $[c/(\omega r_{\mathrm{A}})]^2$ times stronger than the quite weak induced fields actually excited by current antennas [see relationship (2.1)].

To clarify the model of an HF antenna used in Refs [35, 37], we shall unfold the current distribution presented in Fig. 4 into the plane, as shown in Fig. 7a. In this figure, the extreme left conductor is to be identified with the extreme right one, and the axis of the system is vertical. This current distribution can be obtained as the sum of two distributions, one of which can be represented as two parallelograms in which the direction of a closed current flow alters on the diagonals (Fig. 7b). In the second distribution, the size of each of the parallelograms is reduced by the similarity factor $1 - \delta$, while the direction of the current flow is changed to the opposite one. The resultant sum of these current distributions is given in Fig. 7c.

The quantities J_{θ} and $J_{\|}$ in relationships (2.15), (2.16) are coefficients of the Fourier expansion in the longitudinal coordinate. The basis functions over which the expansion is performed depend on the boundary conditions. In the absence of electron emission from the end plates ($j_{\|}(\pm L) = 0$), the boundaries are to be considered impenetrable and, in accordance with expressions (2.12)–(2.14), the derivatives of the tangential components of the electric field $E_r(z)$, $E_{\theta}(z)$ should turn to zero on the surface of the end plates. Whence follows that it is expedient to expand the even parts of both the external charge and the transverse electric field in a set of functions $\cos(p(\pi/L)z)$, and the odd parts in a set of functions $\sin[(p - 1/2)\pi z/L]$, where p is an integer number, and $1 \leqslant p < \infty$. The expansion coefficients for a helical current antenna were obtained in Refs [35, 37]:

$$J_{\theta;p}^{(s,a)} = J_{\theta;p}^{(s,a)}(L')\Big|_{L'=L_{\mathrm{A}}} - J_{\theta;p}^{(s,a)}(L')\Big|_{L'=L_{\mathrm{A}}(1-\delta)}\,,$$

where

$$\begin{aligned} J_{\theta;p}^{(s)}(L') = \frac{2I}{\pi L}\,\frac{\omega}{c}\Bigg\{ & (2A+1) \\ & \times \left[\frac{\sin\left[(A_+ + p\pi/L)L'\right]}{A_+ + p\pi/L} + \frac{\sin\left[(A_+ - p\pi/L)L'\right]}{A_+ - p\pi/L}\right] \\ & + (2A-1)\left[\frac{\sin\left[(A_- + p\pi/L)L'\right]}{A_- + p\pi/L} + \frac{\sin\left[(A_- - p\pi/L)L'\right]}{A_- - p\pi/L}\right] \\ & - 4A\cos\left(\frac{\pi}{2}\,\frac{L'}{L_{\mathrm{A}}}\right)\left[\frac{\sin\left[(A_0 + p\pi/L_1)L'\right]}{A_0 + p\pi/L}\right. \\ & \left. + \frac{\sin\left[(A_0 - p\pi/L_1)L'\right]}{A_0 - p\pi/L}\right]\Bigg\}\,, \end{aligned}$$

$$\begin{aligned} J_{\theta;p}^{(a)}(L') = \frac{2I}{\pi L}\,\frac{\omega}{c}\Bigg\{ & (2A+1)\left[\frac{\sin\left[(A_+ - (p-1/2)\pi/L)L'\right]}{A_+ - (p-1/2)\pi/L}\right. \\ & \left. - \frac{\sin\left[(A_+ + (p-1/2)\pi/L)L'\right]}{A_+ + (p-1/2)\pi/L}\right] \\ & + (2A-1)\left[\frac{\sin\left[(A_- - (p-1/2)\pi/L)L'\right]}{A_- - (p-1/2)\pi/L}\right. \end{aligned}$$

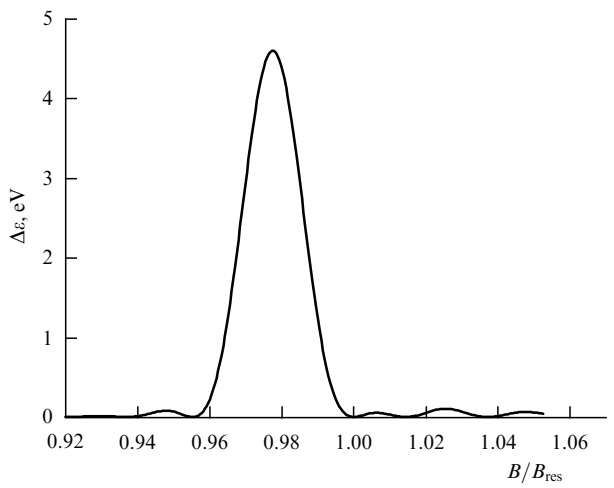

Figure 8. Ion energy increment in ICR interaction in a homogeneous magnetic field, depending on the field intensity. Calculation parameters are as follows: $B_{\text{res}} = 1.75$ kG, ion mass number $A = 100$, current in the single-wave antenna 25 A, $L_{\text{A}} = 1.5$ m, and $r_{\text{A}} = 0.3$ m. The ions were considered to enter the heating system with an ion-acoustic velocity corresponding to $T = 2$ eV, and a transverse energy equal to zero.

$$
\left. - \frac{\sin\left[(A_- + (p - 1/2)\pi/L)L'\right]}{A_- + (p - 1/2)\pi/L} \right]
$$

$$
- 4A\cos\left(\frac{\pi}{2}\frac{L'}{L_{\text{A}}}\right)\left[\frac{\sin\left[(A_0 - (p - 1/2)\pi/L)L'\right]}{A_0 - (p - 1/2)\pi/L}\right.
$$

$$
\left.\left. - \frac{\sin\left[(A_0 + (p - 1/2)\pi/L)L'\right]}{A_0 + (p - 1/2)\pi/L}\right]\right\},
$$

$A_0 = A\pi/L_{\text{A}}$, $A_\pm = A_0 \pm \pi/(2L_{\text{A}})$, and the relative width of the conductors was considered equal to $\delta = 10^{-2}$; it was also assumed that $r_{\text{A}} = L_{\text{A}}/10$, $r_{\text{B}} = 2r_{\text{A}}$, $L = 2L_{\text{A}}$, and $L_{\text{A}} = 10^{-3}$. We recall that all the lengths are normalized to c/ω; here, $N_\parallel = p\pi/L$ for the symmetric part of HF fields, and $N_\parallel = (p - 1/2)\pi/L$ for the antisymmetric part.

HF fields generated by a helical current antenna are characterized by a property that might appear at first sight to be paradoxical. Under conditions that seem most favorable for the realization of ICR interaction (a homogeneous magnetic field, and the HF field frequency equal to the ion cyclotron frequency), ions are actually 'excluded from the resonance' (Fig. 8). The point is that, in accordance with resonance condition (1.2), the HF field at $\omega = \omega_{\text{i}}$ should be homogeneous in the longitudinal direction ($k_\parallel = 0$). Meanwhile, in the case of a bifilar supply of electric current, used in helical antennas, the current can be considered to become closed within the confines of the antenna. Consequently, the values of its components averaged over the z-coordinate are equal to zero. Owing to the linearity of equations (2.3) for HF fields, the components of HF fields constant in the z-coordinate must also turn to zero together with the average current. In the described simplified model of a helical antenna, the indicated general property manifests itself as a consequence of the electron charge conservation in each of the force lines. Under this condition, it follows from equation (2.14) that the electric field averaged over the z-coordinate vanishes.

Owing to the noted regularity, the frequency at which the HF field excited by a helical current antenna interacts most effectively with ions is no longer determined by the resonance condition $\omega = \omega_{\text{i}}$, but is displaced by the value of the Doppler shift [see formula (1.2)]. In expression (1.2), one must set $k_\parallel \approx \pi p/L_{\text{A}}$, where p is the number of turns of the helical conductors within the antenna confines (the number of 'waves' that can be along the whole length of the antenna).

It must, however, be noted that even if the current rings at the antenna flanks are connected by straight ($p = 0$), instead of helical, conductors, the HF field of this antenna must also interact resonantly with the ions. In such a geometry of the conductors, the longitudinal inhomogeneity of the HF field. leading to the presence of components with $k_\parallel \neq 0$ in the HF field spectrum, is due to the antenna boundedness in the longitudinal direction ($k_\parallel \approx 1/L_{\text{A}}$). If the HF field 'flows out' of the antenna along the basic magnetic field, its action on the ion flow is restricted by the dimension L ($k_\parallel \approx 1/L$) of the whole system. These factors determine the effective width of the HF monochromatic field acting on the ions: $\delta\omega \approx v_\parallel/L_{\text{A}}$ (Doppler broadening) or $\delta\omega \approx v_\parallel/L$ (time-of-flight broadening).

The above-indicated effects are especially important in the case of a homogeneous magnetic field which is usually exploited in ICR isotope separation. In SNF processing systems, the inhomogeneity factor of the magnetic field, in the main determining the character of ICR interaction (see Section 3), is much more essential.

3. Ion-cyclotron resonance interaction in spent nuclear fuel processing systems

3.1 Effects imposing restrictions on the ion-cyclotron resonance interaction intensity

The ion-cyclotron resonance phenomenon permits, with the aid of the HF electromagnetic field, increasing the energy of the Larmor rotation of charged particles. Cyclotron heating is particularly effective if the HF field possesses a left-polarized component. Under the action of a left-polarized field in a reference system rotating together with the ion, the ion velocity vector is stretched out along the HF electric field:

$$
\mathbf{v}_\perp = \mathbf{v}_{\perp 0} + \frac{e}{m_{\text{i}}}\,\mathbf{E}_+ t\,.
$$

Whatever the initial ion velocity vector, after a sufficiently long time its direction becomes close to that of the left-polarized electric field, and the ion energy will vary according to the law

$$
\varepsilon_\perp \approx \frac{(eE_+ t)^2}{2m_{\text{i}}}\,.
$$

The energy spread for an ensemble of ions distributed isotropically over the initial velocity is given by the approximate expression

$$
\delta\varepsilon_\perp \approx 4(\varepsilon_{\perp 0}\varepsilon_\perp)^{1/2}\,, \tag{3.1}
$$

where $\varepsilon_{\perp 0}$ is the average initial energy of Larmor rotation.

The stationary magnetic field in the SNF processing systems we are interested in varies in the longitudinal direction (along the z-coordinate) — it weakens along the course of the plasma flow. Ions moving in such a field receive an energy increment from the HF field when passing through the zone z_{s} ($\omega = \omega_{\text{i}}(z_{\text{s}})$) of ion-cyclotron resonance. The duration of resonance interaction is determined by the condition of misphasing between the Larmor rotation of an

ion and the HF field, i.e., the time required for the phase difference

$$\Phi(t) = \int^t \omega_{\rm i}\big(z(t)\big)\,{\rm d}t - \omega t \tag{3.2}$$

to become approximately π.

In a magnetic field varying according to a linear law, namely

$$\omega_i(z) = \omega\left(1 - \frac{z - z_{\rm s}}{L_B}\right), \tag{3.3}$$

the duration of resonance interaction is expressed as

$$\Delta t_{\rm s} = \left(\frac{2\pi L_B}{\omega v_\parallel}\right)^{1/2}.$$

The energy increment received by an ion during the time period $\Delta t_{\rm s}$ is (see, e.g., book [39])

$$\Delta\varepsilon_\perp = \pi\,\frac{e^2 E_+^2 L_B}{m_{\rm i}\omega_{\rm i} v_\parallel}. \tag{3.4}$$

Expression (3.4) is exact if the quantities ${\rm d}B/{\rm d}z$ and $v_\parallel$ are constant. Owing to the small size of the resonance zone, the first condition is usually fulfilled with a good precision. At the same time, there are a number of factors causing a change in $v_\parallel$.

One of the effects leading to a change in the ion longitudinal velocity is due to the action of the diamagnetic force $\mathbf{F} = -\mu\nabla B$ that pushes ions out toward the lower magnetic field ($\mu = \varepsilon_\perp/B$). ICR interaction increases the energy of Larmor rotation and at the same time the diamagnetic force. If the HF field is sufficiently high, the diamagnetic force will lead to a significant increase in the ion longitudinal velocity. As a result, the duration of the resonance interaction will be reduced and, consequently, the ion energy increment will be reduced. This effect manifests itself in the case of resonance ion-cyclotron interaction of both ions and electrons in an inhomogeneous magnetic field. It was revealed precisely by the example of the latter [40].

Let us clarify under what conditions this effect becomes significant. For this purpose we will perform triple differentiation of the expression (3.2) for the phase. With account of the relationships $\dot z = v_\parallel$, $\dot v_\parallel = -(\mu/m_{\rm i})(\partial B/\partial z)$ and formula (3.3), we obtain

$$\dddot\Phi \approx -\frac{\omega}{2}\left(\frac{eE_+ t}{m_{\rm i} L_B}\right)^2.$$

Using the last expression, we find that the phase incursion becomes equal to π in a time

$$\Delta t_{\rm s1} \approx \left(\frac{5!\pi}{\omega}\right)^{1/5}\left(\frac{m_{\rm i} L_B}{eE_+}\right)^{2/5}.$$

If the electric field is sufficiently strong, namely

$$\frac{E_+}{B_0} \geqslant \frac{(5!)^{1/2}}{2^{5/4}\pi^{3/4}}\,\frac{v_\parallel}{c}\left(\frac{\rho_{\rm i\parallel}}{L_B}\right)^{1/4},$$

then the condition $\Delta t_{\rm s1} < \Delta t_{\rm s}$ will be fulfilled and, consequently, the HF field itself will govern the duration of the resonant interaction. In this case, the energy increment in the passage through the resonance vicinity will assume the form

$$\Delta\varepsilon_\perp \approx \frac{(5!\pi)^{2/5}}{2}\,m_{\rm i} c^2\left(\frac{L_B\omega}{c}\right)^{4/5}\left(\frac{E_+}{B_0}\right)^{6/5}. \tag{3.5}$$

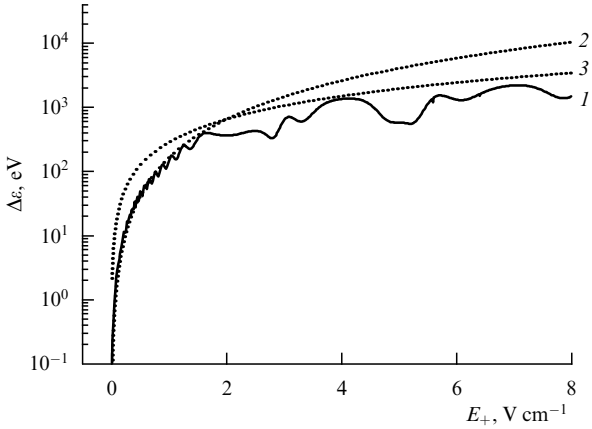

Figure 9. Dependence of ion energy increment resulting from ICR interaction with a homogeneous HF field: curve *1* — solution of equations of motion, *2* — dependence (3.4), and *3* — dependence (3.5). Calculation parameters are as follows: ion mass number $A = 100$, $E_+ = 1$ V cm^{-1}, and $\omega = \omega_{\rm i}(0)$. The ions were considered to enter the heating system with an ion-acoustic velocity corresponding to $T = 2$ eV and the transverse energy equal to zero. The magnetic field was given in the form (1.1) with $B_0(0) = 1.75$ kG, $\beta = 0.3$, and $L_{B0} = 0.75$ m.

The above-described properties of ICR interaction in an inhomogeneous magnetic field are illustrated in Fig. 9.

An ion of mass number $A = 100$ was supposed to be introduced into the ICR heating system with an ion-sound velocity corresponding to the temperature $T = 2$ eV and zero transverse energy. The dependence of the basic magnetic field on the longitudinal coordinate was taken in the form (1.1) for $\beta = 0.3$, $B_0(0) = 1.75$ kG, and $L_{B0} = 0.75$ m. The HF electric field was considered to be independent of the longitudinal coordinate.

From Fig. 9 it is seen that, in the case of weak electric fields, the dependence $\Delta\varepsilon_\perp(E_+)$ corresponds to formula (3.4). However, as the HF field enhances, the rise in $\Delta\varepsilon_\perp$ slows down and the dependence $\Delta\varepsilon_\perp(E_+)$ becomes closer to Eqn (3.5). The oscillations noticeable in Fig. 9 are, apparently, related to the circumstance that, even when leaving the resonance vicinity, the ion continues to interact with the HF field — its energy oscillates with the frequency $\omega - \omega_{\rm i}$. The phase of oscillations with which the ion approaches the boundary of the calculation region depends on the ion longitudinal velocity, which in turn depends on the transverse energy, since in a magnetic field falling along the course of the plasma flow the ion transverse energy transforms into longitudinal energy.

One more effect causing a change in the ion longitudinal velocity in the course of ICR interaction is due to emerging the HF field inhomogeneity in the longitudinal direction. In this case, in accordance with the induction equation

$$\frac{\partial\mathbf{B}}{\partial t} = -c\nabla\times\mathbf{E},$$

the HF magnetic field is related to the left-polarized electric field, and the former is also left-polarized. The following relation holds true for the Fourier components of these fields

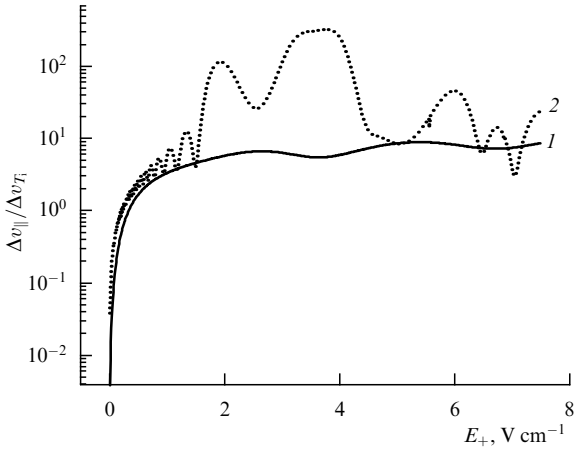

Figure 10. Dependence of ion longitudinal velocity increment due to ICR interaction with the HF field in the form of a wave running along the basic magnetic field: curve *1* — solution of equations of motion, and *2* — dependence with account of Eqns (3.6), (3.7). The wavelength is 1.5 m, the HF field amplitude is 1 V cm^{-1}, and the remaining parameters are the same as in Fig. 9.

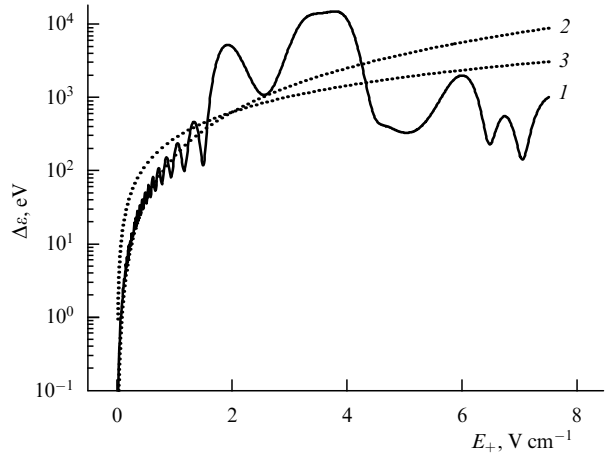

Figure 11. Dependence of ion energy increment due to ICR interaction with the HF field in the form of a wave running along the basic magnetic field: curve *1* — solution of equations of motion, *2* — dependence (3.4), and *3* — dependence (3.5). The calculation parameters are the same as in Fig. 10.

with a longitudinal wave number $k_\parallel$ and frequency ω:

$$\mathbf{B} = N_\parallel \mathbf{b} \times \mathbf{E}\,,$$

where $N_\parallel = k_\parallel c/\omega$.

The magnetic field turns the ion velocity vector, converting the transverse velocity into longitudinal velocity:

$$m_\mathrm{i}\dot{\mathbf{v}}_\parallel = \frac{e}{c}(\mathbf{v} \times \mathbf{B})_\parallel\,.$$

We find from this equation the following approximate relationship for the longitudinal velocity increment in the ion passage through the resonance zone:

$$\Delta v_\parallel \approx \Delta v_\perp \Delta t_\mathrm{s} \omega_\mathrm{i} N_\parallel \frac{E_+}{B_0}\,.$$

With due account of relationships

$$\Delta v_\perp \approx \frac{eE_+}{m_\mathrm{i}}\,\Delta t_\mathrm{s}\,, \qquad \Delta t_\mathrm{s} \approx \frac{2\pi}{\omega_\mathrm{i}}\left(\frac{L_B}{\rho_{\mathrm{i}\parallel}}\right)^{1/2},$$

we arrive at

$$\Delta v_\parallel \approx 2\pi k_\parallel L_B \frac{c^2}{v_\parallel}\left(\frac{E_+}{B_0}\right)^2. \tag{3.6}$$

The same result can be obtained from the general relationship

$$\Delta\mathbf{p} = \frac{\mathbf{k}}{\omega}\,\Delta\varepsilon\,, \tag{3.7}$$

which characterizes the resonance energy and momentum exchanges between an electromagnetic wave and a charged particle.

The longitudinal velocity increments determined by formulas (3.6), (3.7) are compared in Fig. 10 with the result of numerical solution to the equations of motion. Calculations were carried out under the same conditions as in Fig. 9; however, the space–time dependence of the fields was chosen in the form of a wave running along the magnetic field: $\propto \cos(k_\parallel z - \omega t)$ with $k_\parallel = 4\pi/L_B$. The dependence depicted by curve 2 takes into account the change in longitudinal velocity due both to ICR interaction and to transverse energy conversion into longitudinal energy in the case of ions moving in a falling magnetic field:

$$\Delta v'_\parallel = \left[(\Delta v_\parallel)^2 + (\Delta v_\perp)^2\,\frac{\Delta B}{B_\mathrm{min}}\right]^{1/2}, \tag{3.8}$$

where the longitudinal velocity increment is determined by formulas (3.6), (3.7), while the transverse velocity increment is taken from calculations, $\Delta B = B_\mathrm{res} - B_\mathrm{min}$, B_res is the magnetic field at the point of cyclotron resonance, and B_min is the magnetic field at the boundary of the calculation region. Oscillations of curve *2* are due to oscillations of the quantities $\Delta v_\parallel = f(\Delta\varepsilon_\perp)$ and $\Delta v_\perp$ entering into expression (3.8). As was indicated above in the comment on Fig. 9, these quantities also oscillate after the passage of an ion through the resonance zone — in the region where the magnetic field is homogeneous. Actually, as elucidated by a numerical solution to the equations of motion, the HF field in this region affects the longitudinal velocity weakly (see curve *1* in Fig. 10).

Notice the significant difference between curves *1* and *2* in Figs 10 and 11 in the region of transition from the linear regime to the nonlinear one. In this region, the calculated dependence $\Delta\varepsilon(E_+)$ (curve *1* in Fig. 11) also differs significantly from the approximation dependences (curves *2* and *3*). The influence of nonlinearity related to the HF magnetic field leads to the ion energy increment turning out, with a further increase in the HF field amplitude, to be significantly smaller than the increment determined by formula (3.5).

The change in longitudinal velocity, due to the presence of an HF magnetic field, affects the intensity of ICR interaction in the inhomogeneous magnetic field for $\Delta v_\parallel \geqslant v_\parallel$, which takes place under the condition

$$\frac{E_+}{B_0} \geqslant \frac{v_\parallel}{c}\left(\frac{1}{2\pi k_\parallel L_B}\right)^{1/2}.$$

If the magnetic field is homogeneous, then, owing to the cyclotron resonance condition depending on the longitudinal velocity (1.2), the change in longitudinal velocity leads to the ion leaving the resonance state (cf. this with the known problem of resonance interaction of electrons with potential Langmuir oscillations dealt with, for example, in books [41]).

A homogeneous magnetic field is utilized in systems for ICR isotope separation. Attention was drawn to the importance of the discussed effect in such systems in paper [42], while the effect itself was first considered in paper [43].

3.2 Ion-cyclotron resonance interaction of an ensemble of ions

Although changes in the ion longitudinal velocity occurring in the ICR interaction process can restrict its intensity, the practice of plasma experiments reveals that the ICR interaction permits the HF energy to be transferred to the ion plasma component with a high efficiency. No exact analytical expressions exist for the energy increment taking into account the variations in $v_\parallel$. Nevertheless, the parameters characterizing ICR heating in SNF processing systems are such that the change in a longitudinal velocity may turn out to be significant. For this reason, analysis of the ICR heating process in these systems has to be made invoking a numerical solution to the equations of motion.

The method of calculations was described in Refs [24, 28]. It was assumed that a plasma flow moving along the magnetic field with the speed of ion sound and exhibiting a Maxwellian velocity distribution is input into the ICR heating system:

$$f_0(\mathbf{u}) = \frac{2u_\parallel}{\pi A_0} \exp\left[-(u_\parallel - U_0)^2 - u_\perp^2\right], \tag{3.9}$$

where the notation was introduced as follows:

$$\mathbf{u} = \frac{\mathbf{v}}{v_{T_\mathrm{i}}}, \qquad v_{T_\mathrm{i}} = \left(\frac{2T}{m_\mathrm{i}}\right)^{1/2},$$

$$A_0 = \exp\left(-U_0^2\right) + \sqrt{\pi}\, U_0\left(1 + \operatorname{erf}(U_0)\right),$$

$$\operatorname{erf}(U_0) = \frac{2}{\sqrt{\pi}} \int_0^{U_0} \mathrm{d}u \exp\left(-u^2\right),$$

$$U_0 = \frac{V_\mathrm{s}}{v_{T_\mathrm{i}}} = \left(\frac{T_\mathrm{e} + T_\mathrm{i}}{2T_\mathrm{i}}\right)^{1/2}.$$

This distribution is normalized to unity in the regions of $0 < u_\parallel < \infty$, and $0 < u_\perp < \infty$. In numerical calculations, the initial distribution function (3.9) was approximated by the values of a discrete function taken at quite a large number of points, $1.575 \times 10^3 = 35 \times 45$, distributed uniformly within the intervals $0 \leqslant u_\perp \leqslant 3.5$, and $0 \leqslant u_\parallel \leqslant 4.5$. It is natural to consider the distribution over the cyclotron rotation phase with which ions approach the cyclotron resonance zone to be uniform. Owing to the large length of the system, $L_\parallel/\rho_\mathrm{i} \approx 10^2 - 10^3$, the phase spread over the time taken by the ion to approach the resonance zone is quite large: $\Delta\Phi \gg 1$. The phase spread is a function of $v_\perp$ and $v_\parallel$; therefore, the spread in the initial values of these quantities automatically leads to averaging over the phase. Moreover, the assumption was made that in the ensemble of ions input into the processing system four values of the cyclotron rotation phase, differing by $\pi/2$, have equal probabilities.

An example is illustrated in Fig. 12 of the ion energy distribution resulting from ICR interaction of the flow (3.9) proceeding in the inhomogeneous magnetic field (1.1) of the SNF processing system. Calculations were performed in the same conditions as in Fig. 9. In accordance with estimate (3.1), the width of the obtained distribution function is quite significant. We note the irregularity of the distribution function due to the discreteness in partitioning the phase space in the initial state.

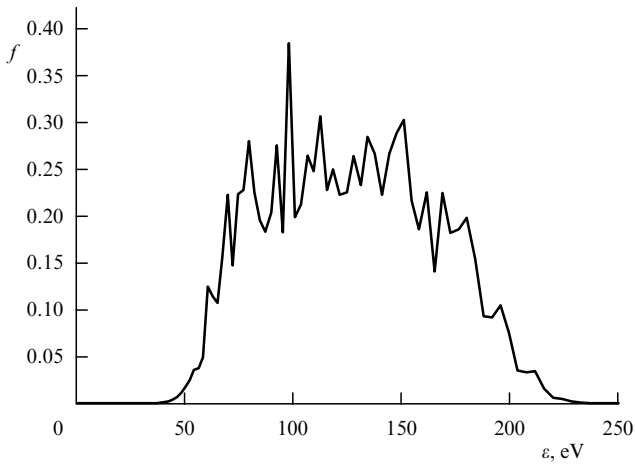

Figure 12. Energy distribution function f of ions in the ensemble (3.9) at the exit of the ICR heating system. Calculation parameters are as follows: $T = 2$ eV, $U_0 = 1$, and $\beta = 0.5$; the remaining parameters are the same as in Fig. 9.

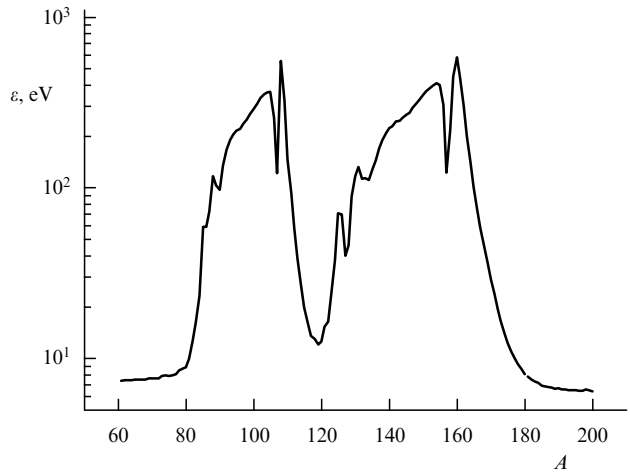

Figure 13. Dependence of mean energy increment of the ion ensemble passing through the ICR heating system on the mass number A: $T = 2$ eV, $I = 0.39$ kA, $r_\mathrm{A} = 0.26$ m, $B_0(0) = 1.75$ kG, $L_{B0} = 0.75$ m, and $L_\mathrm{A} = 1.5$ m.

The content of NA, whose ions are subjected to ICR heating, includes elements differing in mass numbers (see Fig. 2). The points of cyclotron resonance of ions with larger masses are situated in the region of a higher magnetic field and, correspondingly, of smaller radii of the plasma flow moving along the magnetic force lines. According to the results presented in Section 2, a reduction in the plasma radius leads to an enhancement of the transverse electric field excited by a helical current antenna. An increase in the mass number is also accompanied by a decrease in the longitudinal velocity $v_\parallel \propto A^{-1/2}$. Both of these factors lead to enhancement of the ICR interaction intensity: the quantity $\Delta\varepsilon_\perp$ grows within the confines of the ion-cyclotron resonance lines (Fig. 13). In the calculation of $\Delta\varepsilon_\perp$, in accordance with Section 1.3, the assumption was made of two-frequency ICR heating, the values of the frequencies and of the parameter β characterizing the magnetic field inhomogeneity were the same as those in Fig. 9.

In the model adopted for magnetic field (1.1), its spatial scale determined by the formula $L_B = B|\mathrm{d}B/\mathrm{d}z|^{-1}$ increases from the center of the ICR heating system (point $z = 0$)

toward its edges; correspondingly, the size of the resonance zone also increases. Far from the center — in the region where the magnetic field is close to homogeneous — the resonance zone is most extended, being confined from outside by a collector or the chamber wall. Beyond the boundaries of the antenna, the HF electric field remains different from zero, although it weakens. Calculations show that ions being at resonance in this region gain significant energy in the HF field. The spikes at the edges of the cyclotron resonance curves (see Fig. 13) may be linked to these ions. The spikes are clearly identified on the right-hand edges of these curves but much more weakly on the left-hand ones. The distinction is apparently related to the ion energy presented in Fig. 13 representing their energy at the exit from the ICR heating system, where ions of minimal mass, corresponding to the left spikes, are at resonance with the field. Ions with masses differing from resonance masses by a small value interact with the HF field in the so-called adiabatic mode. Their energy oscillates with the difference frequency $\Delta\omega = \omega - \omega_{\rm i}$. These oscillations are taken into account in calculating $\Delta\varepsilon_{\perp}$. The oscillation energy is large in the case of small $\Delta\omega$ ($\varepsilon_{\rm osc} \propto (\Delta\omega)^{-2}$). The contribution from such ions to the resonance curves (see Fig. 13) smooths out the spikes on the left-hand slopes of these curves. On the right-hand edges of the resonance curves, the oscillation energy of ions with maximal masses is large in the region of the maximum magnetic field — at the entrance to the ICR heating system. However, the oscillation energy decreases adiabatically as the ions travel in the decaying magnetic field, and it turns out to be quite small at the collectors, which favors identification of spikes on the right-hand edges of the resonance curves. It should be pointed out that, in accordance with Fig. 2, the number of ions in the region of spikes is insignificant.

4. Extraction of nuclear ash ions

NF and NA ions must be accumulated on different collectors. This is possible since the NF ions are to a significant extent 'attached' to the magnetic force lines, while at the same time the NA ions can shift across the magnetic field through quite large distances owing to an increase in their transverse velocity (see Section 1.3). A collector of heated NA ions can be installed directly at the exit of the UCR heating system or at the end of the curvilinear magnetic field segment, if it is used for extracting NA ions. Such a collector, while capturing NA ions, must at the same time let the cold NF ions pass through. Two versions of collectors, termed transverse and longitudinal, are possible. To explain the operation principle of the collectors, we shall consider a cylindrical surface of radius $r_{\rm cl}$ placed in a homogeneous longitudinal magnetic field. The trajectories of ions for which one of the conditions $r_+ < r_{\rm cl}$ or $r_- > r_{\rm cl}$ is fulfilled lie either completely inside or outside the cylindrical surface, respectively. Here, $r_+ = r_{\rm L} + \rho_{\rm i}$ and $r_- = |r_{\rm L} - \rho_{\rm i}|$ are the maximum and minimum distances between the ion and the axis, and $r_{\rm L}$ is the radius of the center of the Larmor circle. When the condition $r_+ > r_{\rm cl} > r_-$ is fulfilled, the ion trajectory intersects the surface considered.

The transverse collector represents a plane surface oriented across the magnetic field and having a round hole of radius $r_{\rm cl}$ in it. This collector captures all the ions for which the condition $r_- > r_{\rm cl}$ is fulfilled, ignoring at the same time those for which $r_+ < r_{\rm cl}$. Ions with $r_+ > r_{\rm cl} > r_-$, depending on the Larmor rotation phase with which they approach the collector plane, may settle on it or pass by. In the case of a uniform phase distribution, the ion flow onto the transverse collector is proportional to $\int_{r_{\rm cl}}^{r_{\max}} rn(r)\,{\rm d}r$.

All the ions with $r_+ > r_{\rm cl}$ will be extracted from the flow if the collector is made in the form of a cylinder with its axis parallel to the magnetic field and of length exceeding the step of the ion helical trajectory in the magnetic field (longitudinal collector). A longitudinal collector is essentially identical to the receiving plates utilized in the ICR isotope separation systems (see Section 1.4). Notice that if among the heated NA ions there are ions for which $r_- > r_{\rm cl}$, then to accumulate them it is necessary to use an additional transverse collector with $r'_{\rm cl} > r_{\rm cl}$.

Analogs of the longitudinal and transverse collectors can also be applied for ion separation in a curvilinear magnetic field. Such collectors are characterized by the same relationships as the ones described above, but involving the following changes of coordinates: $r_{\rm L} \to y_{\rm L}$, $r_\pm \to y_\pm = y_{\rm L} \pm \rho_{\rm i}$, $r_{\rm cl} \to y_{\rm cl}$. Here, y is the coordinate along the binormal to the force lines of the curvilinear magnetic field.

The longitudinal collector is significantly more effective than the transverse one in ion separation in an axisymmetric magnetic field, for separation in which it is necessary that the Larmor radius of NA ions become comparable to $r_{\rm cl}$. Ion separation in a curvilinear magnetic field is possible in the case of a weaker heating and, respectively, at a smaller Larmor radius of the NA ions. The distinctions between the collectors are less significant in this case.

ICR interaction causes the Larmor radius to increase, while the center of the Larmor circle oscillates, remaining on the average motionless. Therefore, in the case of a known (given) distribution of the Larmor centers, calculation of the distribution of ions over the maximum deviation of their trajectories from the axis $r_+ = r_{\rm L} + \rho_{\rm i}$ or $y_+ = y_{\rm L} + \rho_{\rm i}$ reduces to averaging over the value of the Larmor radius.

Calculation of the ion density $n(\mathbf{r})$ is more complicated. In Refs [24, 28], such a calculation was done for the simplest — parabolic — distribution of Larmor centers over the radius:

$$n_{\rm L}(r) = \frac{2}{\pi r_0^2}\left[1 - \left(\frac{r}{r_0}\right)^2\right], \quad 0 < r < r_0\,. \tag{4.1}$$

This distribution was normalized to unity.

The ensemble of ions with Larmor radii equal to $\rho_{\rm i}$ and centers of Larmor circles situated at a distance $r_{\rm L}$ from the axis and distributed uniformly over the azimuth gives rise to the density distribution

$$n(r, r_{\rm L}, \rho_{\rm i}) = \frac{1}{\pi^2}\,\frac{1}{\left[(r_{\rm L}+\rho_{\rm i})^2 - r^2\right]^{1/2}\left[r^2 - (r_{\rm L}-\rho_{\rm i})^2\right]^{1/2}}\,,$$
$$|r_{\rm L} - \rho_{\rm i}| < r < r_{\rm L} + \rho_{\rm i}\,. \tag{4.2}$$

Averaging formula (4.2) over the distribution (4.1) of Larmor centers, we arrive at

$$n(r, \rho_{\rm i}) = \frac{2}{\pi r_0^2}\begin{cases} 1 - \dfrac{r^2+\rho_{\rm i}^2}{r_0^2}\,, & r + \rho_{\rm i} < r_0\,, \\ \left(1 - \dfrac{r^2+\rho_{\rm i}^2}{r_0^2}\right)\left(\dfrac{1}{2} + \dfrac{1}{\pi}\arcsin\dfrac{r_0^2 - r^2 - \rho_{\rm i}^2}{2r\rho_{\rm i}}\right) \\ \quad + \dfrac{1}{\pi}\left[\left(\dfrac{2r\rho_{\rm i}}{r_0^2}\right)^2 - \left(1 - \dfrac{r^2+\rho_{\rm i}^2}{r_0^2}\right)^2\right]^{1/2}, \\ & |r - \rho_{\rm i}| < r_0 < r + \rho_{\rm i}\,, \\ 0\,, & r_0 < |r - \rho_{\rm i}|\,. \end{cases}$$

The last expression must be averaged over the distribution of Larmor radii, which is uniquely related to the ion transverse velocity distribution at the exit of the ICR heating system, the result obtained numerically in Refs [24, 28].

For the distribution (4.1) of Larmor centers, the fraction of ions with a particular Larmor radius, on the trajectories of which r_+ lies within the interval $(r_+, r_+ + \mathrm{d}r_+)$, is given by the expression

$$n(r_+, \rho_\mathrm{i}) = \frac{2}{\pi r_0^2}\left[1 - \left(\frac{r_+ - \rho_\mathrm{i}}{r_0}\right)^2\right], \qquad 0 < r_+ - \rho_\mathrm{i} < r_0 .$$

If heated NA ions are extracted via their drift in a curvilinear magnetic field, the axial symmetry of collectors might be replaced by a plane symmetry. The initial distribution (at the entrance to the curvilinear magnetic field segment) of the centers of Larmor circles is obtained by integration of formula (4.1) over the x-coordinate orthogonal to the drift direction y:

$$n_\mathrm{L}(y) = \frac{8}{3\pi r_0}\left[1 - \left(\frac{y - \Delta y_\mathrm{dr}}{r_0}\right)^2\right]^{3/2}, \quad |y - \Delta y_\mathrm{dr}| < r_0 , \quad (4.3)$$

where Δy_dr is the displacement of the center of a Larmor circle resulting from a drift in the curvilinear magnetic field [see Eqn (1.3)].

An ensemble of ions with centers of Larmor circles situated at $y = y_\mathrm{L}$ and distributed uniformly over the Larmor rotation phase gives rise to the density distribution

$$n(y, y_\mathrm{L}, \rho_\mathrm{i}) = \frac{1}{\pi\left[\rho_\mathrm{i}^2 - (y - \Delta y_\mathrm{dr} - y_\mathrm{L})^2\right]^{1/2}} ,$$
$$|y - \Delta y_\mathrm{dr} - y_\mathrm{L}| < \rho_\mathrm{i} .$$

This expression is the plane limit of expression (4.2).

If functions $n_\mathrm{L}(y)$ and $n(y, y_\mathrm{L}, \rho_\mathrm{i})$ are known, the ion density distribution over the y-coordinate is found by the integration:

$$n(y, \rho_\mathrm{i}) = \int_{\max(-r_0, y'_-)}^{\min(r_0, y'_+)} \mathrm{d}y'\, n_\mathrm{L}(y')\, n(y, y', \rho_\mathrm{i}) ,$$
$$|y - \Delta y_\mathrm{dr}| < r_0 + \rho_\mathrm{i} ,$$

where $y'_\pm = y_\mathrm{L} \pm \rho_\mathrm{i}$.

The distribution over $y_+ = y_\mathrm{L} + \rho_\mathrm{i}$, which must be known in order to determine the fraction of ions accumulating on the longitudinal collector, is found with the aid of Eqn (4.3):

$$n(y_+) = \frac{8}{3\pi r_0}\left[1 - \left(\frac{y_+ - \Delta y_\mathrm{dr} - \rho_\mathrm{i}}{r_0}\right)^2\right]^{3/2},$$
$$|y_+ - \Delta y_\mathrm{dr} - \rho_\mathrm{i}| < r_0 .$$

Figure 14 provides an idea concerning the state of the ion component of SNF plasma in the case of ion separation performed in an axisymmetric magnetic field directly at the exit of the ICR heating system. The results of calculations indicate that in a plasma with parameters specified in the caption to Fig. 14, and when a longitudinal NA ion collector is used, ion heating to the (mean) energy $\varepsilon \approx 0.37$ keV is necessary. In the vicinity of the collector, the cyclotron frequency of doubly charged NF ions is close to the frequency of one of the HF fields, namely ω_2 (see Fig. 3). Owing to oscillations in this field, the mean energy of doubly charged NF ions increases up to $\varepsilon \approx 50$ eV, while the energy of singly charged ions remains close to the initial value of $\varepsilon \approx 8$ eV. The energy distribution of ions is depicted in Fig. 14a.

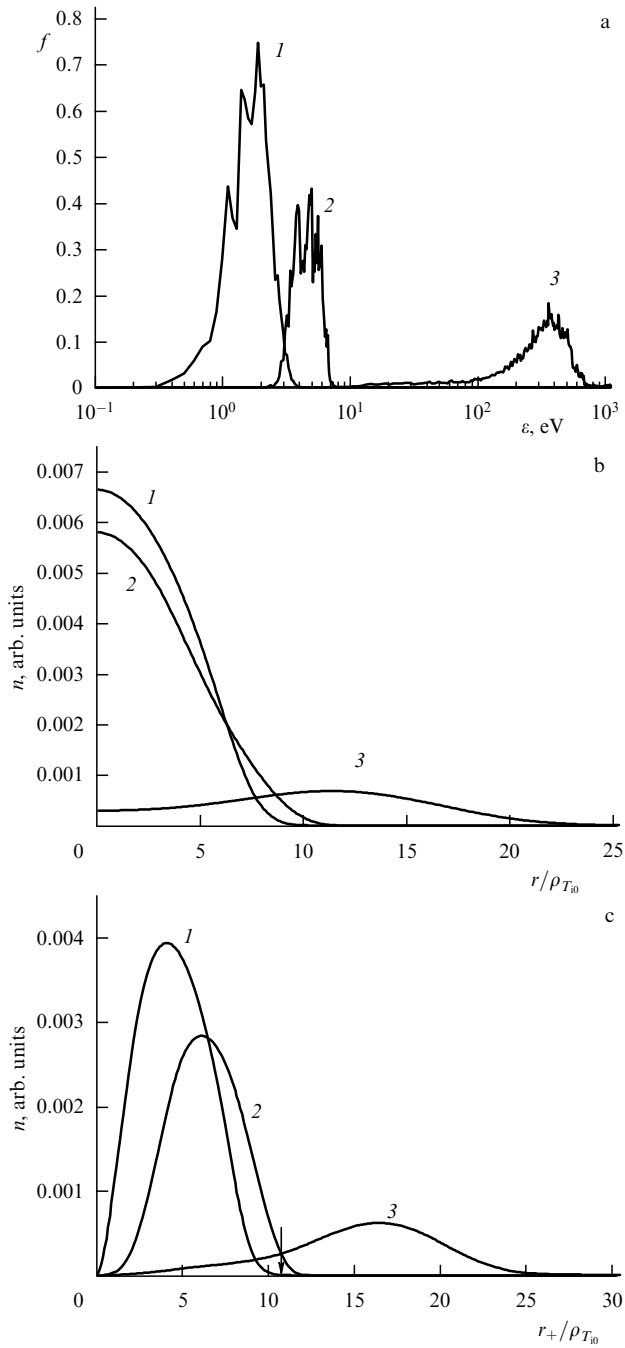

Figure 14. Ion separation in an axisymmetric magnetic field. Distributions are: (a) over energy, (b) over radii, and (c) over the value of r_+. Curves: *1* — singly charged NF ions, *2* — doubly charged NF ions, and *3* — NA ions. The position of the longitudinal collector is indicated by an arrow. Calculation parameters are as follows: $T = 2$ eV, $I = 1.6$ kA, $r_\mathrm{A} = 0.48$ m, $B_0(0) = 1.75$ kG, $\beta = 0.11$, $L_{B0} = 0.75$ m, $L_\mathrm{A} = 1.5$ m, $\omega_1 = \omega_{\mathrm{i},97}(0)$, and $\omega_2 = \omega_{\mathrm{i},143}(0)$. The total length of the ICR heating system measures 3.75 m.

The calculation of ion spatial distributions requires averaging both over ion velocities and over the location (4.1) of Larmor centers; therefore, spatial distributions turn out to be smoother than energy distributions. Oscillations in the HF

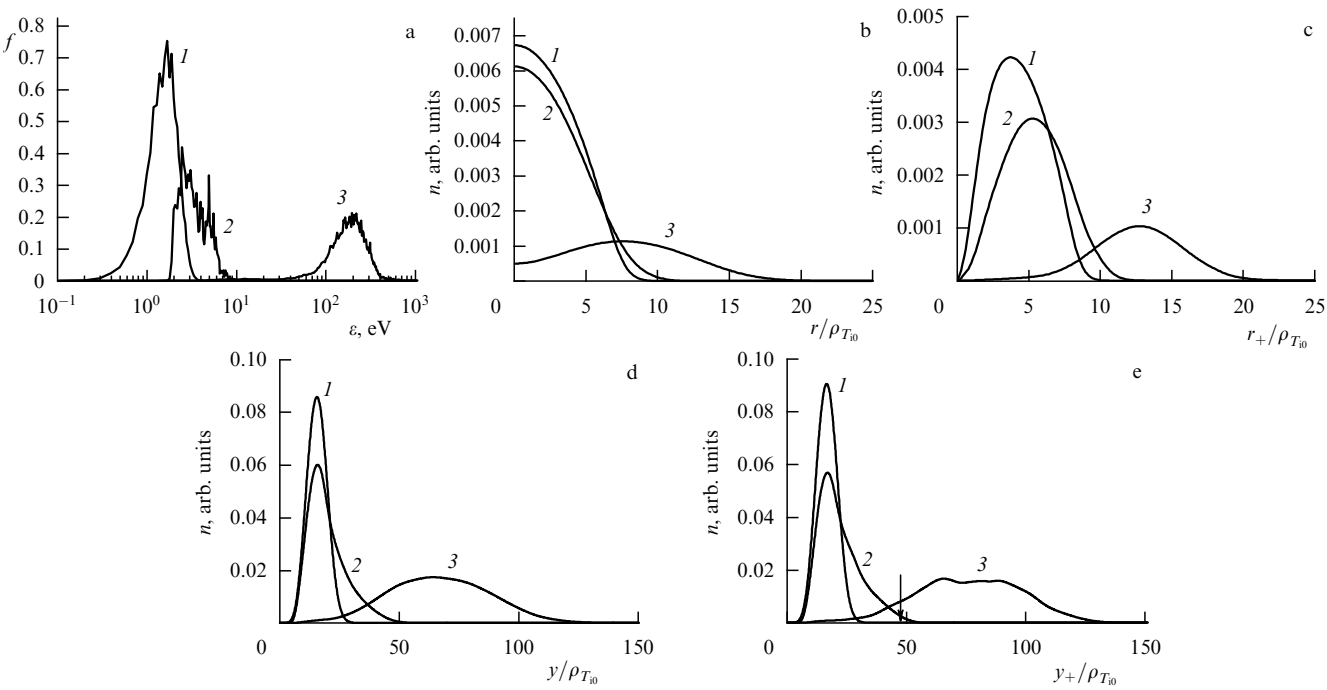

Figure 15. Ion separation in a curvilinear magnetic field. Distributions are (a) over energy, (b) over the radius, (c) over the r_+ distance, (d) along the binormal, and (e) over y_+. Curves are: *1* — singly charged NF ions, *2* — doubly charged NF ions, and *3* — NA ions. The position of the longitudinal collector is indicated by the arrow. Calculation parameters are as follows: $I = 0.55$ kA, $r_A = 0.29$ m, the total length of the system is 9 m, the radius of magnetic force lines along the curvilinear field segment is 1.5 m, $\Delta\chi = \pi$, and the remaining parameters are the same as in Fig. 14.

field somewhat smear the spatial distributions of doubly charged ions. The increase in Larmor radii of NA ions due to ICR heating leads to a significantly greater smearing of the spatial distributions of these ions, which precisely permits their extraction from a cold SNF plasma stream. The distributions over the maximum distances r_+ of ions from the axis are shifted relative to radius distributions by the mean Larmor radius. Since the Larmor radius of NA ions is significantly superior to the Larmor radius of NF ions, ion separation with the aid of a longitudinal collector is easier to perform — it requires less heating of the NA ions.

When using a transverse collector, it is necessary to enhance the HF field, which leads to a rise in the oscillation amplitude of doubly charged ions: $\Delta r \approx eE/[m_i(\omega - \omega_i)^2]$. Here, this quantity rises more rapidly than the Larmor radius of NA ions in the case of ICR heating in the nonlinear regime: $\rho_i \propto E^{3/5}$ [see Eqn (3.5)]. As a result, it turns out that there is a certain critical value of the HF field, starting from which its further enhancement worsens the quality of ion separation. At the parameter values given in the caption to Fig. 14, this HF field corresponds to the mean energy $\varepsilon \approx 0.59$ keV of NA ions and to the energy $\varepsilon \approx 80$ eV of doubly charged NF ions. Here, the fraction $\eta_1 \approx 0.15$ of NA ions remaining in the NF stream somewhat exceeds the desirable fraction $\eta_1 \approx 0.1$, which could be achieved if a longitudinal collector were used (see above).

Processes involving the ion component of SNF plasma during ion separation in a curvilinear magnetic field are illustrated in Fig. 15. In passing through the curvilinear magnetic field segment, ions are displayed along the binormal by the distance Δy_{dr} (1.3). To estimate the pitch angle θ entering into expression (1.3), we shall take account of ICR heating leading to predominant enhancement of the transverse ion energy, which is partially converted into longitudinal energy in the case of motion in the decaying magnetic field of the ICR heating system. Assuming the cyclotron resonance to be realized at the center of the system ($z = 0$), at its exit we obtain $\cos\theta = v_\parallel/v \approx \beta^{1/2}$, where β is a parameter characterizing the drop in the magnetic field within the confines of the ICR heating system [see formula (1.1)]. If $\Delta\chi = \pi$, $\beta = 0.11$, then the average ion displacement is $\Delta y_{dr} \approx 5\langle\rho_i\rangle$. Since the latter is essentially superior to the average Larmor radius, the employment of a curvilinear magnetic field permits noticeably reducing the energy of NA ions. Naturally, the distinctions between transverse and longitudinal collectors separating ions in accordance with the $n(y)$ and $n(y_+)$ distributions become in this case less significant. These distributions are close to each other, being displayed by a distance on the order of the Larmor radius (Fig. 15d, e).

In ion separation in a curvilinear magnetic field, it is necessary to heat the NA ions to the average energy $\varepsilon \approx 0.23$ keV when using a transverse collector, and to the average energy $\varepsilon \approx 0.2$ keV if a longitudinal collector is applied. These energy values are smaller than those required for ion separation in an axisymmetric magnetic field (see above and also Figs 14b, c and 15b, c).

5. Jet of nuclear ash ions in a curvilinear magnetic field and the 'flute mechanism'

The utilization of a curvilinear magnetic field for extracting NA ions with high energies from a cold SNF plasma jet may be impeded by the so-called flute mechanism which ejects plasma into the region of a weak magnetic field. Electrons and ions in an inhomogeneous magnetic field drift toward each other, so, if the plasma is confined in the drift direction, its electric polarization must occur. The originating electric field is directed so that the plasma as a whole drifts in crossed fields toward the weak magnetic field. Precisely this mechanism

leads, in particular, to the development of flute instability in axisymmetric open magnetic traps.

Magnetic traps are designed for the prolonged confinement of charged particles; therefore, the plasma density distribution in traps should not depend on the coordinate reckoned along the particle drift velocity in an inhomogeneous magnetic field and, in the case of axisymmetric open magnetic traps, from the azimuth. In such systems, the instability develops from azimuthally nonsymmetric perturbations. SNF processing systems are those involving moving plasma. In such systems, the stationary plasma density distribution is certain to be nonuniform in the drift direction (the binormal to the magnetic force lines), and the entire plasma stream can be considered a perturbation with a large amplitude. B B Kadomtsev showed that such structures evolve like a plasma column under the action of the first mode of flute instability that propels itself as a whole into the region of a weak magnetic field [44]. At present, such structures are conventionally called blobs (see, for example, Ref. [45]).

The plasma ejection mechanism may be neutralized in the systems with open magnetic force lines that are in electric contact with the end plates (the line-tying phenomenon). Such a contact permits us to discard the plasma electric polarization that triggers the flute mechanism. In the region where the excess negative charge is released, electrons can leave it along the magnetic force lines onto the end plates. In principle, there are two possible ways of introducing electrons into the regions of excess positive charge: by extraction from the emitting end plates, and by initiating a gas discharge. In the gas discharge, such fluxes of charged particles onto the end plates, maintaining the plasma quasineutrality, are established automatically.

The flow of NA ions in the SNF processing system, owing to their drift in the inhomogeneous magnetic field, occupies only a part of the region between the end plates; therefore, in the absence of cold plasma the electrons from the emitting end plates will be compelled to pass through the vacuum gap. Estimates show that for traversing the current that compensates for the ion charge an extremely high electric potential, significantly distorting the ion motion, must be maintained. Therefore, below we shall only consider the process of neutralization with the aid of gas-discharge plasma.

The removal mechanism of the charge polarization of plasma in a gas discharge in contact with the end plates was considered, for example, in Ref. [46]. In a gas discharge, the flux densities of electrons and ions onto the end plates are usually equal to one another at each point of the end plate surfaces. In the case of distinct electron and ion thermal velocities, equalization of the fluxes is achieved using the drop of potential in the Langmuir layer near the walls. If the magnetic force lines are bent and the plasma density is inhomogeneous in the direction of a charged particle drift, the flute mechanism will lead to the emergence of charges in the force lines. In this case, the plasma quasineutrality is maintained by variations in the wall vicinity of the potential jump. In those force lines where a positive charge is released, the jump increases, which reduces the electron flux. In force lines where a negative charge is released, the potential jump decreases, which leads to the ejection of excess electrons. The wall layer does not affect the flux of ions that approach the wall with velocities on the order of the ion-acoustic velocity; therefore, in a bent magnetic field the electric currents that close on the end plate will flow through the Langmuir layer. Here, various force lines acquire different potentials and, consequently, an electric field is induced, directed across the magnetic field. This field has the same sign as the electric field arising in the case of isolated end plates and, consequently, it will also lead to the plasma drifting outward. However, the plasma motion will acquire, instead of the character of an accelerated ejection, the character of a viscous flow. We shall estimate below its rate.

In a gas-discharge plasma, one usually has $T_e > T_i$; therefore, the main factor causing charge polarization of plasma in an inhomogeneous magnetic field is the drift of electrons. In a tube of unit cross section, the electron drift results in the release of the charge per unit time equal to

$$\delta\dot{Q} \approx e\,\frac{\mathrm{d}n_c}{\mathrm{d}y}\,V_{\mathrm{dr,e}}L_1\,, \tag{5.1}$$

where $\mathrm{d}n_c/\mathrm{d}y \approx n_c/l_y$, n_c is the density of cold (gas-discharge) plasma, l_y is the characteristic scale of the plasma density change in the drift direction, $V_{\mathrm{dr,e}} \approx v_{T_e}\rho_{T_e}/R$ is the mean drift velocity in an inhomogeneous magnetic field, v_{T_e} is the electron thermal velocity, ρ_{T_e} is the average electron Larmor radius, R is the radius of curvature of magnetic force lines, and $L_1 = \Delta\theta R$ is the longitudinal size of the curvilinear magnetic field segment.

If the value of $\delta\dot{Q}$ is small compared to the electron charge flowing down the magnetic field, $\dot{Q} \approx en_cV_s$ (where V_s is the ion-acoustic velocity), then for maintaining quasineutrality of the given tube in the inhomogeneous magnetic field the wall jump in potential must change by

$$\delta\varphi \approx \frac{T_e}{e}\,\frac{\delta\dot{Q}}{\dot{Q}}\,. \tag{5.2}$$

The potential $\delta\varphi$ is related to the transverse electric field $E \approx \delta\varphi/l_y$. In the presence of such a field, charged particles drift with the velocity $c\mathbf{E}\times\mathbf{B}/B^2$. During the lifetime of cold charged particles in the discharge, $\tau_c \approx L_1/V_s$, the displacement due to their drift will be small compared to the characteristic plasma scale l_0 in this direction under the condition

$$\frac{(\Delta\theta\rho_{ie})^2 R}{l_y^2 l_0} \ll 1\,, \tag{5.3}$$

where ρ_{ie} is the Larmor ion radius calculated from the electron temperature.

The electric contact with the end flanks can be improved (by reducing the wall jump in potential) if electrons are emitted from them. Here, however, the heat exchange between the plasma and the end plates becomes more intense, which leads to a decrease in the electron temperature. This impedes the flow of electric current through the plasma.

The above estimates were obtained considering the potential to be constant along the force lines everywhere except the layer near the wall. In the gas discharge, along with the potential jump near the wall, there is also actually a fair change of potential from the center to the end plates that is on the order of T_e/e. To provide the flow of electric current, which is necessary for the maintenance of plasma quasineutrality, this distribution is distorted. In estimating the distortions, we shall take advantage of Ohm's law

$$j_\parallel = \sigma E_\parallel\,,$$

where $j_{\parallel} \approx \delta\dot{Q}$ [see Eqn (5.1)], $\sigma = ne^2/(m_e \nu_e)$ is the plasma conductivity, and ν_e is the frequency of electron collisions.

Assuming $E_{\parallel} \approx \delta\varphi_1/L_1$, we find

$$\delta\varphi_1 \approx (\Delta\theta)^2 \frac{R}{l_y} \frac{\nu_e}{\omega_e} \frac{T_e}{e} .$$

The above-presented ideas concerning the processes in gas-discharge plasma in an inhomogeneous magnetic field will hold valid if, together with inequality (5.3), the condition $e\,\delta\varphi_1/T_e \ll 1$ is also satisfied.

To an order of magnitude, the assumed parameter values of the analyzed systems are the following: $R = 1$ m, $l_0 = 0.1$ m, $\Delta\theta = \pi$, and $B = 1$ kG. Owing to the fraction of NA in SNF being small, the gas plasma density can be by an order of magnitude lower than the SNF plasma density $n_c \approx 10^{11}$ cm^{-3}. The energy distribution of heated NA ions is characterized by a significant scatter (see Section 4). Therefore, owing to the drift in an inhomogeneous magnetic field, the characteristic scale l_y is several times larger than l_0 (see Fig. 15). For the indicated parameter values, the condition $e\,\delta\varphi_1/T_e \ll 1$ is fulfilled with a good reserve, while no such reserve is present in condition (5.3).

The processes discussed above can be considered as a manifestation of flute instability caused by the gradient of electron pressure. Let us trace how they are described in the standard formalism. Owing to the low plasma pressure ($\beta \approx 10^{-3}$), the oscillations are assumed to be electrostatic. We shall use the simplest, so-called local, quasiclassical approximation and choose the space–time dependence of perturbed quantities in the form $\propto \exp(-\mathrm{i}\omega t + \mathrm{i}k_y y)$.

Flute oscillations are usually characterized by equations and quantities averaged along the magnetic force lines. As was shown above, quasineutrality in gas-discharge plasma is maintained owing to automatic adjustment of the electron fluxes along the magnetic field onto the end plates. In accordance with formula (5.2), for taking this effect into account, it is necessary to introduce the following term into the averaged electron continuity equation:

$$\delta n_{1e} \approx \mathrm{i}\,\frac{V_s}{\omega L_1}\, n_c\, \frac{e\varphi_1}{T_e} .$$

The dispersion relation for flute oscillations, obtained in the standard way (see, for example, Ref. [24]), assumes the form

$$\omega^2 + \mathrm{i}\omega\,\frac{V_s}{L_1 k_y^2 \rho_{ie}^2} + \frac{V_s^2}{l_0 R} = 0 .$$

To an order of magnitude, the characteristic instability increment is expressed as

$$\mathrm{Im}\,\omega \approx \frac{(k_y \rho_{ie})^2 L_1 V_s}{l_0 R} .$$

It is quite natural that for most large-scale perturbations, $k_y \approx l_y^{-1}$, the condition $\mathrm{Im}\,\omega\tau_c \ll 1$, under which, if it is fulfilled, the given instability cannot develop during the characteristic plasma lifetime $\tau_c \approx L_1/V_s$, coincides by order of magnitude with condition (5.3).

As to the instability caused by NA ions of high energies, it should be stabilized by effects of the finite Larmor radius, as the radial distribution of NA ions is comparable to the transverse dimension of the plasma stream. The finite Larmor radius effects do not affect the so-called first mode of flute instability. In the system considered, the first mode would be manifested as a plasma jet eruption outwards, into the weak magnetic field region. Methods for countering such outward eruptions were considered above.

Stable passage of the plasma flow through the curvilinear magnetic field segment is possible owing to the line-tying phenomenon. An analysis performed without taking this phenomenon into account predicts a plasma ejection from the curvilinear magnetic field region at extremely low densities [47]. These predictions are disproved by the results of experiments performed in the 1960s for the purification of hydrogen plasma bunches, obtained in plasma guns, from heavy ion admixtures. In Refs [17–21], the stable passage was observed of plasma bunches with a density reaching $\sim 10^{12}$–10^{13} cm^{-3} at an energy on the order of several keV. In these studies, neutralization of the flute mechanism was considered to be related to the line-tying phenomenon; however, the details of how this phenomenon acted under the conditions of the experiments performed were not clarified, so even if the indicated phenomenon did exert any influence, it was spontaneous, without the experimentalists having made any efforts.

At present, curvilinear magnetic fields are used in the low-temperature plasma of arc discharges for its removal of the microscopic metal droplets escaping from a cathode. The plasma parameters in these experiments (temperature, density, degree of ionization of the substance) differ significantly from the plasma parameters in SNF processing systems. However, even in this case suppression is observed of the flute mechanism, which is also ascribed to the line-tying phenomenon [48, 49].

6. Influence of viscosity on plasma diffusion across a magnetic field

This section is concerned with the results of work presented in Ref. [29]. Plasma is considered to be magnetized if the condition $\nu_j \ll \omega_j$ ($j = \mathrm{i}, \mathrm{e}$) is fulfilled. Partial magnetization (finiteness of the ratio ν_j/ω_j) is the cause of plasma diffusion across a magnetic field and of so-called transverse viscosity. The influence of these factors on the plasma density distribution across a magnetic field is characterized by the frequencies $\Omega_{dif} = \nu_{ie}(\rho_i/r_0)^2$ and $\Omega_{vis} = \nu_{ii}(\rho_i/r_0)^4$, where r_0 is the plasma radius. Electron viscosity can be neglected here, since the ion frequency is $(m_e/m_i)^{3/2}$ times larger than the respective characteristic one.

The ratio

$$\frac{\Omega_{dif}}{\Omega_{vis}} = \frac{\nu_{ie}}{\nu_{ii}} \left(\frac{r_0}{\rho_i}\right)^2$$

is the product of a small, $\nu_{ie}/\nu_{ii} \approx (m_e/m_i)^{1/2} \approx 1.5 \times 10^{-3}$ (for uranium ions), factor and of a big, $(r_0/\rho_i)^2$, factor. Therefore, in analyzing the evolution of the distribution of an SNF plasma flow moving along a magnetic field, it is, generally speaking, necessary to take into account both the ion diffusion and transverse ion viscosity. The diffusion of plasma across a magnetic field is ambipolar, while ion viscosity acts only upon ions. Here, plasma quasineutrality can be maintained owing to the line-tying phenomenon (see Section 5).

As is well known, viscosity tends to level the velocity profile. Plasma in a magnetic field exhibits a special form of

motion: a diamagnetic (Larmor, ambient, gradient) drift with the velocity $\mathbf{V} = c/(eB^2)\,\mathbf{B}\times\nabla p/n$. It follows from this equation that in the case of a uniform temperature distribution, when $\nabla p = T\nabla n$, viscosity tends to render the density profile across the magnetic field close to exponential in the plane case, $n \propto \exp(-x/a)$, and to Gaussian, $n \propto \exp(-(r/a)^2)$, in the axisymmetric case. Solid-state azimuthal rotation corresponds to the latter.

The plasma diffusion equation in axisymmetric systems, which takes the influence of viscosity into account, was devised in Ref. [28]. In spite of the axial symmetry of the problem, it turned out to be more convenient to apply Cartesian coordinates in intermediate calculations. The starting equation of motion was taken in the form

$$-T_{\mathrm{i}}\,\frac{\partial n}{\partial x_\alpha} - \frac{\partial \pi_{\alpha\beta}}{\partial x_\beta} + \frac{en}{c}\,\mathbf{V}\times\mathbf{B}\Big|_\alpha = 0\,. \tag{6.1}$$

Neglecting viscosity to begin with, from equation (6.1) we obtain $\mathbf{V}_0 = (-y, x, 0)V_0/r$, where $V_0 = [cT/(eB)]\,\partial\ln n/\partial r$. In viscosity tensor [50], we shall take into account the components proportional to the viscosity coefficient $\eta_1 = 0.3(v_{\mathrm{ii}}/\omega_{\mathrm{i}}^2)nT_{\mathrm{i}}$:

$$\pi_{xx} = -\pi_{yy} = 2xy\,\frac{\eta_1}{r}\,\frac{\mathrm{d}}{\mathrm{d}r}\,\frac{V_0}{r}\,,$$

$$\pi_{xy} = \pi_{yx} = (y^2 - x^2)\,\frac{\eta_1}{r}\,\frac{\mathrm{d}}{\mathrm{d}r}\,\frac{V_0}{r}\,.$$

Then, applying the method of successive approximations, we find

$$\mathbf{V}_1 = \frac{c}{enB}\,\frac{\partial}{\partial x_\alpha}(-\pi_{y\alpha}, \pi_{x\alpha}, 0)\,. \tag{6.2}$$

Expression (6.2) provides the following contribution to the continuity equation:

$$G_\chi = \chi\,\frac{\partial^2}{\partial\xi^2}\left(\xi^2 n^2\,\frac{\partial}{\partial\xi}\,\frac{1}{n}\,\frac{\partial n}{\partial\xi}\right), \tag{6.3}$$

and taking it into account yields the continuity equation in the form

$$\frac{\partial n}{\partial t} - \mu\,\frac{\partial}{\partial\xi}\,\xi n\,\frac{\partial n}{\partial\xi} + \chi\,\frac{\partial^2}{\partial\xi^2}\left(\xi^2 n^2\,\frac{\partial}{\partial\xi}\,\frac{1}{n}\,\frac{\partial n}{\partial\xi}\right) = S(\xi)\,, \tag{6.4}$$

where $\xi = (r/r_0)^2/2$, $S(\xi)$ is the plasma source, and

$$\mu = \frac{2v_{\mathrm{ie}}\rho_{\mathrm{i}}^2(1+\tau_{\mathrm{e}})}{r_0^2 n} \approx 3.2\times 10^{-8}\,\frac{(1+\tau_{\mathrm{e}})\rho_{\mathrm{H}}^2}{r_0^2 T_{\mathrm{e}}^{3/2}}\,,$$

$$\chi = \frac{0.3v_{\mathrm{ii}}\rho_{\mathrm{i}}^4}{r_0^4 n} \approx 0.55\times 10^{-6}\,\frac{A^{3/2}\rho_{\mathrm{H}}^4}{r_0^4 T_{\mathrm{i}}^{3/2}}\,,$$

$\tau_{\mathrm{e}} = T_{\mathrm{e}}/T_{\mathrm{i}}$, $\rho_{\mathrm{i}} = (T_{\mathrm{i}}/m_{\mathrm{i}})^{1/2}/\omega_{\mathrm{i}}$ is the average ion Larmor radius, and ρ_{H} is the Larmor radius calculated for hydrogen ions. The second term in the left-hand part of equation (6.4) allows for the plasma diffusion (see, for example, book [51]).

Equation (6.4) must be supplemented by boundary conditions. The point $\xi = 0$ is a singular point of this equation. In an equation of the fourth order, the requirement of analyticity permits the exclusion of two solutions having a singularity at this point. The other two solutions in the vicinity of point $\xi = 0$ can be represented in the form of the series

$$n(t,\xi) = \sum_{p=0}^{\infty} n_p(t)\xi^p\,.$$

It can be readily shown that, setting the first two coefficients (n_0, n_1) in this expansion and equating the coefficients of increasing powers of ξ in equation (6.4) to zero, it is possible to determine successively all the remaining $n_{p\geqslant 2}$. To prove this assertion, it is sufficient to take into consideration that the action of operator $(\partial^2/\partial\xi^2)\xi^2$, entering into the 'viscous' term in Eqn (6.4), on the power function $f(\xi) = \xi^p$ does not alter the exponent.

Since plasma 'perishes' on the wall of the vacuum chamber, it is necessary to put $n(1/2) = 0$. Therefore, the boundary point, as follows from equation (6.4), is also a singular point of this equation. The second boundary condition on the wall can be obtained analyzing the expression for a plasma flow in the vicinity of the wall:

$$J = -\mu\xi n\,\frac{\partial n}{\partial\xi} + \chi\,\frac{\partial}{\partial\xi}\left\{\xi^2\left[n\,\frac{\partial^2 n}{\partial\xi^2} - \left(\frac{\partial n}{\partial\xi}\right)^2\right]\right\}.$$

It is easy to verify that a density dependence on the coordinate in the form

$$n(\xi) \underset{\xi\to 1/2}{\approx} \gamma\xi'^{3/2}\,,$$

where $\xi' = 1/2 - \xi$, ensures that the plasma flow $J \approx (3/2)\chi\gamma^2$ is constant in the vicinity of the boundary $(\xi \approx 1/2)$. The actual value of the flow depends on the joint action of diffusion and viscosity on the whole plasma column.

In accordance with ideas concerning the solution in the region close to the wall, it must be considered that n'_ξ also turns to zero at the boundary.

It should be noted that the problem of the diffusion of 'nonviscous' plasma $(\chi = 0)$ was highlighted in book [51]. In this case, the condition that the flow in the vicinity of the wall be constant is fulfilled for

$$n(\xi) \underset{\xi\to 1/2}{\approx} \gamma\xi'^{1/2}\,.$$

In anticipation of a numerical solution to equation (6.4), we shall analyze the properties of the viscous term in this equation. The Gaussian plasma density distribution along the radius, $n(\xi) = (N/\pi a^2)\exp(-\xi/a^2)$, corresponds to solid-state rotation of the plasma. In accordance with the above, in the case of such a distribution the quantity $F(n) = nn''_{\xi\xi} - n'^2_\xi$ turns to zero, as does the expression $G_\chi(n)$.

The operator entering into expression G_χ conserves the total number of particles $N = 2\pi r_0^2\int n(\xi)\,\mathrm{d}\xi$. Another integral is the value of the azimuthal moment of the generalized momentum, which for $\rho_{\mathrm{i}} \ll r_0$ coincides with $L = 2\pi m_{\mathrm{i}}\omega_{\mathrm{i}} r_0^4\int\xi n(\xi)\,\mathrm{d}\xi$. Indeed, the moment density is expressed as

$$l_\theta = r\left(\frac{e}{c}\,A_\theta + m_{\mathrm{i}}V_\theta\right)n\,, \tag{6.5}$$

where $A_\theta = (r/2)B_0$, and $V_\theta = \omega_{\mathrm{i}}\rho_{\mathrm{i}}^2(1/n)\,\partial n/\partial r$ is the diamagnetic (Larmor) drift velocity.

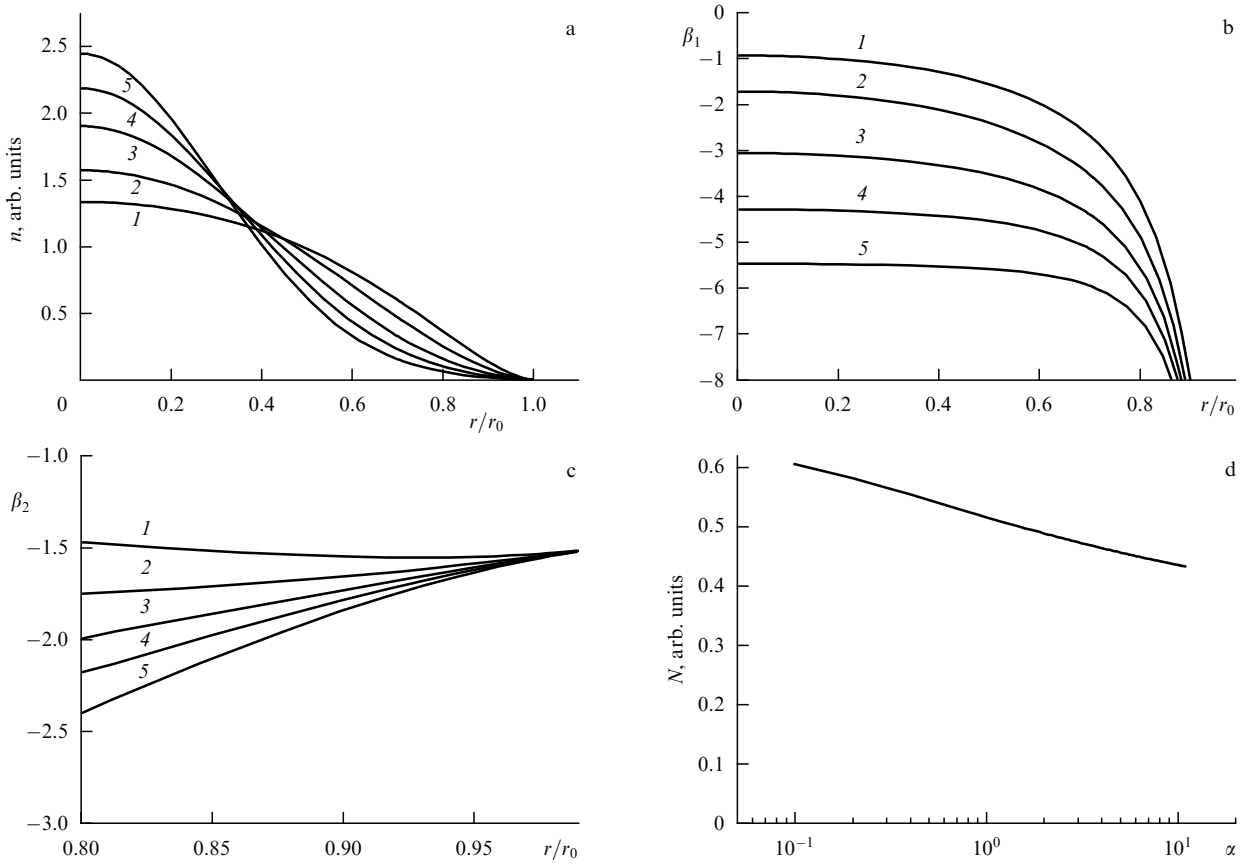

Figure 16. Stationary state of a plasma column in a magnetic field: (a) dependence of density on the radius, (b) dependence of $\beta_1 = n'_\xi/n$ on the radius ($\xi = (r/r_0)^2/2$), (c) dependence of $\beta_2 = (1/2 - \xi)n'_\xi/n$ on the radius, and (d) dependence of the total number of particles N on α. Curves are as follows: *1* — $\alpha = 0.1$, *2* — $\alpha = 0.3$, *3* — $\alpha = 1$, *4* — $\alpha = 3$, and *5* — $\alpha = 10$.

Using formula (6.5), we arrive at the total generalized angular momentum:

$$L_\theta = 2\pi \int r l_\theta \, \mathrm{d}r = 2\pi m_\mathrm{i} \omega_\mathrm{i} r_0^4 \int \xi \left(n + \frac{1}{2} \left(\frac{\rho_\mathrm{i}}{r_0} \right)^2 \frac{\partial n}{\partial \xi} \right) \mathrm{d}\xi \,. \quad (6.6)$$

With the aid of integration by parts, the integrand in formula (6.6) can be represented as $(\xi - 2\rho_\mathrm{i}^2)n$. The first term in parenthesis in the integration element in formula (6.6) is determined by the magnetic part of the generalized momentum, and the second by the mechanical part. Each of them is conserved individually. Since the ion Larmor radius in the hydrodynamical approximation is considered small compared to the characteristic spatial scale, the mechanical part can be dropped:

$$L_\theta \approx L = m_\mathrm{i} \omega_\mathrm{i} \langle \xi \rangle r_0^2 N \,,$$

where $\langle \xi \rangle$ is the average of ξ.

The aforementioned properties of the 'viscous term' permit us to work out a general idea of the influence exerted by viscosity on the evolution of a plasma column. Viscosity tends to transform the initial radial plasma density distribution into a Gaussian distribution, which, by analogy with the plasma profile originating during its evolution in a tokamak, can be called 'consistent' — optimal (see, for example, Ref. [52]). Since plasma is bounded along the radius, this process is accompanied by plasma particles escaping onto the wall. Owing to both the total number of particles and the quantity $\langle \xi \rangle$ being conserved under the influence of viscosity, the remaining particles must be drawn together to the center of the column. As a result, the characteristic scale of the Gaussianlike distribution a (see above) must become smaller. Plasma diffusion, which tends to broaden the radial distribution, counteracts this process.

In Ref. [29], the regularities characterizing the influence of viscosity on plasma diffusion across a magnetic field was illustrated on the base of an analysis of the stationary state established in the presence of a plasma source. The source function in paper [29] was chosen in the form

$$S(\xi) = \begin{cases} S_0(1 - 16\xi^2) \,, & \xi < \dfrac{1}{4} \,, \\ 0 \,, & \xi > \dfrac{1}{4} \,. \end{cases}$$

The parameter $\alpha = \chi/\mu$ was applied in characterizing the relative intensity of diffusion and viscosity. Figure 16a shows that, although the dependence of the source upon the coordinate is far from Gaussian, when α increases, the density distribution along the radius tends to be Gaussian. The Gaussian distribution is characterized by a constant value of $n'(\xi)/n(\xi)$. Referring to Figs 16a, b, it is seen that the region in which this condition is not fulfilled is drawn toward the boundary as α increases. It was found above that the density dependence on the coordinate in the vicinity of the boundary has the form $n(\xi) \approx C(1 - 2\xi)^{3/2}$, where C is a certain constant. This conclusion is confirmed by the results presented in Fig. 16c.

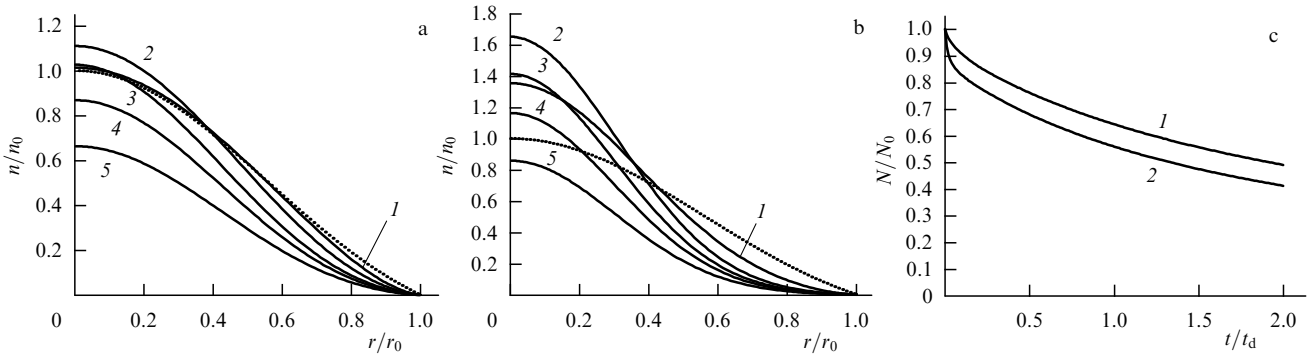

Figure 17. Decay of the initial distribution $n(0,\xi) = n_0 \exp(-2\xi)(1-2\xi)$. Dependence of density on the radius for (a) $\alpha = 1$, and (b) $\alpha = 10$. Dotted curves — $t = 0$, solid curves: *1* — $t = 2 \times 10^{-2} t_d$, *2* — $t = 10^{-1} t_d$, *3* — $t = 0.5 t_d$, *4* — $t = t_d$, and *5* — $t = 2t_d$ ($t_d = (\mu n_0)^{-1}$). (c) Dependence of the total number of particles on time: curve *1* — $\alpha = 1$, and *2* — $\alpha = 10$.

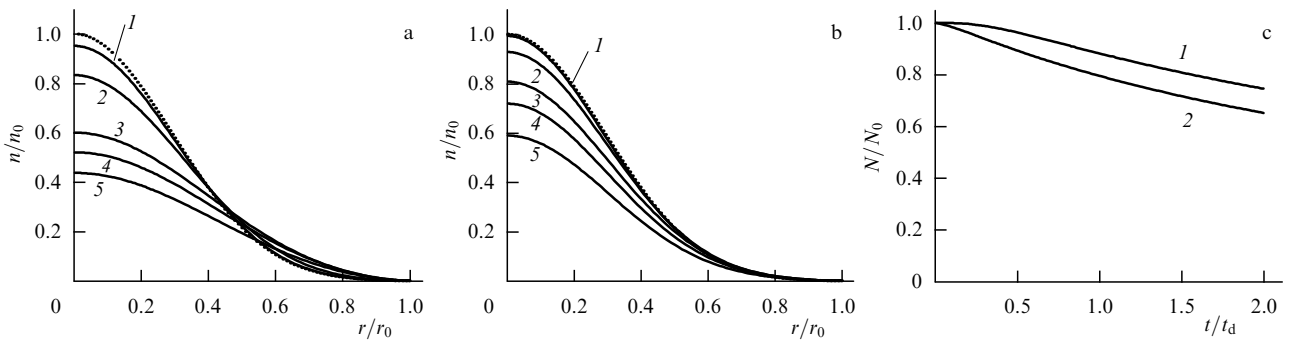

Figure 18. Decay of initial distribution $n(0,\xi) = n_0 \exp(-10\xi)(1-2\xi)$. Dependence of density on the radius for (a) $\alpha = 1$ and (b) $\alpha = 10$. Dotted curves — $t = 0$, curves: *1* — $t = 2 \times 10^{-2} t_d$, *2* — $t = 10^{-1} t_d$, *3* — $t = 0.5 t_d$, *4* — $t = t_d$, and *5* — $t = 2t_d$. (c) Dependence of total number of particles on time: curve *1* — $\alpha = 1$, *2* — $\alpha = 10$.

Although viscosity may influence the density profile, it weakly affects the intensity of plasma losses (Fig. 16d).

In Ref. [29], the decay of initial distributions for different values of α was also analyzed. Both the distribution $n(0,\xi) = n_0 \exp(-2\xi)(1-2\xi)$, spread out over the entire interval $(0, r_0)$, and the distribution $n(0,\xi) = n_0 \exp(-10\xi)(1-2\xi)$, contracted to the center, were considered. In the case of low viscosity ($\alpha = 1$), the first distribution varies little in the course of decay (Fig. 17a). When viscosity is high ($\alpha = 10$), the deformations are more significant. At the center of the column, the plasma density first increases, and its profile approximates to the Gaussian one. In the course of decay, the density profile remains close to Gaussian (Fig. 17b). At the same time, as is seen from Fig. 17c, the viscosity quite weakly affects the decay rate. This conclusion also holds valid in the case of an initial distribution concentrated around the center of the column (Fig. 18). If the viscosity is insignificant ($\alpha = 1$), the distribution quite rapidly spreads out over the entire interval $(0, r_0)$ under the influence of diffusion. Then the plasma density decreases with time without essential changes in the radial distribution. The initial distribution $n(0,\xi) = n_0 \exp(-10\xi)(1-2\xi)$ in the central region differs weakly from the Gaussian one. Naturally, the distribution retains its form when the viscosity is significant ($\alpha = 10$).

In the case of choosing characteristic parameters of the plasma flow through the SNF processing system: $T = 2$ eV, $B = 1.75$ kG, and $r_0 = 10$ cm (see Section 5), the approximate equality $\alpha \approx 2$ holds valid. The analysis performed reveals that for such values of α the viscosity can exert a certain influence on the form of the radial plasma density distribution, but the plasma decay rate depends on diffusion to a greater extent than on viscosity.

The plasma flow passes through SNF processing systems of interest to us in a time t that is short compared to the diffusion time t_d: $t \approx 0.5 \times 10^{-2} t_d$, when ion separation is performed in an axisymmetric magnetic field ($L_\parallel \approx 3.75$ m), and in a time $t \approx 1.2 \times 10^{-2} t_d$, when separation is effected in a magnetic field with curvilinear force lines ($L_\parallel \approx 8.75$ m). In such time periods, neither diffusion nor viscosity can exert a significant influence on the spatial distribution of NF ions.

7. Spatial instabilities of plasma flows along a magnetic field

7.1 Transverse stratification of subsonic flows

In this section, we shall follow the results reported in Ref. [53].

7.1.1 Effective mass and effective heat capacity of plasma flows. The plasma flow rate in SNF processing systems is an important characteristic that affects, in particular, the system throughput. At first sight, there are no obstacles to the motion of a flow with a rate determined by the difference in electric potential, $\Delta\varphi$, in the plasma source. Usually, the quantity $e\Delta\varphi$ is considered to be equal to several electron temperatures and, correspondingly, the plasma flow rate coincides by order of magnitude with the ion-acoustic velocity. However, below, we shall see that the motion of the plasma flow is accom-

panied by quite complex processes. Their analysis provides arguments in favor of the assertion that laminar plasma motion turns out to be possible in systems of sufficient length only if the plasma flow rate is close to the propagation velocity of an acoustic signal, $c_s = [(T_e + 5T_i/3)/m_i]^{1/2}$. In this expression, it is taken into account that sound is to be considered isothermic in electrons, but adiabatic in ions, owing to the large respective electronic and small ionic thermal conductivities under the conditions we are interested in. It is interesting that precisely such a value of the plasma flow rate is presented in paper [22], where ICR isotope separation in the plasma of a number of metals was investigated experimentally.

Irreversible transport phenomena due to viscosity and heat conductivity significantly affect the spatial evolution of plasma flows moving along a magnetic field. In the case of subsonic flows, this means charge particle transportation across the magnetic field. In analyzing the dynamics of subsonic flows, it is expedient, considering the plasma to be ideal, to examine in the hydrodynamic set of equations the terms taking into account viscosity and heat conductivity as due to external factors acting on the plasma — the force and heat source (outflow):

$$\frac{\mathrm{d}}{\mathrm{d}x}\, nV = 0\,, \tag{7.1}$$

$$m_i nV \frac{\mathrm{d}}{\mathrm{d}x}\, V + \frac{\mathrm{d}}{\mathrm{d}x}\, n(T_i + T_e) = F_{ex}\,, \tag{7.2}$$

$$\frac{3}{2}\, n_i V \frac{\mathrm{d}}{\mathrm{d}x}\, T_i + n_i T_i \frac{\mathrm{d}}{\mathrm{d}x}\, V = Q_{ex}\,. \tag{7.3}$$

We shall first assume that $F_{ex} \neq 0$, $Q_{ex} = 0$. In this case, from equation (7.3) we find $T_i = T_{i0}(V_0/V)^{2/3}$. Taking into account a high electron heat conductivity (see also Section 7.1.2), we can consider $T_e = \text{const}$. Having regard to the relation $n = n_0 V_0/V$, following from equation (7.1), and expressing the pressure force in equation (7.2) via the velocity derivative, we obtain

$$m_i \left[1 - \left(\frac{c_s}{V}\right)^2\right] nV \frac{\mathrm{d}}{\mathrm{d}x}\, V = F_{ex}\,. \tag{7.4}$$

The last expression shows that the influence of pressure on the response of a flow to an external force can be taken into account performing renormalization of the ion mass: $m_i \to m_{i,\mathrm{eff}} = m_i[1 - (c_s/V)^2]$. The effective mass $m_{i,\mathrm{eff}}$ is negative for $V < c_s$, and positive when $V > c_s$.

In a subsonic flow, the thermal energy density is relatively high; therefore, a redistribution of pressure is the main effect which the action of an external force leads to. The pressure gradient compensating for the external force accelerates the plasma flow towards this force, which can be interpreted as the consequence of a negative effective mass. In a supersonic flow, the influence exerted by the thermal energy of charged particles on the plasma dynamics is less significant — the effective mass is positive.

The introduction of effective mass permits giving a simple interpretation to the operation of a Laval nozzle. For the flow propagating in this nozzle, the external force is the reaction of the nozzle walls to the (gas) plasma pressure. Owing to the axial symmetry of the nozzle, the force acting on the flow and averaged over the nozzle cross section is directed against the motion in the subsonic part of the nozzle, and along the motion in the supersonic part (Fig. 19). Since together with a change of the sign of the external force a change of the sign of the effective mass also occurs, the flow is accelerated both in the subsonic and in the supersonic parts of the nozzle.

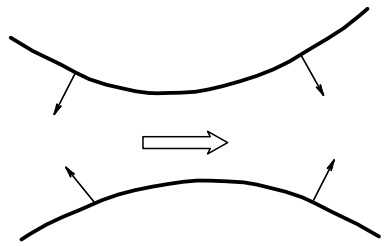

Figure 19. Laval nozzle: thin arrows — reaction force of the walls to the flow pressure; wide arrow indicates the direction of the flow motion.

We shall now assume that $F_{ex} = 0$, $Q_{ex} \neq 0$. Expressing the plasma density and flow rate via the ion temperature with the aid of equations (7.1), (7.2), we transform equation (7.3) into the following:

$$\frac{3}{2}\, n\, \frac{1 - (c_s/V)^2}{1 - (V'_T/V)^2}\, \frac{\mathrm{d}}{\mathrm{d}x}\, T_i = Q_{ex}\,,$$

where $V'_T = [(T_i + T_e)/m_i]^{1/2}$.

The effective heat conductivity

$$C_{\mathrm{eff}} = \frac{3}{2}\, n\, \frac{1 - (c_s/V)^2}{1 - (V'_T/V)^2}$$

is negative within the interval of flow rates $V'_T < V < c_s$. This peculiarity, like the negative effective mass in the subsonic flow, is due to the influence of plasma pressure. The redistribution of this quantity under the action of the heat source (outflow) leads to an adiabatic change in temperature, when $V'_T < V < c_s$, turning out to be more significant than the direct heating (cooling) of plasma.

7.1.2 Spatial instability of subsonic plasma flows. We shall now consider the spatial evolution of velocity and temperature perturbations under the action of viscosity and heat conductivity in a plasma flow moving along the magnetic field. We shall assume a homogeneous plasma flow to be subject to perturbations depending on a coordinate transverse to the magnetic field and take into account transportation in this direction. In this case, equations (7.2), (7.3) assume the forms

$$\rho V \frac{\partial}{\partial z}\, V + \frac{\partial}{\partial z}\left[n(T_e + T_i)\right] = \mathrm{div}_\perp(\eta_{\perp i} \nabla_\perp V)\,, \tag{7.5}$$

$$\frac{3}{2}\, nV \frac{\partial T_i}{\partial z} + nT_i \frac{\partial V}{\partial z} = \mathrm{div}_\perp(\kappa_{\perp i} \nabla_\perp T_i) + \eta_{\perp i}(\nabla_\perp V)^2\,. \tag{7.6}$$

Here, $\eta_{\perp i} = 1.2 n m_i \rho_i^2 \nu_{ii}$ is the ion viscosity coefficient, $\kappa_{\perp i} = 2n\rho_i^2 \nu_{ii}$ is the coefficient of ionic heat conductivity, $\rho_i = (T_i/m_i)^{1/2}/\omega_i$ is the mean ion Larmor radius, and ω_i is the ion-cyclotron frequency; we introduce a Cartesian reference system with the z-axis directed along the magnetic field. We consider the distribution of electron temperature to be uniform (see Section 7.1.1). The diffusion of plasma across the magnetic field is not taken into account, since it is due to weak electron–ion collisions.

Linearizing the set of equations (7.1), (7.5), (7.6) over small perturbations in the form $\exp(\lambda x + \mathrm{i}k_\perp y)$, we obtain the following solvability condition of the linearized set of

equations:

$$\Lambda^2\left[1-\left(\frac{c_s}{V}\right)^2\right]+\frac{4}{3}\Lambda\left[1.9-\left(\frac{V'_T}{V}\right)^2\right]+1.6=0\,, \qquad (7.7)$$

where $\Lambda = \lambda V/[(k_\perp\rho_i)^2\nu_{ii}]$, and $V'_T = [(T_e + T_i)/m_i]^{1/2}$.

Equation (7.7) has two solutions, one of which is positive for $V < c_s$, which corresponds to a downstream enhancement in perturbations. If $V < V'_T$, only the effective mass is negative, while the effective heat capacity is positive (see Section 7.1.1). In this case, temperature variations affect the evolution of perturbations insignificantly. As $V \ll V'_T$, then, when approximate calculations are performed of the increment λ of a spatial increase in perturbations, the ion temperature can be considered not to be subject to perturbations. Also discarding the inertial term in the equation of motion yields

$$\lambda \approx k_\perp^2\,\frac{\eta_{\perp i}}{m_i n}\,\frac{V}{V'^2_T} = 1.2(k_\perp\rho_i)^2\nu_{ii}\,\frac{V}{V'^2_T}\,.$$

Naturally, this expression can also be obtained from formula (7.7).

In the other limiting case of $V \to c_s$, the increment increases indefinitely:

$$\lambda \approx \frac{4}{3}\,\frac{(k_\perp\rho_i)^2\nu_{ii}}{c_s}\,\frac{1.9-(V'_T/c_s)^2}{(c_s/V)^2-1}\,.$$

The instability increment increases as the spatial scale of perturbations, $\propto k_\perp^2$, decreases. Its value is limited by the applicability condition of the hydrodynamic approximation $k_\perp \ll \rho_i^{-1}$. Notice that this condition also permits neglecting the ion longitudinal viscosity and the ion longitudinal heat capacity in equations (7.5), (7.6).

The spatial instability considered is a consequence of the effective mass and effective heat conductivity of subsonic flows being negative. In a flow, the rate of which varies in the transverse direction, viscosity tends to slow the faster part of the flow and to accelerate the slower one. However, owing to the effective mass negativeness, the result of the action of viscosity will be opposite. A change of sign, not only of mass, but also of the viscosity coefficient, will also lead to the same consequences. Indeed, if the viscosity force, which in the case of small perturbations of the uniform stream has the form $F_{ex} = \eta_{\perp i}\Delta V$, is substituted for the external force in equation (7.4), and then this equation is divided by $1-(c_s/V)^2$, we obtain an equation of motion for a medium, the particles of which for $V < c_s$ have positive mass but a negative viscosity coefficient $\eta_{eff} = \eta_{\perp i}[1-(c_s/V)^2]^{-1}$.

In a similar manner, in flows with rates within the interval $V'_T < V < c_s$, a negative effective heat capacity coefficient or a negative coefficient of transverse heat conductivity, which is equivalent, instead of smoothing out, causes intensification of irregularities of the ion temperature profile.

Frequently, an exponential rise in parameters characterizing the state of a medium is a manifestation of its instability. Let us discuss how justified the introduction of the new term 'spatial instability' is with respect to the structure considered. Doubtless, instability can only develop in a nonequilibrium medium. Usually, a medium is called unstable if its eigen-oscillations are increasing with time. If at the boundary of such a medium an external source generates eigen-oscillations with a constant amplitude, then such oscillations will build up as they propagate in space. This situation differs from the one considered in the present article. We assume static perturbations to exist at the boundary of the plasma flow. This implies the presence of external bodies that are at rest in the laboratory reference system, with respect to which the plasma moves. The departure of a system from equilibrium is revealed only owing to the existence of external bodies — the sources of perturbations. A uniform stream left on its own is, naturally, stable in the conventional sense of this term — all eigen-oscillations of such a stream decay with time.

An essential condition of the spatial instability considered is the one-dimensional character of the motion of plasma particles due to the existence of a sufficiently strong magnetic field. The role of magnetic force lines for an ordinary gas can be assumed by a set of thin contiguous tubes. The walls of the tubes prevent the momentum from flowing transversely, but heat can be transported in the transverse direction. Therefore, conditions exist in the proposed system for the development of spatial instability due to the negativeness of the effective heat capacity (effective coefficient of heat conductivity). Naturally, when analyzing the issue of realizing such a system, it is necessary to take into consideration both the friction of the gas on the walls of the tubes and the penetration of heat flows through them.

7.1.3 Spatial evolution of Gaussian perturbations. If the shape of perturbations at the entrance to the system is not harmonic, it will change downstream. In Ref. [53], numerical analysis was performed of the spatial evolution of Gaussian perturbations. We note that the specific character of the spatial instability dealt with permits us to investigate it only within a limited interval of coordinate variations. Indeed, as follows from the expressions obtained in Section 7.1.2, the increment of instability increases as the characteristic spatial scale of perturbations, $\lambda \propto k_\perp^2$, decreases. However, uncontrollable small-scale perturbations are introduced in the course of any numerical calculations, which are due to space discretization and limited calculation accuracy.

The SNF ICR plasma processing systems we are interested in can be subject to the instability considered. In these systems, ICR heating of the plasma flow must be completed during a passage of the flow through the quite extended segment of a homogeneous or weakly inhomogeneous magnetic field. The plasma flow has a complex ion content, and the fraction of ions that are to be heated is small, so the main part of ions remains cold; their behavior can be examined within the framework of hydrodynamics.

Reference [53] reported on a uranium plasma flow in a magnetic field $B_0 = 15$ kG; the plasma density was $n_0 = 10^{13}$ cm^{-3}, and the temperatures were $T_i = 1$ eV, $T_e = 3$ eV. The choice of calculation parameters was due to the necessity of satisfying the applicability conditions of the hydrodynamic approximation.

Owing to the change of sign of the effective heat capacity at $V = V'_T$, flows were considered with rates both superior and inferior to this value. Calculations were performed for three values of the initial flow rate: $V_0 = [(T_e + 2T_i/3)/m_i]^{1/2}$, $V_0 = [(T_e + T_i)/m_i]^{1/2}$, and $V_0 = [(T_e + 4T_i/3)/m_i]^{1/2}$, which were smaller than the propagation velocity of an acoustic signal, $c_s = [(T_e + 5T_i/3)/m_i]^{1/2}$.

Figure 20 illustrates the spatial evolution of initial velocity perturbations $V_1(y) = 10^{-2}V_0\exp(-y^2/a^2)$ (dotted curve in Fig. 20a); the plasma density and the ion temperature were considered nonperturbed at $x = 0$. The distance at which the

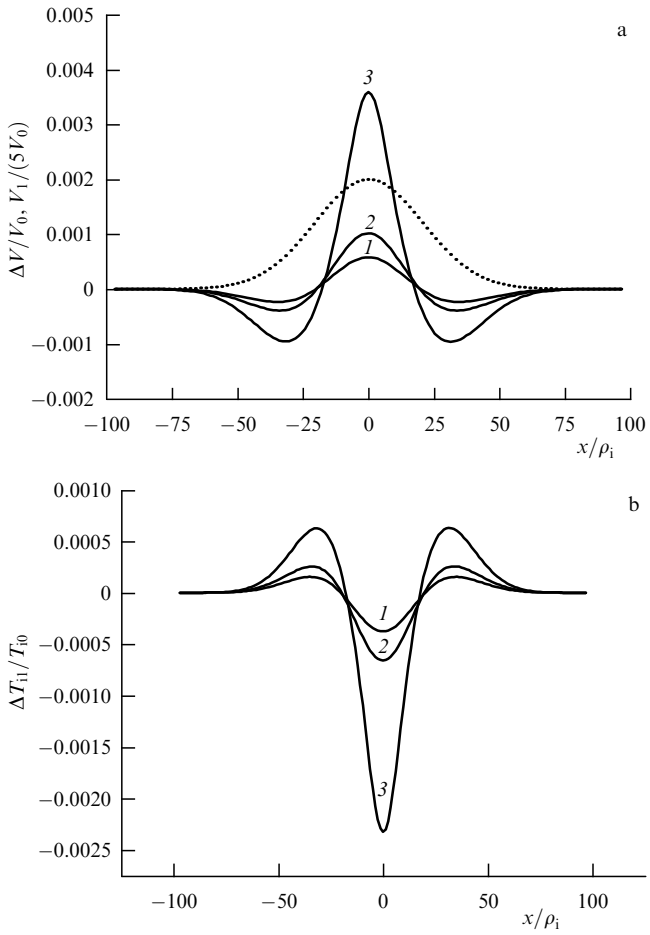

Figure 20. Change in parameters of plasma flow in the case of velocity perturbation $V_1(0, y) = 10^{-2} V_0 \exp(-y^2/a^2)$: (a) velocity, and (b) ion temperature. Curves *1* — $V_0 = [(T_e + 2T_i/3)/m_i]^{1/2}$, curves *2* — $V_0 = [(T_e + T_i)/m_i]^{1/2}$, curves *3* — $V_0 = [(T_e + 4T_i/3)/m_i]^{1/2}$, dotted curve — velocity perturbation at entrance to the system. Distance from the entrance to the system is $x = 0.5$ cm.

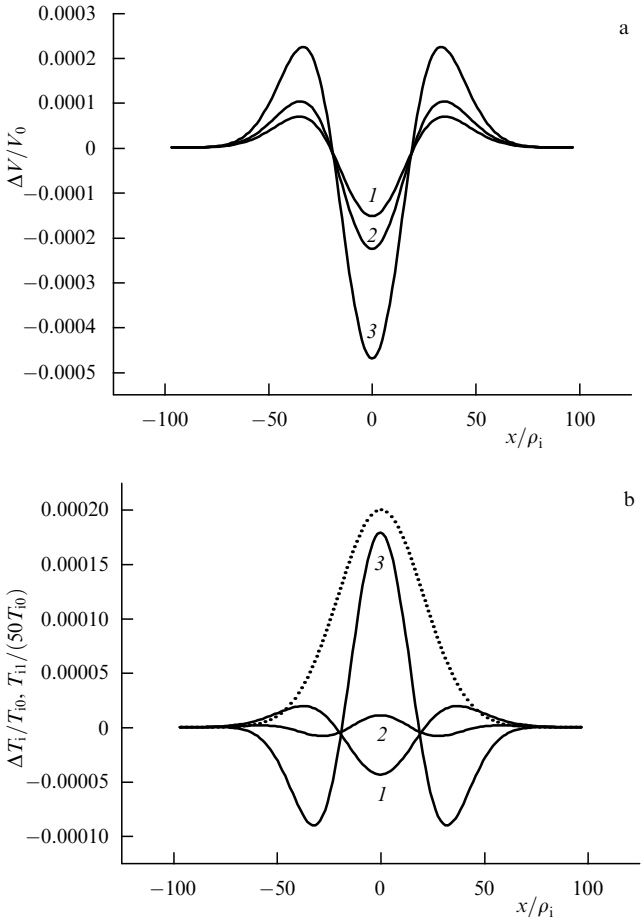

Figure 21. Variation of plasma flow parameters in the case of ion temperature perturbation $T_{i1}(0, y) = 10^{-2} T_{i0} \exp(-y^2/a^2)$: (a) velocity, and (b) ion temperature. Curves *1* — $V_0 = [(T_e + 2T_i/3)/m_i]^{1/2}$, curves *2* — $V_0 = [(T_e + T_i)/m_i]^{1/2}$, curves *3* — $V_0 = [(T_e + 4T_i/3)/m_i]^{1/2}$, dotted curve — ion temperature perturbation at entrance to the system. Distance from the entrance to the system is $x = 0.5$ cm.

numerical instability indicated above has no time to manifest itself is not large. The interval considered in calculations was (0, 0.5 cm). At such distances, the variations in plasma parameters are small. To render them more illustrative, Figs 20 and 21 show, instead of the actual parameters, their variations $\Delta V = V - V_0$, $\Delta T_i = T_i - T_{i0}$. Referring to Fig. 20a, it is seen that, as the flow moves, the velocity perturbations tend to contract to the center, where the flow accelerates due to a slowing down of the peripheral regions. Sharpening of the velocity profile enhances the momentum exchange between different perturbation regions owing to viscosity, which accelerates the rise in perturbations — the spatial instability increment increases as the transverse scale of perturbations decreases (see Section 7.1.2). Notice that in accordance with the results presented in Section 7.1.2, the rate of perturbation evolution increases with the flow rate.

Although the ion temperature and plasma density at the entrance of the system are not considered to be perturbed, the change in velocity along the flow entails a change in the parameters indicated and, owing to the dependences $n = C_1/V$, $T \approx C_2/V^{2/3}$ (see Section 7.1.1), the density and ion temperature vary opposite toward the velocity. The relative perturbations in the plasma density are about one and a half times greater than the relative perturbations in ion temperature, but the shape of these perturbations is practically the same. Therefore, we only demonstrate the variation in ion temperature (Fig. 20b).

As pointed out in Section 7.1.1, when analyzing the dynamics of a subsonic flow, one can consider the effective heat capacity or the effective coefficient of heat conductivity, which is equivalent, to be negative for $c_s > V > V'_T$. Therefore, if the ion temperature at the entrance to the system is perturbed, the perturbation profile will become more sharp as $V > V'_T$ and smooth out when $V < V'_T$. This conclusion is confirmed by Fig. 21a, in which the dependences of the ion temperature on the transverse coordinate are presented at $T_{i1}(y, 0) = 10^{-2} T_{i0} \exp(-y^2/a^2)$, $V_1(y, 0) = n_1(y, 0) = 0$ at the same distance ($x = 0.5$ cm) from the entrance to the system as in the case illustrated in Fig. 20.

It should be noted that within the framework of the hydrodynamic approximation adopted by us, owing to the influence of viscosity, the subsonic flow is unstable relative to harmonic perturbations both for $V > V'_T$ and for $V < V'_T$, independently of the transverse wavenumber value (Fig. 21b). Therefore, the smearing of temperature perturbations over small distances for $V < V'_T$ should be considered to be due to the interference between harmonic components correlated in a certain manner. However, at a sufficient distance from the

entrance to the system, the most rapidly increasing components will separate from the initial perturbation, and they will determine the evolution of perturbations. Regretfully, the computational difficulties mentioned in Section 7.1.3 impede performing an analysis of this process.

The issue of what the development of spatial instability may lead to is quite intricate. From the heat balance equation for ions it follows that, owing to the existence of viscosity, the ion thermal energy increases downstream along the flow [see the last term in the right-hand side of equation (7.6)]. The increase in ion temperature should reduce the increment of instability, while an increase in pressure $(p = n(T_\mathrm{i} + T_\mathrm{e}))$ reduces the flow rate. It cannot be excluded that a stationary state might be achieved in a system of small length. On the other hand, enhancement of the inhomogeneity of flow parameters in extended systems caused by spatial instability may lead to the excitation of plasma eigen-oscillations. In this case, the arising fluctuating electric fields penetrate into the plasma source and may alter its state in such a way that the plasma flow rate at the exit from the source exceeds the velocity of sound. Such a flow would be stable with respect to transverse stratification. The spatial evolution of supersonic flows is examined in Section 7.2.2.

7.2 Shock waves in supersonic plasma flows

7.2.1 Basic equations and boundary conditions. Longitudinal stratification, as opposed to transverse stratification peculiar to subsonic flows, is characteristic of supersonic plasma flows moving along magnetic fields. Therefore, we shall describe the state of such a flow by a set of one-dimensional hydrodynamic equations (see, for example, review [50]):

$$\frac{\mathrm{d}}{\mathrm{d}x}\, nV = 0\,, \tag{7.8}$$

$$m_\mathrm{i} nV\,\frac{\mathrm{d}}{\mathrm{d}x}\,V + \frac{\mathrm{d}}{\mathrm{d}x}\,n(T_\mathrm{i} + T_\mathrm{e}) = \frac{4}{3}\,\frac{\mathrm{d}}{\mathrm{d}x}\,\eta_\mathrm{i}\,\frac{\mathrm{d}}{\mathrm{d}x}\,V\,, \tag{7.9}$$

$$\frac{3}{2}\,nV\,\frac{\mathrm{d}}{\mathrm{d}x}\,T_\mathrm{i} + nT_\mathrm{i}\,\frac{\mathrm{d}}{\mathrm{d}x}\,V = \frac{4}{3}\,\eta_\mathrm{i}\left(\frac{\mathrm{d}V}{\mathrm{d}x}\right)^2 + \frac{\mathrm{d}}{\mathrm{d}x}\,\kappa_\mathrm{i}\,\frac{\mathrm{d}}{\mathrm{d}x}\,T_\mathrm{i}\,, \tag{7.10}$$

$$\frac{3}{2}\,nV\,\frac{\mathrm{d}}{\mathrm{d}x}\,T_\mathrm{e} + nT_\mathrm{e}\,\frac{\mathrm{d}}{\mathrm{d}x}\,V = \frac{\mathrm{d}}{\mathrm{d}x}\,\kappa_\mathrm{e}\,\frac{\mathrm{d}}{\mathrm{d}x}\,T_\mathrm{e}\,. \tag{7.11}$$

Here, $\eta_\mathrm{i} = 1.5\times10^{-12} nT_\mathrm{i}/\nu_\mathrm{ii}$, $\kappa_\mathrm{i} = 6.2\times10^{-12} nT_\mathrm{i}/(m_\mathrm{i}\nu_\mathrm{ii})$, and $\kappa_\mathrm{e} 5.1\times10^{-12} nT_\mathrm{e}/(m_\mathrm{e}\nu_\mathrm{ei})$ are the coefficients of ion viscosity, ion heat conductivity, and electron heat conductivity, respectively, $\nu_\mathrm{ii} = 1.8\times10^{-6}\, n/(A^{1/2}T_\mathrm{i}^{3/2})$, $\nu_\mathrm{ei} = 2.9\times10^{-5}\, n/T_\mathrm{e}^{3/2}$, temperature is expressed in electron-volts, and the remaining quantities are given in CGSE units (absolute electrostatic system of units).

The simplest state described by the set of equations (7.8)–(7.11) is a homogeneous flow, all the parameters of which are kept constant along its path. In numerical simulations of this state or of states close to it, difficulties arise that are due to the instability of the corresponding solution (spatial instability). For the investigation of spatial instability, we shall consider the perturbation of a uniform stream, assuming the form $\propto \exp(\lambda x)$. Linearization of the set of equations (7.8)–(7.10) leads to the following equation for λ:

$$\frac{4}{3}\,\alpha\beta\lambda^2 - V\left[2\alpha + \left(1 - \frac{V_{T_\mathrm{i}}^2}{c_\mathrm{s}^2}\right)\beta\right]\lambda + \frac{3}{2}(V^2 - c_\mathrm{s}^2) = 0\,, \tag{7.12}$$

where $\alpha = \eta_\mathrm{i}/(m_\mathrm{i}n)$, $\beta = \kappa_\mathrm{i}/n$, $V_{T_\mathrm{i}}^2 = (T_\mathrm{i} + T_\mathrm{e})/m_\mathrm{i}$, and $c_\mathrm{s}^2 = (5T_\mathrm{i}/3 + T_\mathrm{e})/m_\mathrm{i}$. Equation (7.11) has been excluded from our consideration, since, owing to the high electron heat conductivity, the electron temperature may be considered constant in the cases of practical interest (see Section 7.2.2).

We shall restrict ourselves to considering flows with rates close to the speed of sound, $V \approx c_\mathrm{s}$. In this case, from (7.12) we obtain

$$\lambda_1 \approx \frac{3}{2}\,\frac{V - c_\mathrm{s}}{\alpha + \beta v_{T_\mathrm{i}}^2/(3c_\mathrm{s}^2)}\,, \qquad \lambda_2 \approx \frac{3}{2}\,\frac{\alpha + \beta v_{T_\mathrm{i}}^2/(3c_\mathrm{s}^2)}{\alpha\beta}\,,$$

where $v_{T_\mathrm{i}}^2 = T_\mathrm{i}/m_\mathrm{i}$. The positive values of λ_1 for $V > c_\mathrm{s}$ and of λ_2, independently of the relation between V and c_s, testify to a downstream increase in perturbations (spatial instability). The expression for λ_1, which does not go beyond the limits of the hydrodynamic approximation ($\lambda_1 l_\mathrm{i} \ll 1$, where l_i is the ion mean free path), describes, as we shall see in Section 7.2.2, the precursor of a shock wave (SW). At the same time, the hydrodynamic approximation is violated for the second solution ($\lambda_2 l_\mathrm{i} \approx 1$). To discard this fictitious instability, we take advantage of the fact that in the hydrodynamic approximation at a plasma flow rate on the order of the ion thermal velocity the right-hand side of equation (7.10), taking into account dissipative effects, is much smaller than the left-hand side; therefore, it can be considered as a small correction within the framework of the method of successive approximations. Such an approach to equation (7.9) would not be correct, since in the approximation of ideal hydrodynamics the left-hand side of equation (7.9) vanishes if the plasma flow rate turns out to be equal to the speed of sound.

In the right-hand side of equation (7.10), setting

$$\frac{\mathrm{d}T_\mathrm{i}}{\mathrm{d}x} = -\frac{2}{3}\,\frac{T_\mathrm{i}}{V}\,\frac{\mathrm{d}V}{\mathrm{d}x}\,,$$

we reduce it to the form

$$\frac{\mathrm{d}T_\mathrm{i}}{\mathrm{d}x} + \frac{2}{3}\,\frac{T_\mathrm{i}}{V}\,\frac{\mathrm{d}V}{\mathrm{d}x} \approx \frac{4}{9}\,\frac{\kappa_\mathrm{i}T_\mathrm{i}}{nV^2}\left(\frac{10}{3}\,\frac{1}{V}\left(\frac{\mathrm{d}V}{\mathrm{d}x}\right)^2 - \frac{\mathrm{d}^2V}{\mathrm{d}x^2}\right) + \frac{8}{9}\,\frac{\eta_\mathrm{i}}{nV}\left(\frac{\mathrm{d}V}{\mathrm{d}x}\right)^2. \tag{7.13}$$

The set of equations (7.8), (7.9), (7.11), (7.13) is equivalent to six first-order equations for the quantities n, V, $\mathrm{d}V/\mathrm{d}x$, T_i, T_e, $\mathrm{d}T_\mathrm{e}/\mathrm{d}x$. To obtain an unambiguous solution for this set of equations, the same number of boundary conditions is required. In a consistent theory, the values of the main plasma flow parameters (density, rate, electron and ion temperatures) at the entrance to the SNF processing system should be determined from an ionization analysis of the SNF matter in the plasma source. Such an analysis has not been performed; however, the source of SNF plasma will be apparently similar to the sources of metal plasma in ICR isotope separation systems, the plasma in which was created with the following parameter values (by order of magnitude): $n \approx 10^{12}$ cm^{-3}, $T_\mathrm{e} \approx 3$ eV, $T_\mathrm{i} \approx T_\mathrm{e}/2$, and $V \approx c_\mathrm{s}$ [22]. Precisely such a plasma will be considered below.

One more boundary condition can be obtained by analyzing the process of electron escape from the ICR heating system to the receiving plate. As is well known, a so-called Langmuir layer arises in the vicinity of the surface where the plasma is lost. The potential jump in this layer levels the electron and ion fluxes onto the absorbing surface, which is necessary for maintaining the plasma quasineutrality. The magnitude of the jump is given by the expression (see, for

example, Ref. [54])

$$\Delta\varphi = \frac{T_e}{2e} \ln\left(\frac{1}{2\pi}\frac{m_i}{m_e}\frac{T_e}{m_i V^2}\right).$$

If the plasma flow rate is equal to the propagation velocity of an ion-acoustic signal (see Section 7.2.2), then one arrives at

$$\Delta\varphi = \frac{T_e}{2e} \ln\left[\frac{1}{2\pi}\frac{m_i}{m_e}\tau_e\left(1+\frac{3}{5}\tau_e\right)^{-1}\right], \tag{7.14}$$

where $\tau_e = T_e/T_i$. Setting the ion mass number to $A = 240$, and $\tau_e = 2$, we obtain $\Delta\varphi \approx 5.3T_e/e$.

Only the most energetic electrons from the 'tail' of the Maxwellian distribution over longitudinal velocities are able to leave the plasma for the receiving plate. The energy needed for overcoming the barrier of the electric potential is supplied to the Langmuir layer owing to heat conductivity and to the convective heat flux.

The energy flux of particles of the kind $j = \mathrm{e}, \mathrm{i}$ is given by the expression (see, for example, Ref. [50])

$$S_j = \frac{1}{2} m_j n V^3 + \frac{5}{2} n V T_j - \kappa_j \frac{\mathrm{d}T_j}{\mathrm{d}x} - \frac{4}{3}\eta_j V \frac{\mathrm{d}V}{\mathrm{d}x}. \tag{7.15}$$

In evaluating the electron heat flux, the first and last terms in the right-hand side of Eqn (7.15) can be dropped. Equating the electron energy flux S_e to the energy lost by electrons escaping to the receiving plate, $S'_e = nV(e\Delta\varphi + T_e)$, we obtain the second boundary condition:

$$\kappa_e \frac{\mathrm{d}T_e}{\mathrm{d}x} + nV\left(e\Delta\varphi - \frac{3}{2}T_e\right) = 0, \tag{7.16}$$

where $\Delta\varphi$ is given by expression (7.14).

We shall see in Section 7.2.2 that the remaining boundary condition for the velocity or its derivative exerts a decisive influence on the character of the solution.

7.2.2 Shock waves and the spatial instability of supersonic plasma flows. The behavior of a plasma flow moving along a strong magnetic field is similar to that of a one-dimensional flow of compressible gas. This is clear from the similarity of the considered set of equations and the set of equations describing the behavior of a gas flow (see, for example, Ref. [55]). As is well known, the rate of a supersonic gas flow drops spontaneously to a subsonic rate owing to the origination of shock waves. Precisely in the same way, SWs arise in plasma flows if their velocity exceeds the ion-acoustic velocity. The results of calculations presented in Fig. 22 show that the ion-acoustic velocity is indeed a threshold velocity for the SW origin. When $V_0 < c_s$, the influence of $\mathrm{d}V_0/\mathrm{d}x$ variations on the $V(x)$ profile is extremely weak. Thus, the dependences obtained for different signs of $\mathrm{d}V_0/\mathrm{d}x$, but for the same absolute value of this quantity, cannot be distinguished from each other in Fig. 22 (see curve *1*). If $V_0 > c_s$, a change in the sign of $\mathrm{d}V_0/\mathrm{d}x$ alters the character of the $V(x)$ dependence drastically. Thus, if $\mathrm{d}V_0/\mathrm{d}x < 0$, an SW originates (curve *2*), while when $\mathrm{d}V_0/\mathrm{d}x > 0$, the velocity rises sharply (curve *3*) and the solution goes beyond the applicability limits of the hydrodynamical approximation. The last case will be further analyzed.

It should be noted that in the case of moderate rates of the incoming flow, $V - c_s \leqslant c_s$, the SW characteristic spatial scale Δx is expressed as $\Delta x \approx l_i c_s/(V - c_s)$, where l_i is the ion mean free path (see, for example, Ref. [55] and also below). If $V - c_s \ll c_s$, Δx is significantly superior to l_i. In this case, the quite smooth transition of the supersonic plasma flow to the subsonic flow can only arbitrarily be called an SW; however, only such a transition can be described by the equations of hydrodynamics.

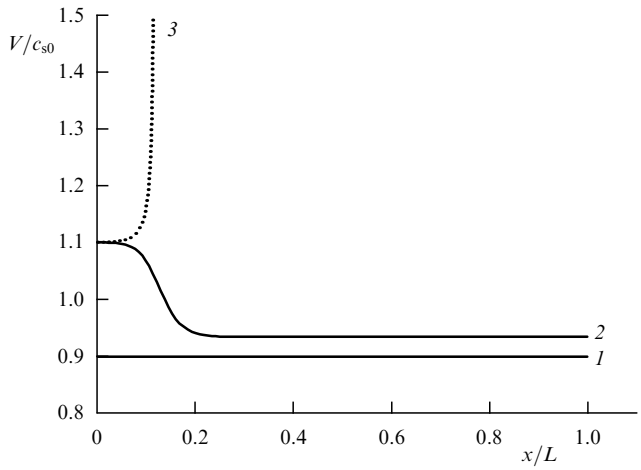

Figure 22. Plasma velocity profiles for $V \approx c_s$: curve *1* — $V_0/c_{s0} = 0.9$, $|\mathrm{d}V_0/\mathrm{d}x| = 10^{-2}V_{00}/L$; curve *2* — $V_0/c_{s0} = 1.1$, $\mathrm{d}V_0/\mathrm{d}x = -10^{-2}V_{00}/L$, and curve *3* — $V_0/c_{s0} = 1.1$, $\mathrm{d}V_0/\mathrm{d}x = 10^{-2}V_{00}/L$; $V_{00} = (2T_e/m_i)^{1/2}$, and $L = 3$ m.

The parameters of a flow that has passed through an SW can be related, as in the case of ordinary gas, to the surging flow parameters with the aid of ion mass, momentum, and energy conservation laws:

$$n_0 V_0 = n_1 V_1, \tag{7.17}$$

$$n_0\left(V_0^2 + \frac{T_{i0} + T_e}{m_i}\right) = n_1\left(V_1^2 + \frac{T_{i1} + T_e}{m_i}\right), \tag{7.18}$$

$$V_0^2 + 5\frac{T_{i0}}{m_i} - 2\frac{T_e}{m_i}\ln V_0 = V_1^2 + 5\frac{T_{i1}}{m_i} - 2\frac{T_e}{m_i}\ln V_1. \tag{7.19}$$

Here, account has been taken of the fact that at sufficiently large distances from the SW and on both sides of it the flow is uniform, the subscript 0 indicates values of quantities in front of the SW, and the subscript 1 points to quantities behind the SW. Owing to the high electron heat conductivity, the electron temperature is considered not to alter within the SW boundaries. We also assume the electron distribution function to be close to equilibrium one — to the Boltzmann distribution function. In this case, the plasma density jump in the SW will be accompanied by a jump in the electric potential, $\Delta\varphi \approx (T_e/e)\ln(n_1/n_0)$. The energy spent by ions in overcoming the electric potential barrier is given by the expression [see the last terms in both parts of Eqn (7.19)]

$$A = T_e \int^x \mathrm{d}x\, V \frac{\mathrm{d}n}{\mathrm{d}x} = T_e n V \ln\frac{V_0}{V_1}.$$

Relationships (7.17)–(7.19) are valid independently of the values of $V_0 > c_s$, while the set of hydrodynamic equations holds valid only if $V_0 - c_s \ll c_s$. Figure 23 demonstrates that the hydrodynamical approximation provides good accuracy for V_0 values right up to $V_0 \approx (1.5-2.0)c_s$.

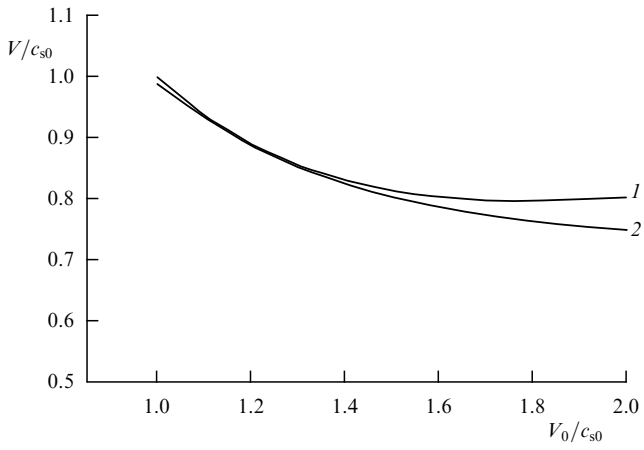

Figure 23. The rate of plasma flow abandoning the SW vs. the incoming flow rate: curve *1* — calculation based on conservation laws, and curve *2* — calculation with the aid of hydrodynamical equations.

The dependences obtained in this approximation at $V_0 = 1.5c_s$ are presented in Fig. 24. The region of drastic transition from the supersonic to the subsonic flow — the SW — stands out quite clearly in Fig. 24a. Figure 24b shows that, as assumed above, the electron temperature within the system boundaries varies little, while within the SW boundaries it is practically constant. The dependences plotted in Fig. 24 were obtained at $\mathrm{d}V_0/\mathrm{d}x = -10^2 V_{00}/L$.

If $\mathrm{d}V_0/\mathrm{d}x > 0$, the spatial structure of the solutions to hydrodynamic equations differs drastically from the structure represented by curves *2* in Figs 22 and 24c. When $\mathrm{d}V_0/\mathrm{d}x > 0$, both the plasma flow rate and the ion temperature increase downstream (see curve *3* in Fig. 22). The characteristic spatial scale of the solution reduces in the same direction. As a result, the hydrodynamical approximation is violated at a relatively small distance from the entrance.

We shall try to clarify the meaning of the results obtained. Integrating equation (7.15) over x, we obtain

$$m_i n V^2 + p - \frac{4}{3}\,\eta_i\,\frac{\mathrm{d}V}{\mathrm{d}x} = \mathrm{const}\,. \tag{7.20}$$

In accordance with the applicability condition of the hydrodynamical approximation, the velocity difference $V - c_s = \delta V$ will be considered small compared to the velocity of sound, c_s. We the aid of equations (7.8) and (7.13), we represent the plasma pressure in the form

$$p = p_0 - m_i n_0 c_{s0}^2\,\frac{\delta V}{V_0} + \frac{20}{9}\left(1 + \frac{9}{20}\,\tau_e\right) n_0 T_{i0}\left(\frac{\delta V}{V_0}\right)^2 - \frac{4}{9}\,\frac{\kappa_{i0} T_{i0}}{V_0^2}\,\frac{\mathrm{d}}{\mathrm{d}x}\,\delta V\,, \tag{7.21}$$

where $\tau_e = T_e/T_{i0}$.

In formula (7.21), terms that are quadratic in the small quantity $\delta V/V_0$ are taken into account, since when the difference $V_0 - c_s$ is small, weak dissipative and nonlinear effects become essential. The quantity T_e is considered constant (see above). The source is assumed to be situated at $x = -\infty$, where the plasma flow is uniform. Under this condition, equation (7.20) reduces to the form

$$(\delta V)^2 + \alpha(V_0 - c_s)\,\delta V - \beta\,\frac{\mathrm{d}}{\mathrm{d}x}\,\delta V = 0\,, \tag{7.22}$$

where

$$\alpha = \frac{3}{2}\,\gamma\,, \qquad \beta = \frac{\eta_{i,\mathrm{eff}}\,\gamma}{m_i n_0}\,, \qquad \gamma = \frac{1 + 3\tau_e/5}{1 + 9\tau_e/20}\,,$$

$$\eta_{i,\mathrm{eff}} = \eta_{i0} + \frac{1}{5}\,\frac{m_i \kappa_{i0}}{1 + 3\tau_e/5}\,.$$

Equation (7.22) has a solution describing a stationary SW in an infinite spatial interval (see, for example, Ref. [55]):

$$\delta V = -\frac{\Delta V}{2}\left(1 + \tanh\frac{x}{\Delta x}\right), \tag{7.23}$$

where the x-coordinate is reckoned from the SW center (the point at which the value of $|\mathrm{d}V/\mathrm{d}x|$ is maximum), and

$$\Delta V = \frac{3}{2}(V_0 - c_s)\,\gamma\,, \qquad \Delta x = \frac{4}{3}\,\frac{\eta_{i,\mathrm{eff}}}{m_i n_0}\,\frac{1}{V_0 - c_s}\,.$$

The expression $V(x) = V_0 + \delta V(x)$, where $\delta V(x)$ is determined by formula (7.23), describes the transition of the flow rate from its initial value V_0 to the final value $V_1 = V_0 - \Delta V$:

$$V \approx \begin{cases} V_0 - \Delta V \exp\dfrac{2x}{\Delta x}\,, & x \to -\infty\,, \\ V_1 + \Delta V \exp\left(-\dfrac{2x}{\Delta x}\right), & x \to \infty\,. \end{cases} \tag{7.24}$$

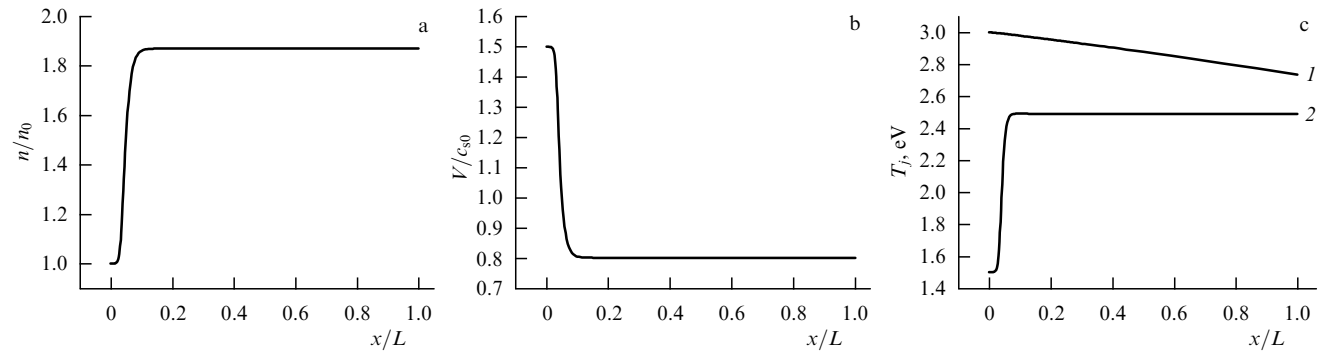

Figure 24. Profiles of plasma flow parameters at $V_0/c_{s0} = 1.5$: (a) plasma density, (b) rate, and (c) electron temperature (curve *1*) and ion temperature (curve *2*).

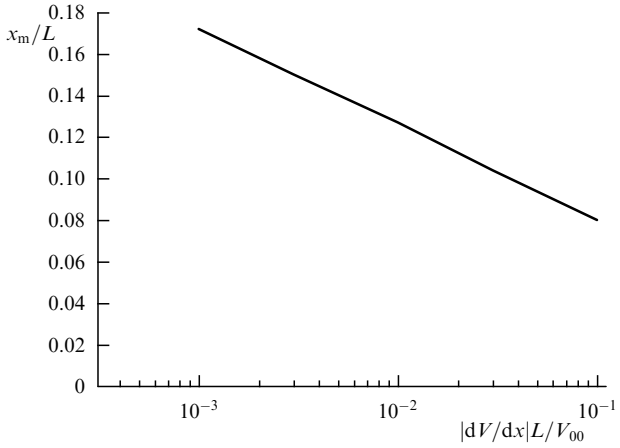

Figure 25. SW position vs. condition on the boundary.

In accordance with expression (7.23), (7.24), in the region $x < 0$ there is a uniform flow, upon which a small perturbation increasing downstream is imposed. When the perturbation amplitude becomes comparable to the difference $V - c_s$, nonlinear effects, restricting the perturbation, come into action — an SW arises.

For this solution to be applicable in the case of systems of a finite length, it is necessary for the plasma flow to slow down at the entrance to the system ($d\delta V/dx < 0$). The slowdown may be caused by friction on neutral atoms. For this purpose, it is also possible to use a wire lattice. The distance between the source of perturbation at the entrance and the SW (the region of the largest velocity gradient) depends logarithmically on the amplitude of the initial perturbation, $\propto \ln(V_0/|\delta V_0|)$ (Fig. 25). The smaller the value of $|dV/dx|$ at the entrance to the system, the farther the SW is from the entrance. In sufficiently short systems, the SW will have no time to originate and the perturbation will depend exponentially on the coordinate.

The spatial dependence of δV can be determined for its small values from equations (7.20), (7.22) by their linearization over small perturbations. Such an approach leads to the following result (compare with formulas (7.24) in the region $x < 0$):

$$V(x) \approx V_0 + C \exp \frac{2x}{\Delta x}\,, \tag{7.25}$$

where C is an arbitrary constant, and $\Delta x = 2\lambda_1$ (see Section 7.2.1).

When $C = -\Delta V$, expression (7.25) coincides with the solution of equation (7.22) describing SW in the region $x < 0$, $|x| \gg \Delta x$.

We shall now clarify the meaning of solution (7.25) for $C > 0$. It describes a plasma flow, the rate of which increases downstream (see curve *3* in Fig. 22). The plasma flow considered is close to adiabatic one (see above) under the applicability condition of the hydrodynamical approximation, and acceleration is achieved mainly by the downstream drop in the plasma pressure. However, the influence of viscosity turns out to be decisive in this process — the energy flux is maintained constant precisely owing to viscosity. The term that takes viscosity into account in expression (7.15) is negative when $dV/dx > 0$, and it describes the upstream energy transfer. Momentum transfer in the same direction is also due to viscosity. Such a motion, corresponding to the sign of $C > 0$ in formula (7.25), requires the maintenance of specific conditions at the receiving plate, and such motion is apparently difficult to realize. The case of $C < 0$, when formula (7.25) describes an exponentially rising SW precursor, is more realistic. We also note that, when $dV/dx > 0$, as the flow accelerates the characteristic scale of velocity variation decreases (see Fig. 22), and the solution rapidly goes beyond the limits of the hydrodynamical approximation.

There are numerous examples in physics showing that stationary perturbations exponentially decrease with the distance from a certain body that constitutes their source. In this case, the term 'spatial instability' is inappropriate in spite of the exponential increase in perturbations as their source is approached. In the problem we are interested in, such a situation arises if $dV/dx|_{x=0} > 0$, when the exponential downstream increase in perturbations is due to energy being pumped into the plasma at the receiving plate (see above). However, if $dV/dx|_{x=0} < 0$, the receiving plate is passive, while the region of exponential growth of perturbations is restricted by the SW which is itself 'attached' to the source of perturbations at the entrance to the system.

The analysis performed shows that if the plasma flow rate at the entrance to the system is significantly higher than the velocity of sound, then, upon covering a small distance, the flow becomes subsonic owing to the formation of an SW. Meanwhile, as shown in Section 7.1, the spatial instability of subsonic flows leads to their transverse stratification. It is well known that stratified flows are not stable relative to the setup of eigen-oscillations.

Thus, we arrive at the conclusion that a plasma flow will be laminar if its velocity at the entrance to the system is a little superior to the velocity of sound. Then, an SW will not have time to originate within the limits of the system, and the flow rate will change insignificantly under the action of longitudinal viscosity and heat conductivity.

8. Conclusion

For SNF plasma processing, it is necessary to ionize it, to separate NA ions from NF ions, and, finally, to accumulate them at different collectors. From experiments on ICR isotope separation, it follows that the problems of creating a plasma of the metals making up the main part of SNF matter and of ion collection can, in principle, be resolved.

In the present article, it is shown how specific features of the mass distribution of SNF elements affect the separation process of NA ions from NF ions. The parameters of the devices required for this purpose are conventional for a modern plasma experiment. This conclusion is made under the assumption of a sufficiently small fraction of doubly charged ions in the SNF plasma, which is in agreement with the results of experiments on ICR isotope separation. Naturally, applying the results of these experiments as a base does not deliver one from the necessity of theoretical and experimental investigation of the processes of SNF plasma formation, including control of the charge multiplicity of ions and their collection. The theoretical results presented in this article also require experimental confirmation. SNF matter is radioactive, so all manipulation of it must be remote. In spite of the fact that implementation of the idea of plasma processing requires a large volume of technical development work and physical investigations, the stimulus for realizing this idea is the possibility of significantly

reducing the amount of detrimental waste from that produced in chemical processing.

Acknowledgments
The author gratefully acknowledge V P Smirnov for initiating the investigation of the problem of SNF processing, and also thank V A Zhiltsov and A A Skovoroda for many helpful discussions.

This work was supported by grant NSh-4361.2012.2 of the President, Russian Federation for State Support of Leading Scientific Schools.

Amendment to Russian edition

When analyzing the spatial structure of plasma flows in Section 7, we introduced the notion of spatial instability. It is applied to static perturbations that increase downstream along the flow. The legitimacy of using this term may be validated considering static perturbations as the limits for exponentially varying in time perturbations $\propto \exp(-\mathrm{i}\omega t)$ when $\omega \to 0$. A method is known [see, for example, A I Akhiezer et al. *Elektrodinamika Plazmy* (Plasma Electrodynamics) (Moscow: Nauka, 1974)] that permits, when $\omega \neq 0$, separating the instability phenomenon from the so-called opacity of oscillations. In the latter case, the downstream increase in perturbations along the flow is not due to their enhancement upon excitation at the entrance to the system, but to a weakening in the opposite direction, when their excitation occurs at the exit of the system. The examples of 'spatial instability' presented in Section 7 are precisely of the latter kind.

Thus, the plasma flow along a magnetic field was considered in Section 7.1 taking into account the transverse ion viscosity and heat conductivity. If the flow rate V is small compared to the velocity of sound V_s, then the ion heat conductivity in the case of the perturbations dealt with is insignificant, and, for simplicity, they can be considered to be isothermic. Here, the frequency dependence of the longitudinal wavenumber of oscillations assumes the form

$$k_\pm(\omega) = \frac{-(\omega + \mathrm{i}\chi/2)V \pm \mathrm{i}(\chi^2 V^2/4 - \mathrm{i}\omega\chi V_\mathrm{s}^2 - \omega^2 V_\mathrm{s}^2)^{1/2}}{V_\mathrm{s}^2 - V^2},$$

where the quantity χ accounts for the transverse viscosity coefficient $\chi = \mu k_\perp^2$, μ is the kinematic viscosity coefficient, and $k_\perp$ is the transverse wavenumber.

From the expression for the longitudinal wavenumber $k_\pm$, it follows that, as $\gamma \to \infty$, the spatial dependence of perturbations takes the form

$$\tilde{V}_\pm \propto \exp\left(\mathrm{i}k_\pm(\omega)x\right) \approx \exp\left(\frac{\gamma}{\mp V_\mathrm{s} - V}\, x\right).$$

Thus, in the case dealt with in Section 7.1 ($V_\mathrm{s} > V$), in accordance with the known criterion, perturbations $\tilde{V}_+$ decreasing downstream along the flow must be excited at the entrance to the system (small values of x), whereas the rising $\tilde{V}_-$ are excited at the exit (large x values). In the static limit ($\omega \to 0$), precisely the latter increase along the plasma flow:

$$\tilde{V}_- \propto \exp\left(\frac{\chi V}{V_\mathrm{s}^2 - V^2}\, x\right),$$

and, consequently, are due to 'opacity'.

Similar results can also be obtained for the 'precursor' of a shock wave considered in Section 7.2.

Hence, the phenomena called spatial instability in Section 7 are actually caused by 'opacity'.

References

1. Lopatkin A V et al., in *Yadernyi Toplivnyi Tsikl. Nauchnaya Konf. Minatoma RF, Moskva, Iyun' 2000* (Nuclear Fuel Cycle. Scientific Conf. Minatom RF, Moscow, June 2000) (Moscow: Russian Federation Ministry for Atomic Energy, 2001) p. 65
2. Ohkawa T, Miller R L *Phys. Plasmas* **9** 5116 (2002)
3. Cluggish B P et al. *Phys. Plasmas* **12** 057101 (2005)
4. Fetterman A J, Fisch N J *Phys. Plasmas* **18** 103503 (2011)
5. Kovtun Yu V, Skibenko E I, Yuferov V B *Vopr. Atom. Nauki Tekh. Ser. Fiz. Radiatsionnykh Povrezhdenii Radiatsionnoe Materialoved.* (1 – 2) 149 (2008)
6. Skibenko E I et al. *Tech. Phys.* **54** 1380 (2009); *Zh. Tekh. Fiz.* **79** (9) 138 (2009)
7. Fetterman A J, Fisch N J *Phys. Plasmas* **18** 094503 (2011)
8. Volosov V I *Plasma Phys. Rep.* **23** 751 (1997); *Fiz. Plazmy* **23** 811 (1997)
9. Fetterman A J, Fisch N J *Plasma Sources Sci. Technol.* **18** 045003 (2009)
10. Smirnov V P et al., in *Fiziko-Khimicheskie Protsessy pri Selektsii Atomov i Molekul: Sb. Dokladov IX Vseross. (Mezhdunar.) Nauch. Konf., 4 – 8 Okt. 2004 g., Zvenigorod* (Physical and Chemical Processes in Selection of Atoms and Molecules: Coll. of Talks, IX All-Russian (Intern.) Scientific Conf., 4 – 8 Oct. 2004, Zvenigorod) (Ed. Yu A Kolesnikov) (Moscow: TsNIIatominform, TROVANT, 2004) p. 7
11. Smirnov V P et al. *Plasma Phys. Rep.* **39** 456 (2013); *Fiz. Plazmy* **39** 523 (2013)
12. Morozov A I *Vvedenie v Plazmodinamiku* (Introduction to Plasmodynamics) (Moscow: Fizmatlit, 2006)
13. Zhil'tsov V A et al. *Atom. Energy* **101** 755 (2006); *At. Energ.* **101** 302 (2006)
14. Timofeev A V *Plasma Phys. Rep.* **26** 626 (2000); *Fiz. Plazmy* **26** 667 (2000)
15. Karchevsky A I, Muromkin Yu A, in *Izotopy: Svoistva, Poluchenie, Primenenie* (Isotopes: Properties, Production, Application) Vol. 1 (Ed. V Yu Baranov) (Moscow: Fizmatlit, 2005) p. 307
16. Dolgolenko D A, Muromkin Yu A *Phys. Usp.* **52** 345 (2009); *Usp. Fiz. Nauk* **179** 369 (2009)
17. Eubank H P, Wilkerson T D *Phys. Fluids* **4** 1407 (1961)
18. Eubank H P, Wilkerson T D *Phys. Fluids* **6** 914 (1963)
19. Safronov B G, Voitsenya V S, Konovalov I I *Sov. Phys. Tech. Phys.* **7** 495 (1962); *Zh. Tekh. Fiz.* **32** 678 (1962)
20. Voitsenya V S et al. *Sov. Phys. Tech. Phys.* **9** 221 (1964); *Zh. Tekh. Fiz.* **34** 280 (1964)
21. Voitsenya V S et al., in *Fizika Plazmy i Problemy Upravlyaemogo Termoyadernogo Sinteza* (Plasma Physics and Issues of Controlled Thermonuclear Fusion) Issue 1 *Issledovanie Plazmennykh Sgustkov* (Investigation of Plasma Bunches) (Kharkov: Izd. AN UkrSSR, 1965) p. 119
22. Compant La Fontaine A et al. *J. Phys. D Appl. Phys.* **31** 847 (1998)
23. Compant La Fontaine A, Louvet P *Plasma Sources Sci. Technol.* **8** 125 (1999)
24. Timofeev A V *Plasma Phys. Rep.* **35** 912 (2009); *Fiz. Plazmy* **35** 989 (2009)
25. IAEA. Nuclear Data for Safeguards, http://www-nds.iaea.org/sgnucdat/c1.htm#92-Pu-239
26. Mikhailovskii A B *Theory of Plasma Instabilities* Vol. 2 (New York: Consultants Bureau, 1974); Translated from Russian: *Teoriya Plazmennykh Neustoichivostei* Vol. 2 (Moscow: Atomizdat, 1971)
27. Belavin M I, Zvonkov A V, Timofeev A V, RF Patent No. 742900 of 05.07.1993
28. Timofeev A V *Plasma Phys. Rep.* **33** 890 (2007); *Fiz. Plazmy* **33** 971 (2007)
29. Timofeev A V, Kuyanov A Yu *Plasma Phys. Rep.* **36** 931 (2010); *Fiz. Plazmy* **36** 991 (2010)
30. Mack J M, Radziemski L J *Physica B + C* **102** 66 (1980)

31. Fortov V E (Ed.-in-Chief) *Entsiklopediya Nizkotemperaturnoi Plazmy* (Encyclopaedia of Low-Temperature Plasma) Introductory Vol., Book 1 (Moscow: Nauka, 2000)
32. Longinov A V, Stepanov K N, in *High-Frequency Plasma Heating* (Ed. A G Litvak) (New York: American Institute of Physics, 1992) p. 93; Translated from Russian: in *Vysokochastotnyi Nagrev Plazmy*: *Materialy Vsesoyuz. Soveshchaniya, Gor'kii, 21–25 Iyunya 1982 g.* (Exec. Ed. A G Litvak) (Gor'kii: IPF AN SSSR, 1983) p. 105
33. Stix T H *The Theory of Plasma Waves* (New York: McGraw-Hill, 1962); Translated into Russian: *Teoriya Plazmennykh Voln* (Moscow: Atomizdat, 1965)
34. Compant La Fontaine A, Pashkovsky V G *Phys. Plasmas* **2** 4641 (1995)
35. Timofeev A V *Plasma Phys. Rep.* **31** 1012 (2005); *Fiz. Plazmy* **31** 1087 (2005)
36. Timofeev A V *Phys. Usp.* **49** 1197 (2006); *Usp. Fiz. Nauk* **176** 1227 (2006)
37. Timofeev A V *Plasma Phys. Rep.* **37** 56 (2011); *Fiz. Plazmy* **37** 60 (2011)
38. Abramowitz M, Stegun I A (Eds) *Handbook of Mathematical Functions with Formulas, Graphs, and Mathematical Tables* (New York: Dover Publ., 1972); Translated into Russian: *Spravochnik po Spetsial'nym Funktsiyam s Formulami, Grafikami i Matematicheskimi Tablitsami* (Moscow: Nauka, 1979)
39. Timofeev A V *Rezonansnye Yavleniya v Kolebaniyakh Plazmy* (Resonance Phenomena in Plasma Oscillations) (Moscow: Fizmatlit, 2009)
40. Canobbio E *Nucl. Fusion* **9** 27 (1969)
41. Kadomtsev B B, in *Reviews of Plasma Physics* Vol. 22 (Ed. V D Shafranov) (New York: Kluwer Acad./Plenum Publ., 2001) p. 1; Translated from Russian: *Kollektivnye Yavlenia v Plazme* (Cooperative Effects in Plasmas) (Moscow: Nauka, 1976)
42. Laz'ko V S *Plasma Phys. Rep.* **20** 470 (1994); *Fiz. Plazmy* **20** 523 (1994)
43. Palmadesso P, Schmidt G *Phys. Fluids* **14** 1411 (1971)
44. Kadomtsev B B *Plasma Turbulence* (London: Academic Press, 1965); Translated from Russian: in *Voprosy Teorii Plazmy* (Reviews in Plasma Physics) Issue 4 (Ed. M A Leontovich) (Moscow: Gosatomizdat, 1964) p. 188
45. Krasheninnikov S I, D'Ippolito D A, Myra J R *J. Plasma Phys.* **74** 679 (2008)
46. Timofeev A V *Plasma Phys. Rep.* **19** 488 (1993); *Fiz. Plazmy* **19** 940 (1993)
47. Schmidt G *Phys. Fluids* **3** 961 (1960)
48. Alterkop B et al. *J. Appl. Phys.* **79** 6791 (1996)
49. Papernyi V L, Krasov V I *Plasma Phys. Rep.* **37** 988 (2011); *Fiz. Plazmy* **37** 1057 (2011)
50. Braginskii S I, in *Reviews in Plasma Physics* Vol. 1 (Ed. M A Leontovich) (New York: Consultants Bureau, 1965) p. 205; Translated from Russian: in *Voprosy Teorii Plazmy* Issue 1 (Ed. M A Leontovich) (Moscow: Gosatomizdat, 1963) p. 183
51. Longmire C L *Elementary Plasma Physics* (New York: Interscience Publ., 1963); Translated into Russian: *Fizika Plazmy. Elementarnyi Kurs* (Moscow: Atomizdat, 1966)
52. Kadomtsev B B *Tokamak Plasma*: *A Complex Physical System* (Bristol: Institute of Physics Publ., 1992); *Osnovy Fiziki Plazmy Tokamaka* (Fundamentals of Plasma Physics of Tokamak) (The Results of Science and Technology. Ser. Plasma Physics, Vol. 10, Pt. 1, Ed. V D Shafranov) (Moscow: VINITI, 1991) p. 3
53. Timofeev A V *JETP Lett.* **97** 5 (2013); *Pis'ma Zh. Eksp. Teor. Fiz.* **97** 7 (2013)
54. Chen F F, in *Plasma Diagnostic Techniques* (Eds R H Huddlestone, S L Leonard) (New York: Academic Press, 1965) p. 113; Translated into Russian: *Diagnostika Plazmy* (Moscow: Mir, 1967) p. 94
55. Landau L D, Lifshitz E M *Fluid Mechanics* (Oxford: Pergamon Press, 1987); Translated from Russian: *Gidrodinamika* (Moscow: Nauka, 1986)